Inês da Conceição Duarte Prazeres

Degree in Biochemistry

Development of astaxanthin lipid formulations for nutraceutical application: targeting the gastrointestinal epithelium

Dissertation to obtain the master's degree in
Biochemistry for Health

Supervisor: Ana Matias, PhD, iBET

October, 2019

Inês da Conceição Duarte Prazeres

Degree in Biochemistry

Development of astaxanthin lipid formulations for nutraceutical application: targeting the gastrointestinal epithelium

Dissertation to obtain the master's degree in
Biochemistry for Health

Supervisor: Ana Matias, PhD, iBET

Jury
President: Doctor Teresa Catarino
Arguer: Doctor Vanessa Santos Silva Gonçalves
Vogal: Doctor Margarida Archer Baltazar Pereira da Silva Franco Frazão
ITQB

October, 2019

Development of astaxanthin lipid formulations for nutraceutical application: targeting the gastrointestinal epithelium

Acknowledgments

Gostaria de agradecer a todas as pessoas que, direta ou indiretamente, me ajudaram a chegar aqui. Este trabalho não seria possível sem o meu esforço e dedicação, mas foram vocês que sempre me deram a força necessária para não desistir.

À minha orientadora, Doutora Ana Matias. Por todo o tempo despendido na realização deste trabalho de investigação, por estar sempre disponível para me ajudar e por, essencialmente, me ter permitido, com o seu apoio, chegar a este resultado final.

Aos meus colegas do laboratório de Nutracêuticos e Tecnologia de Processo de Bioativos do iBET, Naiara, Agostinho, João, Liliana, Ana Roda, Miguel, Martim, Sara, Ana Nunes, Melanie e Maha. Agradeço-vos toda a ajuda, disponibilidade e companheirismo demonstrados ao longo destes meses.

Um especial obrigado à Ana Nunes e à Melanie, por estarem incondicionalmente disponíveis para me ajudar. Sem a vossa ajuda não teria sido possível.

Às “meninas da química”, Ana Bárbara, Sheila e Rafaela, agradeço-vos toda a ajuda e, especialmente, a vossa amizade. À Rafaela pela amizade, apoio e sobretudo por me teres animado sempre que precisei.

Às minhas amigas, Andreia, Cátia, Daniela, Joana, Maha, Pimpão e Sara pela vossa amizade, apoio à paciência ao longo do meu percurso académico. Espero que o tempo não apague estes laços que se criaram. Obrigada por me fazerem sempre sorrir.

À minha família, por me terem dado os meios necessários para chegar aqui, nunca me deixarem baixar os braços e estarem sempre lá para mim quando o caminho parecia incerto.

À minha Mãe, porque sem ela nada disto seria possível. Agradeço o amor incondicional que me dás, todos os dias.

Abstract

Astaxanthin is renowned for its powerful antioxidant activity and remarkable therapeutic effects in the prevention and treatment of several diseases. Moreover, astaxanthin could constitute a potential nutraceutical to be used in the treatment and maintenance of Inflammatory Bowel Diseases. However, its therapeutic use is seriously limited by its instability and low bioavailability. Hence, in this work, astaxanthin and a shrimp shells extract rich in astaxanthin were entrapped into nanostructured lipid carriers (NLCs) and structured lipid carriers (SLCs). Furthermore, their permeability was assessed in a Caco-2 monoculture and in a Caco-2:HT29-MTX:Raji-B triple co-culture. Additionally, their capacity to inhibit reactive species of oxygen (ROS) formation was assessed in Caco-2 monolayers.

Astaxanthin- and extract-NLCs were prepared through melt-emulsification. The formulation (presence of organic solvent, amount of bioactive) and process conditions (homogenization time) were optimized. The optimum formulation and conditions led to the production of particles with the smallest particle size (<370 nm) and lowest polydispersity index (<0.3).

Astaxanthin- and extract-SLCs were prepared through Particles from Gas Saturated Solutions (PGSS®) process. The formulation (olive oil or peceol) and process conditions (pressure, contact time with supercritical CO_2) were optimized. The optimum formulation (containing olive oil) and process conditions (250 bar and 15 minutes) led to the particles production with the highest load (9.257±0,796 and 0.0029 mg/g, respectively) and with the smallest particle size (1.5-20 µm).

The permeability studies indicate that SLCs and NLCs may improve astaxanthin cellular uptake. The antioxidant assays revealed that the extract and extract-SLCs possess the most promising antioxidant activities. While, astaxanthin revealed to increase the levels of ROS when incubated with the cells prior to stress induction, and to directly scavenge ROS when co-incubated with the stressor.

In conclusion, formulations that may improve astaxanthin bioavailability were produced and a scalable entrapment process (PGSS®) with potential application in the industry was developed.

Keywords: Astaxanthin; Shrimp shell extract; Nanostructured lipid carriers; Structured lipid carriers; PGSS®; Triple co-culture Caco-2:HT29-MTX:Raji-B

Resumo

Astaxantina é conhecida por possuir potente atividade antioxidante e extraordinários efeitos terapêuticos no tratamento e prevenção de várias doenças. Além disso, poderá ser utilizada como possível nutracêutico para o tratamento e manutenção das Doenças Inflamatórias Intestinais. Contudo a sua instabilidade e baixa biodisponibilidade limitam os seus efeitos terapêuticos. Portanto, neste trabalho, a astaxantina e um extrato de cascas de camarão, rico em astaxantina, foram encapsulados em *nanostructured lipid carriers* (NLCs) e *structured lipid carriers* (SLCs). Ademais, a sua biodisponibilidade foi avaliada em Caco-2 e numa co-cultura tripla de Caco-2:HT29-MTX:Raji-B, e a sua capacidade em inibir a produção de espécies reativas de oxigénio (ROS) foi avaliada em Caco-2.

Astaxantina- e extrato-NLCs foram preparadas por *melt-emulsification.* A formulação (presença de solvente orgânico e quantidade de bioativo) e condições de preparação (tempo de homogeneização) foram otimizados. A formulação e condições ideias permitiram produzir partículas com o menor tamanho (<370nm) e com o índice de polidispersão mais baixo (<0,3).

Astaxantina- e extrato-SLCs formam preparadas através do processo *Particles from Gas Saturated Solutions* (PGSS®). A formulação (azeite ou peceol) e condições do processo (pressão e tempo de contacto com CO_2) foram otimizados. A formulação (contendo azeite) e condições (250bar e 15minutos) ideias permitiram a produção de partículas com o maior *load* (9,257±0,796 e 0,0029 mg/g, respetivamente) e com o menor tamanho de partícula (1,5-20µm).

Os estudos de permeabilidade revelaram que as SLCs e as NLCs podem ter aumentado a absorção celular da astaxantina. O extrato e extrato-SLCs revelaram apresentar a atividade antioxidante mais promissora. Porém, astaxantina revelou aumentar os níveis de ROS quando incubada com as células antes da indução de stress, mas inibiu os ROS quando co-incubada com o indutor de stress.

Concluindo, formulações que poderão melhorar a biodisponibilidade da astaxantina e um processo de encapsulação (PGSS®) com possível aplicação na indústria foram desenvolvidos.

Palavras-chave: Astaxantina; Extrato de cascas de camarão; *Nanostructured lipid carriers*; *Structured lipid carriers*; PGSS®; Co-cultura tripla Caco-2:HT29-MTX:Raji-B

List of Figures

List of Tables

Abbreviation	Full form
AGS cell line	AGS Human Caucasian gastric adenocarcinoma cell line
AP-1	Activator protein 1
ARE	Antioxidant response element
ASX	Astaxanthin
Caco-2	Human erythrocytes from colorectal adenocarcinoma cell line
CAT	Catalase
COX-1	Cyclooxygenase-1 enzyme
COX-2	Cyclooxygenase-2 enzyme
CP	Critical point
DCF	2',7'-Dichlorofluorescein
DCFH	2',7'-Dichlorofluorescin
DCFH-DA	2',7'-Dichlorofluorescin Diacetate
DCM	Dichloromethane
DMEM	Dulbecco's Modified Eagle Medium
DMSO	Dimethyl Sulfoxide
DPPH	2,2-diphenyl-1-picrylhydrazyl
DSC	Differential Scanning Calorimetry
DNA	Deoxyribonucleic Acid
EE(%)	Encapsulation efficiency
Eq.	Equantion
ERK	Extracellular signal–regulated kinases
FBS	Fetal Bovine Serum
FDA	Food and Drug Administration
GIT	Gastrointestinal tract
Gpx	Glutathione Peroxidase
GSH	Reduced form of Glutathione
GSH-px	Glutathione Peroxidase
GST	Glutathione S-transferase
HPLC	High Performance Liquid Chromatography
H.Pluvialis	*Haematococcus pluvialis*
HDL	High density lipoproteins
HO-1	Heme Oxygenase 1
HT29	Human goblet cells from colon adenocarcinoma cell line
HT29-MTX	Human goblet cells from colon adenocarcinoma cell line methotrexate treated
IBD	Inflammatory Bowel Diseases
IkBα	regulatory protein that inhibits NF-kB
iNOS	Inducible nitric oxide synthase
ISO	International Organization for Standardization
LDL	Low density lipoprotein
LPS	Lipopolysaccharide
M-cells	Microfold cells
MAPK	Mitogen-associated Protein Kinases
min	Minutes
MMP	Mitochondrial membrane potential
MTX	Methotrexate
NADPH	Nicotinamide Adenine Dinucleotide Phosphate
NF-kB	Nuclear factor kappa B
NLC	Nanostructured lipid carrier
NO	Nitric oxide
NrF-2	Nuclear Factor Erythroid related factor 2

O/W	Oil in water
P	Pressure
PBS	Phosphate-Buffered Saline
PDI	Polidispersitivity index
PGE2	Prostaglandin 2
P-gp	P-glycoprotein
PGSS	Particles from Gas Saturated Solution
Raji-B	Human B lymphocyte Burkitt's lymphoma cell line
RNS	Reactive species of nitrogen
ROS	Reactive species of oxygen
$scCO_2$	Supercritical carbon dioxide
SCF	Supercritical fluid
SD	Standard deviation
SEM	Scanning electron microscopy
SFEE	Supercritical Fluid Extraction of Emulsions
SLC	Structured lipid carriers
SLN	Solid lipid nanoparticle
SOD	Superoxide Dismutase
sR-A	Class A macrophage scavenger receptor
T	Temperature
TBARS	Thiobarbituric acid reactive substances
TEER	Transepithelial electrical resistance
TGF-β	Transforming Growth Factor β
TLR4	Toll-like receptor 4
TNF-α	Tumor necrosis factor α
UV	Ultraviolet
UV-Vis	Ultraviolet-Visible

1 Introduction

1.1 Nutraceuticals

The term “nutraceutical” was first introduced in 1989 by Stephen De Felice, who defined nutraceutical as “food, or parts of a food, that provides medical or health benefits, including the prevention and treatment of disease” [1]. Nowadays, as population transitions to a more natural and healthier way of life the interest in nutraceuticals as an alternative medicine rose, replacing synthetic drugs with natural medicinal compounds. Hence many pharmaceutical companies are looking for nutraceuticals from natural sources to aid with drug development.

These products are often used to prevent and manage chronic diseases, delay the aging process, increase life expectancy and improve and maintain health. Many nutraceuticals are recognized for their ability to reduce the risk of cardio-vascular diseases, cancer, heart diseases, diabetes, inflammation, arthritis and so on [1–3].

Nutraceuticals range from isolated vitamins, antioxidants, purified food, dietary supplements and herbal products. These nutraceuticals can also refer to bioactives and are often comprised of vitamins, lipids, proteins, carbohydrates, minerals, carotenoids, flavonoids, and others and can be obtained from a variety of sources, such as plants and marine life [3,4].

Some of the bioactive compounds often used in nutraceuticals tend to be sensitive to a variety of factors such as oxygen, light, acidic conditions, and it is often difficult to obtain a pharmaceutical form (tablets, powders, capsules etc.) containing bioactives that present a satisfactory bioavailability. Thus, to improve their bioavailability, these are often encapsulated to protect them from external factors and the harsh conditions of the gastrointestinal tract (GIT) [4,5].

1.2 Astaxanthin

Astaxanthin (3,3’-dihydroxy-β,β-carotene- 4,4’-dione) is a lipid-soluble red-orange pigment that belongs to a group of carotenoids classified as xanthophyll. It is known for having an antioxidant ability 10 times higher than zeaxanthin, lutein, and canthaxanthin [6–9]. Furthermore, it is reported to possess remarkable biological activities including anti-inflammatory, anti-cancer, anti-aging, anti-diabetic, improvement of cardiovascular function, neuronal protection among others [10–12].

It is naturally found in crabs, lobsters, salmon, shrimp and flamingos, being responsible for the red color on the flesh, skin, exoskeleton or feathers of the animals. Astaxanthin is synthesized by some plants, microorganisms and algae. Although animals are not able to synthesize carotenoids, they obtain them from the food chain in nature. The main source of this xanthophyll is a green microalgae known as *Haematococcus pluvialis (H.pluvialis),* which produces it under stress conditions such as high salinity, nitrogen deficiency, high temperature and light [6,7,13].

Astaxanthin is available for purchase from either chemical synthesis or natural sources such as microalgae, yeast, and crustacean byproducts. Synthetic astaxanthin dominates commercially, being its total market value above $200M per year [8,13,14]. Despite the chemical synthesis being a source of large quantities of astaxanthin, Food & Drug Administration (FDA) banned its use from human consumption and animal feed, due to its rising concerns about its biological functions and food safety, since it is derived from petrochemicals. Furthermore, natural astaxanthin is reported to have higher antioxidant activity than synthetic astaxanthin [13,15]. Hence, the only application of synthetic astaxanthin is in aquaculture [8,13,14]. As a result, natural astaxanthin has been very sought after for its application in dietary supplements and for the production of cosmetics, nutraceuticals and pharmaceuticals, due to its evidenced effects in promoting human health. As a consequence, while the price of synthetic astaxanthin is US$2500/kg, the prince of natural astaxanthin is US$7000/kg [15].

Owing to the high astaxanthin concentration, *H.pluvialis* represents the primary natural source of astaxanthin for human applications, and its use in dietary supplements has been approved by the FDA [6,14,16,17].

1.3 Astaxanthin extraction

As mentioned previously, natural astaxanthin is mainly obtained through extraction from *H.pluvialis,* which accumulates up to 9.2 mg/g cell. Despite this, its large-scale cultivation is difficult, and no efficient method has been found due to the thick cell wall of the organism, making it difficult to extract astaxanthin using solvents [17].

Shrimps are another important dietary source of astaxanthin. Seafood processing companies produce large amounts of discarded shrimp shells, which still contain valuable nutrients and functional compounds, such as proteins, chitin, and lipids, as well as astaxanthin. Moreover, often, these wastes are not exploited for their potential use in recovering valuable components on a commercial scale, thus a good and cheap source of carotenoids is lost [18]. As already stated, there is a high demand for natural astaxanthin, hence by using shrimp waste for the extraction of this carotenoid would not only improve the economics of the crustaceans processing business, but, simultaneously, would provide a cheap raw material for the extraction of astaxanthin and other carotenoids, thus decreasing the carotenoids production cost [19,20].

Different extraction methods of astaxanthin from shrimp shells have been reported, such as solvent extraction method, oil-soluble method, pressurized liquid extraction method, high pressure method, supercritical carbon dioxide extraction method, enzymatic digestion, among others [17,18,21–24].

1.4 Biochemistry of astaxanthin

Carotenoids can be divided into two groups accordingly to their chemical structure: carotenes, which are only composed by carbon and hydrogen; and xanthophylls, which are oxygenated derivatives. Astaxanthin belongs to the latter group, and in this case oxygen is present as hydroxyl and carbonyl groups [25].

The properties of astaxanthin are attributed to its unique molecular structure. Its molecule has an extended shape with a polar structure at either end of the molecule and a nonpolar fraction in the middle (Figure 1.1-A). The two oxygenated β-ionone ring systems, that confer the potent capacity for quenching free radicals or other oxidants are linked by a chain of double bonds, which alternate with carbon-carbon single bonds, termed conjugated system (polyene chain). This polyene system allows astaxanthin to act as a strong antioxidant, being able to donate electrons to free radicals. Furthermore, this polar-nonpolar-polar configuration of the molecule of astaxanthin allows it to fit precisely into the polar-nonpolar-polar area of the cell membrane [7,16,26,27](Figure 1.1-B).

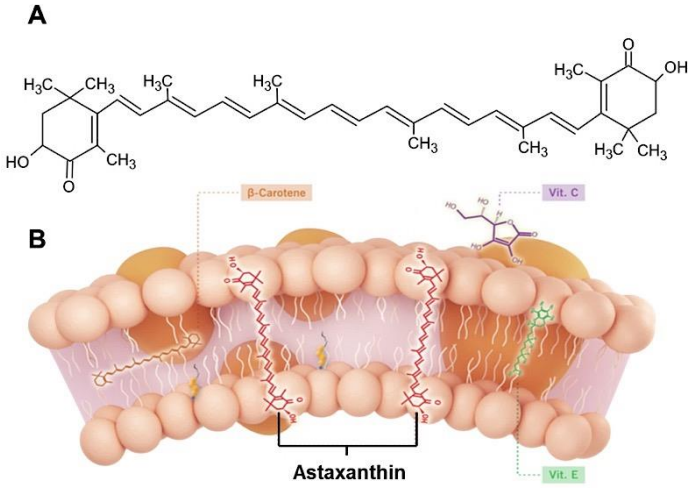

Figure 1.1- A- Chemical structure of pure astaxanthin; B- Phospholipidic membrane integration of astaxanthin (adapted from AstaReal, 2012 [28])

The conjugated system provides astaxanthin its unique molecular structure, chemical properties and light-absorbing characteristics. Depending on the configurations of the double bonds

of the polyene chain, astaxanthin may exist in two geometrical isomers, trans and cis (E and Z) (Figure 1.1). In nature, astaxanthin exists predominantly in the all-trans form [7,16,29].

The presence of the hydroxyl (OH) and carbonyl (C=O) in each ionone ring explains some of the properties of astaxanthin, such as the ability to be esterified, higher antioxidant capacity and a more polar nature than the other carotenoids (Figure 1.1). Due to the presence of two stereogenic carbons (3 and 3′) on the β-ionone rings astaxanthin possess three stereoisomeric forms, two chiral, ((3S,3′S) and (3R,3′R)), and one optical inactive mesoform (3R,3′S) (Figure 1.2). Although in nature the ratio of optical stereoisomers varies accordingly to the biological source, synthetic astaxanthin consists of an equimolar mixture of the racemate and the meso form. In synthetic astaxanthin, the meso compound accounts for half of total astaxanthin, while (3S, 3'S) and (3R, 3'R) enantiomers account for ~25% each. In addition to the natural occurring stereoisomers, the presence of stereoisomer by-products may have an inhibitory effect on the biological activity of synthetic astaxanthin. In nature, astaxanthin exists predominantly in the all-trans 3S,3S' form [16,29,30].

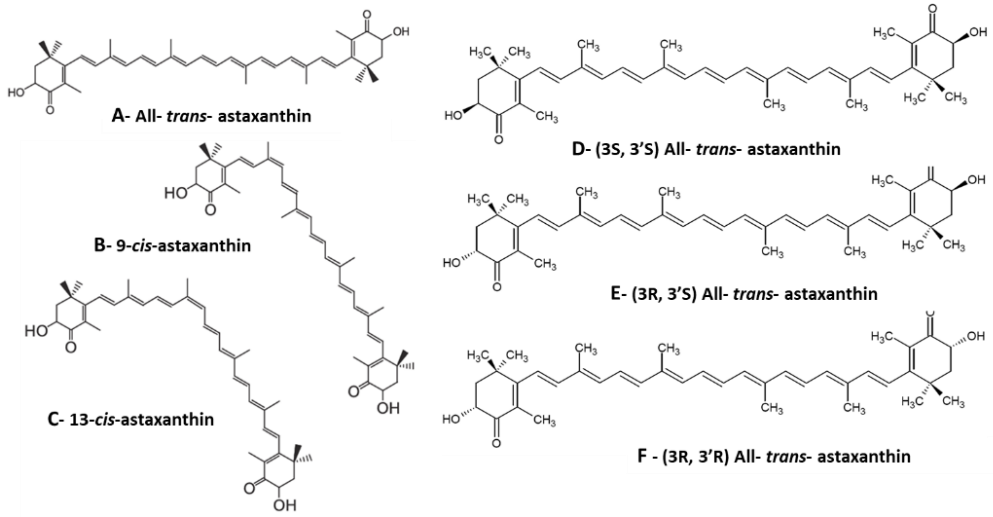

Figure 1.2- Structure of the geometrical isomers of astaxanthin: (**A**) all-trans-astaxanthin, (**B**) 9-cis-astaxanthin, (**C**) 13-cis-astaxanthin, and **stereoisomers of all-trans-astaxanthin:** (**D**) (3S,3 S)-all-trans-astaxanthin, (**E**) (3R,3 S)-all-trans-astaxanthin, and (**F**) (3R,3 R)-all-trans-astaxanthin. (Adapted from: Wang *et al.* [31])

1.5 Biological activities and Health benefits

1.5.1 Antioxidant activity

Reactive oxygen species (ROS) are species of oxygen with unpaired electrons, that can be produced by cells in physiological conditions. The main source of ROS is oxidative phosphorylation, and in a smaller extend the activity of enzymes and cytochrome p450. Moderate levels of ROS can lead to cell functioning alterations by activating and modulating intracellular signaling pathways, such as MAPK pathway, leading to the activation of transcription factors, such as AP-1 and NF-κB, which in turn are involved in the transcription of cell growth regulation genes [32–35].

Increased levels of ROS are referred to as oxidative stress, and are caused by several factors, such as inflammation, infection and imbalance between antioxidant defense and pro-oxidant load (which is caused by an inadequate or excess nutrient supply that results from a poor diet or bad eating habits). Since the membrane systems of cells are composed by polyunsaturated fatty acids, they are particularly vulnerable to free radicals endogenously generated, in metabolic activities, or externally generated. Additionally, when there is an imbalance the free radicals can damage lipids, DNA and proteins, and because these molecules make up for a large part of the body that damage can result in numerous diseases. Extensive research as revealed that continued oxidative stress leads to chronic inflammation and consequently leads to chronic diseases, including cancer, Inflammatory Bowel Diseases (IBD) and skin damage. Furthermore, it is a leading cause of various

other diseases such as metabolic syndromes, neurodegenerative, cardiovascular diseases as well as age-related diseases [32–36].

Recently, astaxanthin has become notorious for its properties as a biochemical messenger and powerful antioxidant, acting as a defense against oxidative damage by being a potent quencher of singlet oxygen and an efficient scavenger of superoxide anion and hydroxyl radical. Thus, astaxanthin protects native molecules (e.g., DNA) and cell membranes from oxidation. Additionally, astaxanthin enhances the immune system function, regulates gene expression and preserves membrane structures by inhibiting lipid peroxidation [37].

The extended π-conjugation system in the molecule of astaxanthin allows it to interact with radicals and ultimately quench singlet oxygen. In this process of quenching, astaxanthin remains intact so that it can undergo further cycles of quenching [16]. Besides lowering the levels of ROS, this xanthophyll is capable of inhibiting H_2O_2-mediated activation of the transcription factor NF-κB, which controls the expression of inducible genes such as heme oxygenase 1 (HO-1), that represents a marker of oxidative stress [35].

Cells have developed strategies to avoid damage caused by oxidative stress. One of which is to activate the nuclear factor erythroid- related factor 2 (Nrf-2)/ antioxidant response element (ARE) signaling pathway, which controls the expression of numerous cytoprotective genes that can combat the harmful effects of oxidative stress. As a result, the Nrf-2/ARE signaling pathway has become a therapeutic target of many antioxidants. This pathway regulates phase II antioxidant responses, which can be activated by small amounts of ROS. Once activated, Nrf2 translocates from the cytosol to the nucleus, and there it increases gene expression, by binding to the antioxidant response element (ARE), of phase II antioxidant enzymes, such as NAD(P)H: quinine oxidoreductase-1 (NQO1), glutathione S-transferase, glutamate-cysteine ligase, and HO-1. Some compounds induce HO-1 expression by activating the Nrf-2/ARE pathway [38,39].

Tingting *et al.* verified that astaxanthin produced small amounts of ROS, rather than directly quench them, implying that astaxanthin could behave as a “prooxidant” like other known carotenoids, that under certain conditions also act as prooxidant. Additionally, the results obtained suggested that astaxanthin by generating ROS in cells promoted the translocation of Nrf-2 from the cytoplasm to the nucleus, and consequently the activation of HO-1 expression and improvement of the expression and activity of GSH-Px via the ERK-Nrf-2/HO-1 pathway [38].

Tripathi *et al.* demonstrated that the administration of astaxanthin reduced the oxidative stress and cell death in rat hepatocyte, through Nrf-2/ARE pathway. Additionally, it was observed an increase in the nuclear Nrf2 and in the associated phase-II enzymes (NQO-1 and HO-1), in response to the treatment of astaxanthin [40].

Therefore, astaxanthin can employ its antioxidant activity not only through direct radical scavenging, but also through the activation of Nrf2/ARE pathway [6,38,41].

McNulty *et al.* suggested that the differences in membrane alignment of the antioxidants may explain their biologic activity. Specifically, the antioxidant and anti-inflammatory activity of these compounds appears to be a consequence of their precise transmembrane alignment in the lipid bilayer of cell membranes. This alignment allows the hydrophilic moieties at the end of the molecule to be exposed and to interact with reactive species in the aqueous environment. Furthermore, the transmembrane alignment may provide proximity to cofactors, such as vitamin C, which serve as a sink for accepting the radical cations, effectively recharging the electron transfer capacity [42] (Figure 1.1).

Since it can fit precisely into the polar-nonpolar-polar area of the cell and mitochondria membranes, astaxanthin displays higher antioxidant activity than other carotenoids [43,44] (Figure 1.1). The polyene chain in astaxanthin traps radicals in the membrane, while the terminal ring of the molecule can scavenge radicals both at the surface and in the interior of the cell membrane [36]. Additionally, McNulty *et al.* demonstrated that astaxanthin when integrating the membrane preserved its structured and reduced the lipid peroxidation [42].

By integrating the phospholipidic bilayers astaxanthin provides numerous antioxidant activities such as: neutralizing free radicals by donating electrons to unpaired electrons; bonding with the radical to form an unreactive “adduct”; conducting electrons or electronic energy out of the membrane; neutralizing radical species of nitrogen, sulfur, or carbon, in addition to oxygen [26].

1.5.2 Anti-inflammatory activity

While inflammation is an essential defense mechanism, excessive and prolonged immune activation can result in destruction of healthy tissues. Hence, the development of pharmaceuticals/nutraceuticals is crucial to handle the excessive release of inflammatory mediators in inflammatory-related diseases.

Inflammation starts as an acute response that aims to limit and eliminate the causes of cellular damage, and clear and/or absorb necrotic cells and tissues. Furthermore, this response is self-limiting and beneficial to the host. On the other hand, prolonged chronic inflammation results in healthy tissue damage and ultimately results in chronic diseases and complications. Chronic inflammation is the cause of numerous diseases such as Inflamed Bowel Diseases (IBD), cardiovascular diseases, type 2 diabetes, Chronic Obstructive Pulmonary Disease (COPD), cancer, among others [45].

Transcription factors, specifically NF-κB, have been associated with inflammation. The NF-kB signaling pathway has long been recognized as one of the main pathways responsible for modulating the inflammatory response and process. This pathway can be activated by specific (TNF-α, IL-1β) and unspecific (excess of ROS, UV radiation) signals, and once activated it triggers a cascade of signals that will result in the transcription of various genes, many of which are inflammatory and immunoregulatory. By blocking the NF-kB cascade the transcription of pro-inflammatory genes is prevented, thus preventing the production of pro-inflammatory molecules and ultimately preventing inflammation [46].

It is known that excess of ROS contributes for chronic inflammation, by continuously activating the NF-κB pathway. Therefore, astaxanthin by being a powerful antioxidant may exert anti-inflammatory effects and contribute for the treatment of chronic inflammatory diseases.

Speranza *et al.* demonstrated that astaxanthin by quenching ROS inhibited the activation of NF-kB and consequently inhibited the production of pro-inflammatory molecules. This author revealed that astaxanthin inhibited the translocation of NF-κB to the nucleus [47].

Furthermore, M.Li *et al.* verified that astaxanthin inhibited the activation of the NF-kB pathway and the degradation of IκBα, a protein that inhibits the activation of NF-kB, by forming a complex with this protein. The last discovery is also reported in many other studies [12,48,49].

1.5.3 Astaxanthin and Inflammatory Bowel Diseases (IBD)

Astaxanthin has become known for its unique chemical properties, high antioxidant activity and emerging evidence of health promotion. Studies revealed the anti-inflammatory, anti-cancer, and protection against UV-radiation-induced photo-toxicity activity of astaxanthin. Moreover, it has been demonstrated that astaxanthin possess a great therapeutic potential, specifically, in the prevention and treatment of cardiovascular, gastrointestinal, hepatic, neurodegenerative, ocular, and dermatological diseases, as well as diabetes, diabetic neuropathy, metabolic syndromes, cancer, and chronic inflammation [50].

Inflammatory Bowel Diseases (IBD) are chronic inflammatory conditions of the gastrointestinal tract (GIT). The two most common types of IBD are Ulcerative colitis and Crohn's disease. The current therapies for IBD aim to ease disease related symptoms and reduce relapse rates, but besides treating the disease they also come with adverse effects. Recently, several studies focused on reactive oxygen species (ROS) and reactive nitrogen species (RNS) as etiologic factors for IBD. The GIT is a major site for generation of pro-oxidants, that are produced by food ingredients and interactions between immune cells. Despite the defense mechanism of the intestinal cells against ROS and RNS, excessive ROS generation leads to lipid peroxidation and could deplete the antioxidant defenses [51].

Because excessive generation of ROS is a big contributor for the inflammation in IBD (since ROS activates NF-kB signaling pathway) the administration of antioxidants with added anti-inflammatory activity could potentially aid the treatment of IBD [51]. Astaxanthin being a powerful antioxidant and with anti-inflammatory activity could be an alternative or complementary treatment for IBD. Additionally, to date, there are no significant adverse effects attributed to astaxanthin supplementation, indicating that it could be a safe compound with no side effects associated.

Shigeki *et al.* studied the potential of astaxanthin as a therapeutic option to treat IBD. In this work it was evaluated the effect of astaxanthin on dextran sulfate sodium (DSS)-induced colitis in

mice. It was verified that astaxanthin suppressed the DSS-induced histological inflammatory changes and suppressed the mucosal mRNA expression of IL-1β, IL-6, IL-36γ. Additionally, this carotenoid blocked the translocation of NF-kB, and AP-1 into the nucleus and suppressed the activation of MAPKs (ERK1/2, p38 and JNK). All in all, astaxanthin prevented the DSS-induced colitis [52].

Mitochondria are crucial for the cellular energy production and are a major source of ROS. Mitochondrial membranes are particularly susceptible to oxidative damage since they are composed by a high content of polyunsaturated fatty acids and because of their proximity to the site of ROS production [53–55].

Oxidative stress can cause mitochondrial dysfunction, which results in functional loss. A major indicator of mitochondrial dysfunction is the disruption of the mitochondrial membrane potential (MMP). The consequence of MMP loss is ATP depletion, decreased metabolic oxygen consumption and low energy metabolism. Ultimately, oxidative damage can result in mitochondrial membrane permeabilization and trigger the mitochondrial apoptotic pathway, thus resulting in cell death [53–55].

Several studies have reported evidence of mitochondrial dysfunction within the intestinal epithelium of patients with IBD and mice undergoing experimental colitis [165]. Furthermore, several new studies with clinical reports associated mitochondrial dysfunction and ROS produced by mitochondria with the pathogenesis of IBD [56–58]. Others studies, however, report that IBD is caused by an immune response dysregulation, environmental changes and gene variants [59]. Despite the evidences in the intestines of patients with IBD of oxidative stress and impaired ATP production, which are known to be caused by mitochondrial dysfunction, it is still unknown whether mitochondrial dysfunction is a cause or a consequence of IBD.

Astaxanthin by inhibiting oxidative stress in cells may suppress oxidative stress-induced mitochondrial dysfunction and mitochondrial ROS production. Furthermore, some authors report that astaxanthin by acting out against ROS can prevent mitochondrial dysfunction [53]. Wolf *et al.* demonstrated that astaxanthin prevented mitochondrial dysfunction by protecting the mitochondrial redox balance [55]. It was also demonstrated that astaxanthin protected mitochondria inner and outer membranes and the cristae against H_2O_2- or bleomycin-induced structural disruption, additionally it increased mitochondrial membrane potential (MMP) [60].

Despite its potential, the clinical use of astaxanthin for IBD treatment has not been reported much, so more investigation needs to be performed to attest its actual potential as an alternative or adjuvant treatment for IBD.

1.6 Astaxanthin pharmacokinetics, bioavailability and stability

As a result of its hydrophobic nature, the digestion and absorption of astaxanthin is similar to other dietary lipids and carotenoids. Briefly, after incorporation into mixed lipid micelles in the lumen, astaxanthin is partially absorbed through passive diffusion by the intestinal mucosal cells and incorporated into chylomicrons to be later released into the lymphatic system. Afterwards, chylomicrons are digested by the lipoprotein lipase, in the liver, and astaxanthin is assimilated by lipoproteins, HDL and LDL, to be further distributed to other tissues [16,30,37].

Bioavailability can be defined as the fraction of ingested component available at the site of action and results from three main steps: (1) digestibility and solubility of the element in the gastrointestinal tract; (2) absorption of the compound by the intestinal cells and transport into the circulation; and (3) transport from the circulation to the target place [61]. The absorption of astaxanthin and other carotenoids is highly influenced by their chemical properties and dietary and non-dietary-related parameters. Astaxanthin is highly hydrophobic and because of this it has low oral bioavailability, which limits its therapeutic potential [16,30,37].

Another explanation for the low bioavailability of astaxanthin is its dissolution limitations in the gastrointestinal fluids and, in high doses, there is a saturation of its incorporation into bile micelles [62]. Moreover, the bioavailability of astaxanthin is influenced by its level of esterification, only free-astaxanthin is absorbed, so before being absorbed esterified astaxanthin needs to undergo hydrolysis [30].

Furthermore, astaxanthin is extremely sensitive and prone to degradation under adverse conditions, such as acidic environments, heat, light, transition metal ions, singlet oxygen, and free radicals. The polyene chain in the molecule is susceptible to oxidation and isomerization [63]. Its

degradation can be verified by the fading of its red-orange color and a corresponding loss of function [64].

Because of its low bioavailability the powerful antioxidant activity of astaxanthin is very limited in the *in vivo* settings. Also, the instability and low bioavailability of this xanthophyll restrict its applications in functional foods, pharmaceutical and cosmetic products. Therefore, to overcome the limitations of astaxanthin caused by its hydrophobic nature, extreme sensibility and poor oral bioavailability it is important to develop delivery strategies to encapsulate astaxanthin.

When astaxanthin is administered/consumed with lipids, its absorption increases [37,62]. As a consequence, its bioavailability is enhanced by lipid-based formulations, not only it present high solubility in lipids, but also by being solubilized in the oil phase the absorption of astaxanthin increases [16,62]. Different delivery strategies can be employed such as nano- or microencapsulation, O/W emulsions, incorporation into liposomes, among others [65–68].

1.7 Bioactive formulation

Due to the powerful antioxidant activity and chemical properties of astaxanthin, it is a very promising bioactive with great nutraceutical applications in human nutrition and healthcare. To act as an antioxidant *in vivo*, astaxanthin would have to be in an appropriate concentration, that is proportionate to the oxidants and the molecules to be preserved, at the right place in the tissues [16].

The oral route is the preferred route for administration of drugs. However, most bioactive compounds (e.g. carotenoids, flavonoids, oil soluble vitamins and nutraceuticals) have hydrophobic nature and poor oral bioavailability, this suggests that insufficient amount of bioactive arrives to the site of action, thus causing lack of pharmacological action [69–71]. Furthermore, there are several barriers encountered in the oral route that difficult the absorption and subsequent activity of lipophilic compounds, such as astaxanthin. The hydrophobic nature of astaxanthin causes it to have poor solubilization in the GIT, increases the risk of metabolization through intestinal metabolic enzymes and through cytochrome P450 enzymes, thus leading to its significant first pass elimination [69,70,72]. Additionally, lipophilic compounds tend to be expelled via P-glycoprotein (P-gp) [69,70,72]. Thus, it is necessary to develop a suitable drug delivery system to overcome these limitations.

Delivery system is defined as the entrapment of a bioactive material in a carrier, to control its release rate. When designing drug delivery systems, it is important to consider the four key design aspects: stability, encapsulation efficiency, controlled release and biocompatibility.

A delivery system may be in the nano- or microscale. A nanomaterial can be defined as “a discrete entity that has one or more dimensions of the order of 100 nm or less” although, in the pharmaceutical field it is defined as particles with a size below 1000 nm (=1 µm) [73]. The application of micro- and nanotechnologies in the pharmaceutical industry has contributed in many aspects for the development of efficient drug delivery systems and formulations with improved bioavailability [71,74].

When comparing micro-delivery systems to nano-delivery systems, the latter offer some advantages over the former, such as [71,75]:

- higher surface area, which translates into a larger surface for functionalization and higher dissolution rate;
- thermodynamically more stable;
- higher mobility and capacity to cross barriers, due to its small size they are easily taken up and can pass through cells (microparticles when injected, for example, tend to stay where they are placed);
- while particles up to 10 µm in diameter can only be absorbed through phagocytosis by phagocytes (macrophages, dendritic cells, and the like), nanoparticles can be taken up through pinocytosis, a mechanism that all cell types possess.

Cellular uptake of particles and small molecules depends mainly on endocytosis, which consists in the active transport of compounds into the cell by engulfing them with its membrane using energy in the form of ATP. The two main endocytosis mechanisms are pinocytosis and phagocytosis. Phagocytosis is carried out by phagocytes (macrophages, neutrophils and dendritic cells) and is achieved by engulfing particles larger than 1 µm. In contrast, pinocytosis involves taking extracellular fluids into the cells. Through this mechanism the cell can internalize fluids using a small amount of

energy [76]. The uptake of the particles through pinocytosis mainly occurs through macro-pinocytosis, clathrin-mediated, caveolin-dependent and caveolin-independent pinocytosis [76]. The particle size, shape, surface charge, and surface functionalization of the particulate systems are the main physicochemical traits that influence the endocytosis-dependent cellular uptake. Nevertheless, it is important to refer that particles with sizes up to 600 nm have been reported to have similar permeability capacity in the human GIT as ones with 1–100 nm [71].

More and more the use of nano-delivery systems contributes to the growth of pharmaceutics, cosmetics and food industries. These systems can generally be divided into two groups: polymer- and lipid-based systems. The use of polymer-based systems is limited due to the low availability of suitable biopolymers, the possibility of toxicity of the polymers, low concentration of active compounds, poor stability of the nanoparticles, the need to use organic solvents, the need of intricate chemical or heat processing and lack of suitable large-scale production methods. Besides this, natural (carbohydrates/proteins) and synthetic polymers are generally hydrophilic, and as already mentioned, astaxanthin is hydrophobic and its absorption is increased with lipid co-administration [71,72,74].

In contrast, lipid-based formulations have many advantages such as: increased solubilization capacity; biocompatibility (since the lipids used to prepare the particles are usually physiological lipids, and thus biocompatible and biodegradable) which in turn result in low toxicity; enhanced membrane permeability; higher encapsulation efficiencies; controlled release; possible to produce without using organic solvents and the production is easier to scale-up. Additionally, when bioactives are administered with digestible lipids their absorption in the GIT is facilitated, because the lipids increase the number and the solubility capacity of mixed micelles available to solubilize and transport hydrophobic compounds [71,74,77,78].

The bioavailability of astaxanthin and stability may increase in lipid-based nanocarriers, which include nanoemulsions, microemulsions, liposomes, micelles, solid lipid nanoparticles (SLN), and nanostructured lipid carriers (NLC) (Figure 1.3). In Table 1.1 it is presented a summary of different lipid-based formulation developed by other authors for the delivery of astaxanthin.

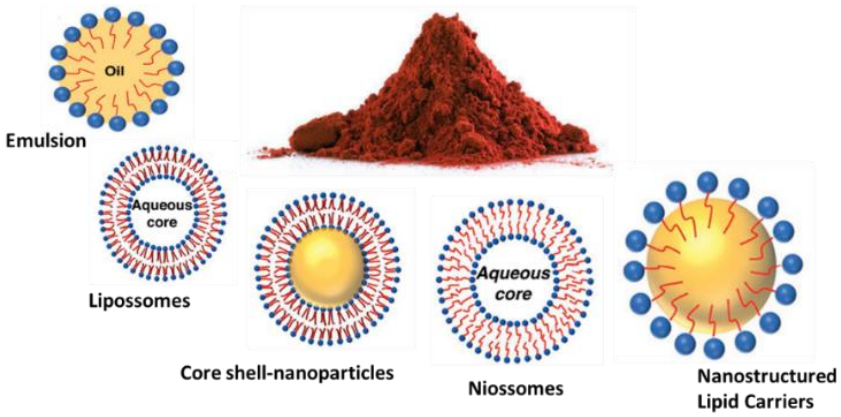

Figure 1.3- Different lipid-based delivery systems that could be used to encapsulate astaxanthin (Adapted from [195]).

Table 1.1- Summary of the different lipid-based formulation used as the delivery system of astaxanthin.

Lipid-based delivery system	Carriers	Research highlight	Ref.
O/W emulsion	Medium chain triacylglycerol	O/W emulsion droplets remained stable at 25 °C with encapsulation efficiency (EE(%)) of over 98% during 15 days of storage.	64
O/W Emulsion	Corn oil	No organic solvents were used. The chemical stability of astaxanthin in the emulsions was not affected by pH, ionic strength, and light exposure.	79
O/W nanoemulsions	Soybean oil	Bioacessibility of astaxanthin in nanoemulsions was higher using modified lecithin than using sodium caseinate.	80
O/W emulsion	Palm oil	Emulsifiers or their combinations influenced the cellular uptake by the colon carcinoma cells line HT-29 and Caco-2.	65
O/W nanoemulsion	Medium chain triaglycerides	The formulation was found to be non-toxic and with antimicrobial properties, ideal to treat and repair wounds.	81
O/W nanoemulsion	Medium chain triaglycerides	The formulation increased intracellular ROS production.	82
Liposomes	phosphatidylcholine (PC)	Astaxanthin-loaded liposomes containing 70% PC had higher EE(%) and higher cellular uptake than liposomes containing 23% PC.	66
Liposomes	SPC and cholesterol	Encapsulation increased water dispersibility and release rate of astaxanthin.	83
Liposomes	Cholesterol	Astaxanthin-liposomes activated antioxidant enzymes like superoxide dismutase, catalase and glutathione S-transferase more effectively than free- astaxanthin.	68
SLN	glycerol monostea-rate, glycerol distearates, stearic acid	SLNs provided a prolonged release of astaxanthin in simulated gastric and intestinal juices.	84
NLC	Compritol 888 ATO; oleic acid	EDTA and α-tocopherol increased the stability of astaxanthin-loaded NLCs without causing physical instability.	85
NLC	Compritol 888 ATO; oleic acid	Size of astaxanthin-loaded NLCs increased at low pH values and high NaCl concentrations.	86
NLC	Precirol ATO 5; SUPRAS	The encapsulation and stabilization of astaxanthin based on the combination of SUPRAS and NLCs was sucessful.	67

Despite the numerous postive results obtained with the lipid-based delivery systems, systems like micelles, liposomes and emulsions, have been reported to be susceptible to degradation during storage and exposure to acidic conditions, intestinal enzymes, bile salts in the GIT and, additionally, they lack controlled release [65,73,79,87]. On the other hand, SLNs and NLCs have attracted a lot of attention from food and pharmaceutical industries because of their numerous advantages.

1.7.1 Nanostructured Lipid Carriers (NLC)

Solid lipid nanoparticles (SLNs) were discovered in 1990 and are often used as drug delivery systems. These are composed of lipids that are solid at body temperature. Despite being

biocompatible and protecting drugs from degradation, they also possess disadvantages, such as poor bioactive loading capacity (due to the highly ordered matrix with little imperfections, that make it difficult for incorporation of bioactives), drug expulsion during storage (due to polymorphic transitions, less ordered α and β′ modifications are transformed into highly ordered β modification), slow release of the bioactive, possible gelation phenomenon, and particle aggregation [73,88].

Nano structured lipid carriers (NLCs) were first discovered in the early 2000s' and developed to overcome SLNs limitations, thus being introduced as their second generation. Like SLNs, NLCs are composed by biocompatible and biodegradable lipids, have low toxicity and slow release. Their solid matrix efficiently protects the loaded bioactive against chemical degradation, and their production does not require the use of organic solvents [88,89].

Bioactive expulsion, a disadvantage of SLNs, was one of the major encouragements for the development of NLCs. The expulsion happens during the process of full-crystallization or recrystallization of the solid lipid, which leads to the decrease of the solubility of the bioactive and, in turn, leads to the bioactive expulsion. This happens particularly when the drug concentration in the formulation is high [88–90].

The matrix of NLCs is composed by a mixture of solid lipids, lipids that are solid at room and body temperature, usually with high melting points, and by liquid lipids, lipids that are liquid at room temperature. Despite the presence of liquid lipids, the matrix of the NLCs is solid at room/body temperature [88–90]. This mixture of different types of lipids causes the partial crystallization of lipid droplets on the NLCS and formation of a less ordered crystalline structure (or amorphous solid structure), in other words, allows the formation of imperfections in the matrix. This less ordered crystalline structure provides more space for bioactive incorporation, and thus NLCs can accommodate a higher amount of bioactive [71,91,92]. Another advantage of incorporating liquid lipids in the formulation is the fact that the majority of bioactives have higher solubility in liquid lipids than in solid lipids. Additionally, this lipid combination has slower polymorphic transitions and low crystallinity index [74,92,93].

NLCs are spherical particles in which the liquid lipid and the bioactive are incorporated into the core of the solid lipid [74,92,93]. Furthermore, NLCs have a higher loading capacity and controlled drug release, as drugs are solubilized in the liquid lipid and simultaneously encapsulated and protected from degradation by the solid lipid [74,92,93].

All in all, NLCs possess the advantages of the SLNs, but have overcome their limitations. Other characteristic features of NLCs include: high encapsulation efficiency and drug loading; high stability; ease to produce and scale-up; and increased dispersibility in an aqueous medium. Therefore, using NLCs as a bioactive delivery system could, not only, improve the chemical stability and oral bioavailability, but also assure a high loaded amount and controlled release of bioactives [72,93].

There are three types of NLCs: Imperfect, Amorphous and Multiple. The Imperfect NLCs, contain imperfections in their matrix to accommodate the bioactive, which resulted from mixing spatially different lipids (solid and liquid lipids). By mixing different chain length fatty acid and mono-, di- and triacylglycerols, the matrix of NLC is not able to form a highly ordered structure, thus creating the imperfections. The Amorphous NLCs are produced by mixing solid lipids with special lipids (hydroxyl octacosanyl hydroxy stearate, isopropyl myristate, dibutyl adipate) that do not recrystallize after cooling, creating an amorphous state. Moreover, the lack of a crystalline structure prevents bioactive expulsion caused by the polymorphic transitions. The third type is the Multiple NLCs, this one takes into account that lipophilic compounds have higher solubility in liquid lipids than in solid lipids, thus this type contains a higher liquid lipid amount than the other types. This type enables controlled bioactive release and prevent bioactive expulsion [88,91,93] (Figure 1.4).

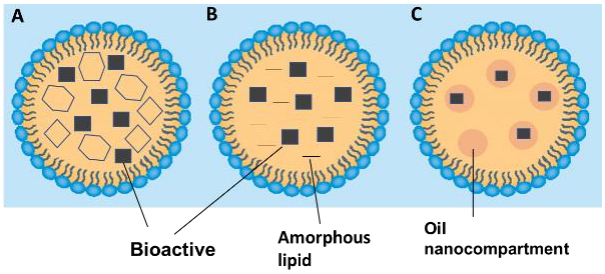

Figure 1.4- **The three different types of NLCs**: A- Imperfect type, B- Amorphous type; C- Multiple type.

Therefore, NLCs could be a promising drug delivery system to entrap astaxanthin, being able to overcome the stability and oral bioavailability issues of this molecule.

Many different methods can be used to prepare NLCs. These methods can be divided into two groups, high energy methods and low energy methods. The high energy methods use high energy machines and comprise of the following techniques: high-pressure homogenization (HHP); hot homogenization; cold homogenization; ultrasonication. The low energy methods include the following techniques: microemulsion; double emulsion; emulsification-solvent evaporation; emulsification solvent diffusion; melt-emulsification (melting dispersion), and others. The most commonly used technique is high-pressure homogenization, which utilizes both high temperature and high pressure [88,93].

In melt-emulsification technique, the bioactive, solid lipid, liquid lipid and organic solvent are melted (oil phase) and simultaneously the aqueous phase is heated until it reaches the temperature of the oil phase. Then, the oil phase is added to the aqueous phase and the mixture is homogenized/stirred at high speed until an emulsion is produced. Then, for particle reduction, the emulsion is further homogenized using a high-pressure homogenizer, or bath sonicator, or probe sonicator. Lastly, the emulsion is cooled down at room temperature or in ice, and left stirring so that the organic solvent evaporates, thus producing a dispersion of nanoparticles [93,86].

Nevertheless, there are some issues associated with the use of conventional methods for the production of particles. Generally, in conventional methods, it is used organic solvents, high temperatures and high shear forces.

Besides the techniques mentioned for the production of the particles, supercritical fluid (SCF) techniques, such as Supercritical Fluid Extraction of Emulsions (SFEE) and Particles from Gas Saturated Solution (PGSS®), can also be used to produce NLCs or micro versions of NLCs termed SLCs (structured lipid carriers). These techniques are based on the use of supercritical fluids such as supercritical CO_2, and they overcome some of the limitations associated with the conventional methods of encapsulation.

1.7.2 Supercritical Fluid (SCF) techniques

The Pharmaceutical industry is one of the industries that spends the highest volumes of organic solvents and is the least efficient of all chemical industries regarding waste produced per unit of product [88]. Nowadays, as society becomes more environmentally conscious, the demand for safer and more sustainable processes from pharmaceutical industries is increasing. Furthermore, regulamentary units urge pharmaceuticals to develop production processes that use the minimum volume of volatile solvents and produce finished products with reduced amount of organic solvent residues [94].

Supercritical fluids (SCF) technologies, characterized as “green”, sustainable, safe, and “environmentally-friendly” has attracted, in the recent years, the attention of pharmaceutical industries for the development of new and/or improved “greener” and “safer” processes and/or products, such as the production of micro- and nano- particles [95].

A supercritical fluid (SCF) is any substance that reaches the supercritical region when heated and pressurized above its critical temperature and pressure, that is, above its critical point (Figure 1.5). In the supercritical region the physico-chemical properties of SCFs are between those of liquids and gases. These fluids often have densities like liquids, thus exhibitt solvating characteristics that are similar to those of liquids, but simultaneously have gas-like mass transfer properties, with similar

viscosity and diffusivity values and an almost zero surface tension. Moreover, because of the high compressibility of SCF, particularly near the critical point, any alteration in the pressure or temperature results in density alterations and, consequently, in solvent power alteration [94,96–100].

The most common SCF used for bioactive/drug encapsulation is CO_2, which is odorless, colorless, nontoxic, highly pure, safe, cost effective, non- flammable and recyclable gas [101]. This fluid can reach the supercritical state at moderate pressures and temperatures (Tc = 304.1 K, Pc = 7.4 MPa) (Figure 1.5). As a result, it allows processes to operate at near- ambient temperatures and thus minimize the risk of thermal degradation of labile compounds [99].

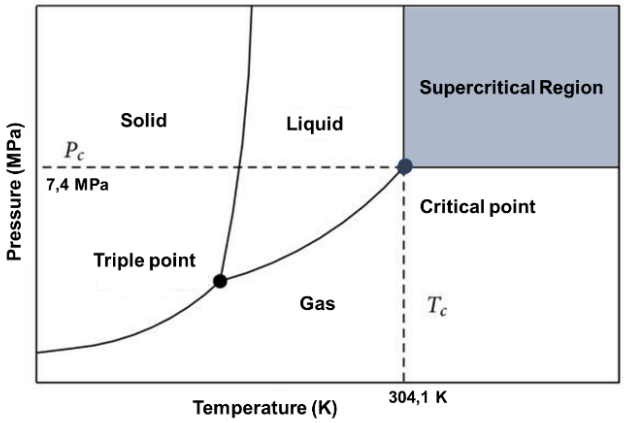

Figure 1.5- **Pressure versus temperature phase diagram of CO_2**: its critical point and the supercritical region (Adapted from [196]).

Additionally, $scCO_2$ also provides an inert medium, oxygen free and without the need to use high shear forces. These conditions benefit the processing of thermally and chemically labile materials, such as bioactives [95]. Also, by using $scCO_2$ the need to use toxic organic solvents in the process is reduced or eliminated, and due to the high solubility of organic solvents in $scCO_2$ these are easily removed. Moreover, at the end of the process the $scCO_2$ evaporates by depressurization, thus no CO_2 remains in the finished product [97]. Besides that, $scCO_2$ is an excellent solvent for nonpolar and slightly polar, low molecular weight compounds[99]. Another advantage of SCF techniques is the reduction in complexity of the process, with reduction of the number of steps [97].

Furthermore the use of SCF techniques overcomes some of the conventional methods limitations, such as thermal and chemical degradation of drugs/bioactives, the use of large amounts of organic solvents, broad particle distribution and solvent residue in the finished products. Hence their advantages justify the application of SCF techniques in pharmaceutical industries, namely for nano and micronization of drugs and bioactives.

The solvent properties of $scCO_2$, i.e. the solubility of polymers and lipids in $scCO_2$ and the solubility of CO_2 in the polymers and lipids, are two key fundamental subjects in this field. There are several processes based on supercritical fluids used for particle production. These processes can be classified according to the role of the SCF in the process, which can act as solvent, anti-solvent, co-solvent or solute, or even propellent gas. The techniques in which the SCF acts as a solvent include: Rapid Expansion of Supercritical Solution (RESS) and Rapid Expansion of Supercritical Solution into a Liquid Solvent (RESOLV). The techniques in which the SCF acts as an anti-solvent include: Gaseous Antisolvent (GAS), Supercritical Antisolvent (SAS), Supercritical Fluid Extraction of Emulsions (SFEE), Solution Enhanced Dispersion by Supercritical Fluids (SEDS). The techniques in which the SCF acts as a solute include: Particles from Gas Saturated Solutions (PGSS) [97,102].

One of the limitations of these SCF techniques is the fact that for most cases the particles obtained are in the micro range, although, nanoparticles can also be obtained using specific techniques, such as SFEE [95]. However, it is important to mention that micronization also improves oral bioavailability and stability of the bioactives, and microparticles also possess some advantages over nanoparticles.

1.7.2.1 Particles from Gas Saturated Solution (PGSS)

The PGSS® technique was patented by Weidner and co-workers and is considered one of the most promising $scCO_2$ based micronization processes, since it eliminates the need for organic solvents and because it does not rely on the solvent strength of CO_2, so it can operate at low pressures [99,103,104].

In comparison with other supercritical-based precipitation methods, the PGSS® process offers some advantages, such as low consumption of CO_2, suitability for micronization of thermo-labile compounds, since it operates under mild conditions, and the compound to be micronized does not need to be soluble in CO_2 [101,103,104]. Hence the PGSS® process is already used at large scale (Natex, Austria, Thar Technologies, USA, Uhde HPT).

The production of particles using PGSS® is based on the high solubility of $scCO_2$ in many substances, including oils and fats. In this process the $scCO_2$ acts as a solute, diffusing and dissolving into a solution, creating a gas-saturated solution [102]. It is noteworthy that as $scCO_2$ dissolves in the solution it reduces the glass transition (of amorphous and semi-crystalline compounds) and/or the melting point (of semi-crystalline substances), as well as the viscosity of the mixture [99,103]. This fact allows to operate at mild processing conditions, and thus reduce energy consumption [105].

The PGSS® process consists of dissolving $scCO_2$ in the mixture of lipids in a stirred high pressure reactor, until saturation is reached. Then the gas saturated solution, which can contain between 5-50 wt. % of the compressed gas, is expanded through a nozzle to ambient temperature, leading to the release of CO_2 with large cooling effect due to the energy consumption (Joule-Thompson effect). Fine particles are produced through atomization and precipitation after the rapid expansion, as a consequence of a drastic reduction in solubility of the CO_2 in the solution [99,102–106].

The morphology, size and apparent density of the produced particles may depend on several parameters, such as structure and viscosity of the compounds to be precipitated, the operating conditions, and the nozzle design of the PGSS® equipment [99]. Usually, the average particle size decreases when using higher pressures (higher carbon dioxide content in the solution) lower temperature values, and smaller nozzle diameters. On the contrary, with the increase of the temperature the particles produced are more spherical, since slower solidification of the droplets helps the diffusion of CO_2 out of the particles [99,105]. The PGSS® process, depending on the operating conditions and the nozzle design, also allows the production of particles with different morphologies, such as spherical and completely solid, distorted, agglomerated, spherical and hollow [107].

Furthermore, for the development of the experimental procedure it is important to have prior thermodynamic knowledge of the solubility of CO_2 in the lipid mixture and prior knowledge of the determination of the solid-liquid transition of a compound in the presence of carbon dioxide, to know the influence of the high pressure on the melting temperature of the lipids [103]. The depression on the melting point of each compound depends on the amount of CO_2 that solubilizes into the compound. The determination of the solid-liquid transitions in the pressurized systems is fundamental, since it provides information on the pressure needed to melt the mixture to be micronized [108].

The main limitations of PGSS® include the fact that the solute has to be melted, which can be an issue for thermo-labile compounds, the fact that the particles produced are in the micro range, and the production of nanoparticles is not possible. Of course the latter “limitation” may not be a limitation at all, it depends on the application of the finished products.

Nevertheless, the PGSS® process is a promising process that can present the pharmaceutical industry with several advantages, such as reduced energy consumption, since it operates under mild conditions; eliminates the need for organic solvents, ensuring that the finished product is solvent free; it can be applied to a wide range of substances; produces microparticles of homogenous and narrow size distribution and the final product is dry and so no need for further processing steps [96,99,107].

Haq *et al.* efficiently encapsulated omega-3 polyunsaturated fatty acids and astaxanthin- rich salmon oil in PEG-6000 polymer using PGSS® process. It was evaluated different process parameters such as temperature, pressure, oil and polymer ratio, and the nozzle diameter on the preparation of the microparticles. The particles obtained had a large range of sizes [107].

Finally, PGSS®, a green and sustainable process, can be used as an alternative less- complex method than the conventional methods to micronize astaxanthin, without risking its degradation and without the use of organic solvents, therefore, producing astaxanthin-loaded microparticles solvent-

free. To the best of the authors knowledge, PGSS process has not yet been used to produce lipid microparticles loaded with pure astaxanthin.

1.7.3 Structured Lipid Carriers (SLCs)

Like previously mentioned NLCs are a promising drug delivery system to improve the stability of astaxanthin and oral-bioavailability. However, using PGSS® the particles produce will not be in the nanorange, but instead in the microrange (1- 1000µm).

So when producing particles through PGSS® process using the same formulation composition used to produce NLCs (solid lipid, liquid lipid, but no organic solvent) the particles obtained will be termed Structure Lipid Carriers (SLCs) [105]. These are homologous to the NLCs, being the only difference the size [105]. Hence, SLCs posess some of the characteristics of NLCs, they are solid at room and body temperature, biocompatible, biodegradable, and because they are also composed by liquid lipids a less ordered crystalline structure (or amorphous solid structure) is formed. The fact that they have more imperfections in their structure leads to higher bioactive loading and minimize bioactive expulsion during storage. Besides, by incorporating liquid lipids it ensures a higher solubilization of lipophilic compounds such as astaxanthin [74,92,93,105]. Thus SLCs are a promising drug delivery system, produced using an alternative and sustainable process, PGSS®, to improve astaxanthin oral-bioavailability and stability, and that overcomes some limitations of the conventional methods used to prepare NLCs.

Particle size is one of the properties of particles that affects the oral bioavailability of any incorporated drugs/bioactives [109,110]. The particles size influences their capacity to cross barriers and to be taken up by cells, furthermore, it influences their loading efficiency, aggregation, dissolution rate and tissue retention [111]. Particles up to 10 µm in diameter can only be taken up through phagocytosis by phagocytes, and by M-cells in the GIT [61,65,112]. Still, microparticles not only have a higher loading capacity than nanoparticles, but similarly to nanoparticles they also protect the compounds from the environment and improve their oral-bioavailability, by being able to protect and deliver the bioactive to the GIT where it can be absorbed by intestinal cells [113,114,115]. Additionally, smaller particles tend to have a higher degradation rate than larger particles, because they have higher surface area and therefore an increased contact area with aqueous phase prooxidants [63].

To the best of the authors knowledge, PGSS® process has not yet been used to produce structured lipid carriers (SLC) loaded with pure astaxanthin.

1.8 Permeability studies of the bioactives

Oral administration is the preferred route for intake of drugs and formulated products, and therefore, their transport across the intestinal epithelium constitutes a major determining factor for *in vivo* bioavailability, which can be defined as the fraction of ingested component available at the site of action [116,117].

During the process of development and optimization of novel drugs and formulated products for oral administration, it is crucial to predict human intestinal absorption, bioavailability and cytotoxicity of a compound. Oral bioavailability is a highly desirable property of a drug candidate: poor permeability and/or absorption makes a molecule unsuitable for further development, but nowadays with the use of delivery systems this issue can be minimized. Meanwhile many formulations are being developed, their permeability across the intestinal barrier is a remaining key factor that needs to be considered in order to design, in a rational way, the delivery systems to improve the bioavailability of a compound. Hence the importance of having a physiological relevant *in vitro* cell model of the intestinal epithelium to assess the intestinal absorption of drug candidates and formulated products, in order to better predict the bioavailability of drugs and formulated products [116–118].

1.8.1 Intestinal composition and characteristics

The intestinal epithelium has two opposing features. Firstly, represents a physical barrier between the contents of the gut lumen and the rest of our body. Secondly, allows the efficient absorption of indispensable nutrients from the gut lumen, and produces mucus with protective properties, anti-microbial peptides and cytokines [61].

The small intestinal epithelium is organized into several units of crypts and villi. The villi project into the lumen to maximize nutrient absorption [61]. The intestinal epithelium is composed by five major cell types enterocytes, goblet cells, enteroendocrine cells, paneth cells and the rare M-cells (Figure 1.6). Goblet cells, the second most abundant cell type in the intestinal epithelium, secrete mucus to the intestinal lumen leading to the production of a mucus layer that surrounds and coats the intestinal villi, this layer protects the intestinal epithelium. Enteroendocrine cells are hormone secreting-cells. Paneth cells are responsible for secreting antimicrobial lysozymes. M-cells (microfold cells) are found in the epithelium overlaying the organized lymphoid tissue and Peyers patches, and are responsible for transporting antiges from the lumen to the lymphoid tissues. Finally, enterocytes, the most abundant cell type, possess tiny microvilli on their apical surface, and responsible for the production of digestive enzymes and for the nutrients absorption [61,119,120].

Enterocytes form a mechanical barrier by being tightly connected through adhesive complexes: the desmosomes, adherens junctions and tight junctions, thus preventing the entry of molecules into the circulation. But besides acting as a barrier, they also allow the absorption of nutrients and other molecules. The selective uptake and transport of molecules across the epithelial cell layer can be done through paracellular and transcellular transport, the latter being passive diffusion, vesicle-mediated transcytosis and carrier-mediated uptake [61,119,120].

Since the oral route is the preferred administration route used, the intestinal barrier has received particular attention. To be absorbed the molecules must diffuse across a series of separate barriers some of which include the mucosal side, the mucus gel layer, the intestinal epithelial cells, the lamina propria and the endothelium of the capillaries. However, the epithelial cells barrier is the major determinant for the absorption of a compound [121]. Several *in vitro* cell models with high-throughput capacity and that can provide an adequate prediction of the absorption in the human epithelial are now available to evaluate the intestinal permeability and transport [116,117,122]. A good cell model is one that best simulates the *in vivo* stettings, and the Caco-2 monolayer is one of the most widely accepted *in vitro* model to study the human oral drug absorption [123,124].

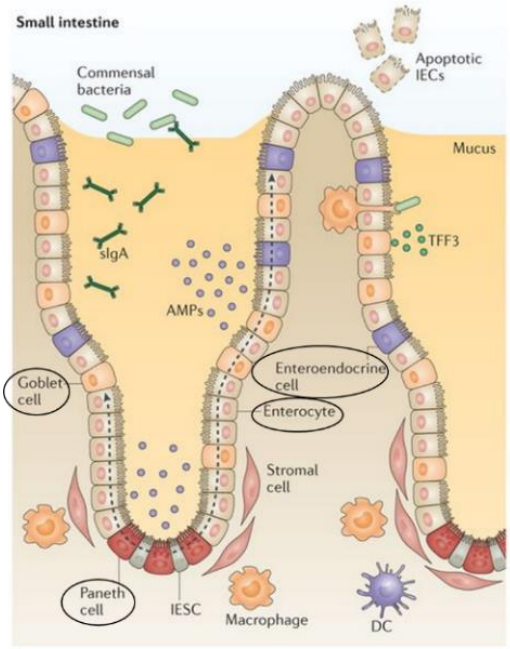

Figure 1.6- Representation of the organization of the small intestine epithelium (Taken from [197])

1.8.2 Caco-2

Caco-2 monolayers are the most accepted and widely used model for high throughput screening of the permeability of compounds and drug delivery systems. This model correlates well with *in vivo* absorption in humans, while considering all the physical, chemical and biological events during intestinal transportation [61,117,118,125].

Caco-2, originated from human colon adenocarcinoma, have the ability to differentiate into enterocyte-like cells, exhibiting functional and morphological elements as those of enterocytes. When cultured on semipermeable porous filter and after reaching confluence, the cells will spontaneously start to differentiate into a polarized cell layer with apical microvilli and intercellular tight junction

complexes [61,117,118,125]. Furthermore, Caco-2 express many of the hydrolytic enzymes and transport systems characteristics of enterocytes.

Still, when compared to the human intestinal epithelium this model presents some limitations, in particular, overexpression of p-glycoprotein, an efflux pump, also the tight junction are tighter than those of the small intestinal cells, and instead resemble those of colon cells. This tightness could decrease the paracellular permeability. Finally, this model only represents the absorptive cells, hence not mimicking completely the human epithelium, that is composed by a combination of different cell types: enterocytes, goblet cells, endocrine cells and M cells [61,116,117,122,125].

1.8.3 HT29- MTX

The mucus layer, a water-insoluble gel, covering the intestinal epithelium represents an important barrier acting as a physical and chemical defense against food particles, chemicals, enzymes and microbial products, additionally it constitutes a significant barrier to the absorption of particles. Mucus protects the underlying epithelium by both lubricating the surface, trapping and removing foreign-particulates. Additionally, mucus has demonstrated to be highly adhesive to pathogens and particulate systems [54].

As mentioned, the Caco-2 monolayer model is not able to translate the *in vivo* settings, and the lack of mucus secretion is one of its main flaws, since its presence influences significantly the absorption of molecules and immobilization of delivery systems. Moreover, goblet cells are the second most abundant cell type in the small intestine, so their representation in an *in vitro* model is important to better mimic the *in vivo* settings. Therefore, new models of Caco-2 and HT29-MTX cells, which represent goblet cells, co-cultures have been proposed [126].

HT29-MTX is a mucus secreting cell type and used as a model to study the mucus role in the absorption of compounds in the small intestine. These cells are derived from the human adenocarcinoma cell line HT29, which were treated with methotreaxate (MTX), allowing the isolation of a subpopulation of mature goblet cells, the HT29-MTX [127]. This cell line is characterized by having similar size and cellular complexity to Caco-2. They have identical morphology to mature goblet cells by having sparse and short microvilli, and at a late confluence they present a dense layer of mucus gel in the apical surface, but this mucus layer is labile and is removed by extensive and rough washings. Additionally, opposed to Caco-2, they do not express P-gp and express less tight junctions, characteristics which are found in mature goblet cells.The reduced number of tight junctions increase the paracellular transport pathway, thus increasing the permeability of hydrophilic compounds [126–128].

1.8.4 Caco-2:HT29- MTX co-culture

As previously mentioned, the Caco-2 monolayer model, despite being a widely accepted model for permeability studies, it is not the best representation of the human small intestine, since it only represents absorptive cells and the epithelium is composed by a variety of cells. Thus, this model does not provide adequate *in vivo* information of the intestinal absorption of a compound [126]. Furthermore, the intestinal epithelium is covered by a layer of mucus, produced by goblet cells, which has a significant influence on the absorption of compounds and mucoadhesion of delivery-systems.

To overcome the limitations of the Caco-2 monolayer model a new model was developed, the Caco-2:HT29-MTX co-culture. As mentioned Caco-2 and HT29-MTX exhibit morphological and functional characteristics of enterocytes and goblet cells, respectively. This model was first characterized by Wikman-Larhed and Artursson *et al.,* and is accepted as a better representation of the small intestine, since the most abundant cells present in the epithelium are both represented in this model, as well as the mucus layer [129].

Moreover, the presence of the mucin-secreting cells in co-cultures not only allow the production of the mucus layer, thus mimicking physiological conditions, but also mimic the tight junctional geometry and “tightness” of the epithelium, since HT29-MTX cells do not form tight junctions as tight as those formed by Caco-2 cells [61,122,126]. This modulation of the “tightness” of the epithelium was first verified by Walter *et al.*, the author verified that the TEER decreased in proportion to the increase of the amount of HT29-MTX [130]. Hence, to closely mimic the permeability features of the intestinal barrier, the ratio of Caco-2 and HT29-MTX has to be adjusted. In the intestinal tract 10% of the cell population constitute of goblet cells, moreover, different studies confirmed that the ratio 9:1 of Caco-

2:HT29-MTX, respectively, is the ratio that best represents the physiologic condition of the small intestine [125]. Several works demonstrated the validity of these co-cultures, and it was verified that the permeability of compounds with paracellular pathway and P-glycoprotein substrates increases [120,122,125,131].

Hilgendorf *et al.* evaluated the Caco-2:HT29-MTX co-culture for its use in screening for drug absorption and intestinal permeability, and compared the results with those obtained for the monocultures (Caco-2 and HT29-MTX). The authors verified that compounds that undergo passive absorption had higher permeabilities in the co-culture than in the Caco-2 monolayers. The compounds transported via paracellular pathway displayed noticeable differences in the permeability values in each model. In the HT29-MTX model the permeabilities were 30 times higher than in the Caco-2 monolayer, while for the lipophilic and highly permeable compounds the difference in permeability values was less noticeable. For compounds undergoing P-glycoprotein mediated secretion the permeability from apical to basolateral increased in the co-culture, but decreased in the opposite direction [125].

All in all, the Caco-2:HT29-MTX co-culture model is a better representation of the human intestinal epithelium, thus providing a better understanding of the human intestinal absorption of compounds. This has been confirmed in several reports where it is established a good correlation between this model and human *in vivo* studies [120,122,125,131].

1.8.5 M-cells

Besides enterocytes and goblet cells, intestinal epithelial Microfold (M) cells also have a significant role in the intestinal absorption. M-cells are part of the follicle-associated epithelium (FAE), an epithelium that covers the lymphoid follicles of gut-associated lymphoid tissues (GALT), such as Peyer's patches (PPs) and isolated lymphoid follicles (ILFs), which are the specialized antigen sampling sites of the intestine [132].

Despite being a minor population, M-cells are the main responsibles for antigen sampling, they bind, transport and deliver macromolecules and microorganisms to the lymphoid follicles. These cells transport the substances through fluid-phase or receptor-mediated endocytosis at the apical membrane, then the substances are transported in vesicles through the cytoplasm of the cells and released by exocytosis in the basolateral membrane [132–134].

Moreover, M-cells are characterized by having sparse and irregular microvilli in the apical membrane and a basolateral cytoplasmic invagination in which the lymphocytes and macrophages are located. Additionally, they are characterized by having lower enzymatic activity than Caco-2 monocultures [122].

The passage of antigens and microorganisms through M-cells is important for the development of mucosal immune responses and for the pathology of many infectious diseases. Particle delivery vehicles are largely prevented from passing between epithelial cells by tight junctions. However, since M-cells have a relative high transcytotic capacity, when compared to enterocytes, these can represent an efficient route for the transport of nutraceuticals carried by delivery systems through the intestinal epithelial barrier [122,134–136]. Furthermore, several reports suggest that nanoparticles and microparticles are capable of permeating the intestinal epithelium via M cells [132,137](Figure 1.7).

The origin of the M-cells still remains unclear and is a long-standing debate, some theories state that M-cells arise as an independent cell line and others that they originate from the differentiation of enterocytes under the influence of immune cells that exist in the dome epithelium [122,133] . This latter theory, suggests that the differentiation of enterocytes into M-cells is caused by soluble factors released by immune cells.

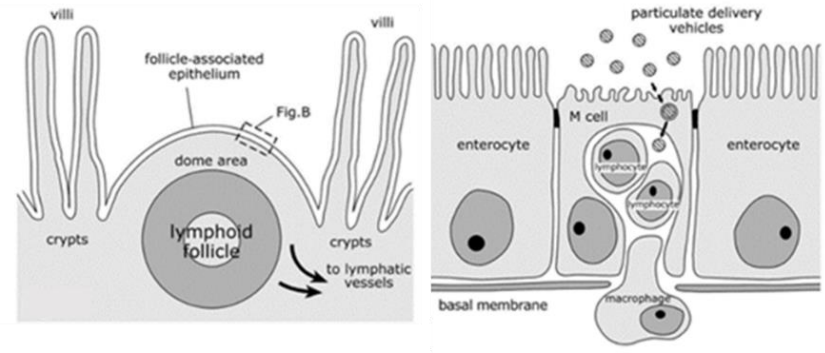

Figure 1.7- Schematic Sections of Peyer's lymphoid follicle and follicle-associated epithelium (FAE), showing the transport of particulate delivery vehicles by M cells. **(A)** The lymphoid follicle is located beneath a dome area which projects into the gut lumen between villi which is covered by the follicle-associated epithelium (FAE), this epithelium is where the M cells are located **(B)** (Taken from [130]).

Kernéis *et al.* constructed the first intestinal *in vitro* co-culture model based on Caco-2 cells and mouse Peyer's patch lymphocytes. The results suggested that the interaction of Caco-2 with lymphocytes triggered the creation of cells-like M-cells, that resemble the functions and morphology of intestinal M-cells [138]. Likewise, Gullberg *et al.* developed a similar model based on a co-culture of Caco-2 cells and human Raji B lymphocytes, a cell line that originates from human Burkitt's lymphoma [136]. Raji cells were used since they exhibit B cell markers, which are major inductive of M-cells phenotype [136]. Furthermore, Rieux *et al.* replicated the model developed by Gullberg *et al.,* and compared the permeability of nanoparticles in Caco-2 monolayers with the permeability in Caco-2: Raji-B co-culture. The findings revealed that the transport in the co-culture was 50-fold higher than in the Caco-2 monolayer [135,139].

1.8.6 Triple Co-culture- Caco-2:HT29-MTX:Raji-B

More recently, a new and improved *in vitro* model has been developed by Antunes *et al.,* to achieve a cell model that better resembles the human intestinal epithelium [116]. This model more closely mimics small intestine epithelium, since it comprises the three major cell types involved in the absorption: enterocytes (Caco-2), goblet-cells (HT29-MTX) and M-cells (differentiated Caco-2 in the presence of Raji-B cells). Moreover, this model, not only takes advantage of the characteristics of Caco-2:HT29-MTX co-culture, which maintain their intrinsic properties and primary functions (such as production of mucus), and the fact that this model is already accepted as a good representation of the small intestine, but also have improved it by introducing another cell type with great influence in the intestinal absorption [116,122,126,133]. This model was developed based on previous findings which report that Caco-2 when cultured with Raji B lymphocytes acquire M-cell phenotype [116,133].

As described by Antunes *et al.* to obtain the M-cell phenotype a common approach is to use a 21 days *in vitro* model, that consist in a co-culture with ratio 9:1 of Caco-2:HT29-MTX, respectively, seeded on Transwell® membranes inserts (normal oriented) and Raji B lymphocytes, which are added to the basolateral chamber of the insert after 14 days [116]. In this system it was possible to detect the development of cells with M-cell like morphology (Figure 1.8).

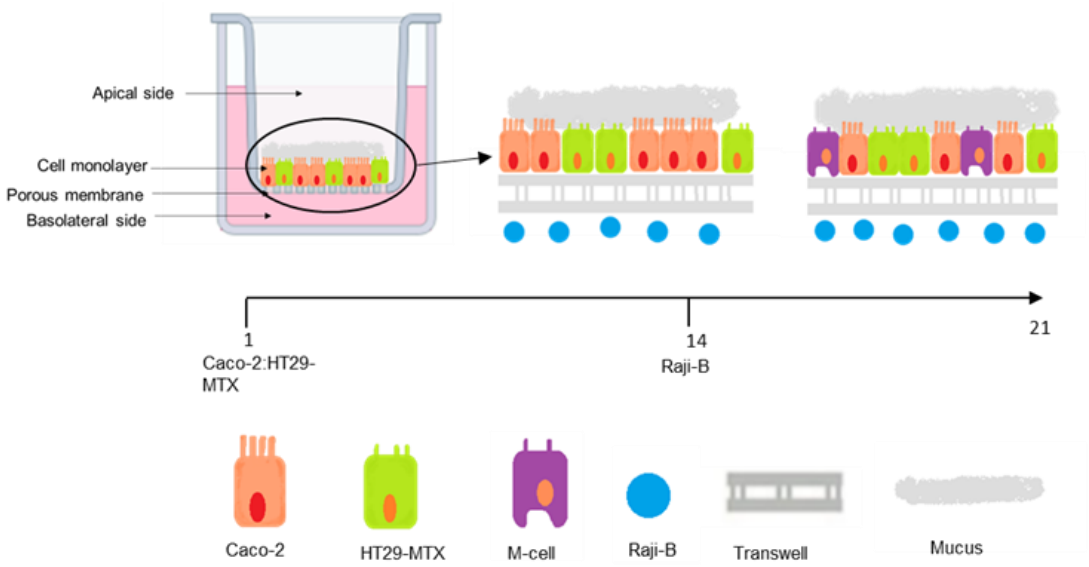

Figure 1.8- Illustration of the triple co-culture (Caco-2:HT29-MTX:Raji-B) set-up process. Initially only Caco-2 and HT29-MTX, with 9:1 ratio, were seeded, then at the 14th day Raji-B were added to induce the alteration of Caco-2 phenotype to M-cell phenotype.

Araújo *et al.*, stated that HT29-MTX maintained their intrinsic properties, producing mucus in the co-cultures with Caco-2 and Raji B cells, thus suggesting that the primary function of HT29-MTX is not influenced by the presence of the other cells. Additionally, Caco-2 successfully acquired the M-cells phenotype without being influenced by the presence of HT29-MTX, as demonstrated by the loss in apical brush border and microvilli, characteristic of M-cells. It was also stated that the change in phenotype only occurred in a few cells, and it was hypothesized that just a subpopulation of enterocytes is affected by the factors released by the lymphocytes. Another important trait of the model that enhances its resemblance with the human intestinal epithelium is the monolayer tightness, which is more identical to the physiological tissue, due to the different strength of the tight junctions formed by the three cell types. This tightness was assessed by measuring the TEER and the authors verified that the TEER was lower in the triple co-culture and highest in Caco-2 monolayer [122].

Schimpel *et al.* replicated the triple co-culture model described by Antunes *et al.*, tested the permeability of nanoparticles, and compared the results with those obtained for the Caco-2 monolayer model and Caco-2:HT29-MTX co-culture model [116,135]. It was verified that the uptake is greatly influenced by the mucus and that the uptake was higher in the triple co-culture than in the Caco-2:HT29-MTX co-culture, confirming what was expected, provided that M-cells are reported to have a high transcytosis activity [116,135].

Moreover, Antunes *et al.* used the triple co-culture to study the permeability of insulin, in solution and in mucoadhesive dextran/sulfate chitosan nanoparticles. The author verified that the P_{app} values for the permeability of insulin-loaded nanoparticles were comparable to the data collected from studies using an *ex vivo* rat ileum model [116].

All in all, taking in consideration all the advantages of the Caco-2:HT29-MTX co-culture and the importance that M-cells have in the intestinal absorption, as well as the reported data of other authors stating that the results obtained correlated well with *in vivo* studies. This model could provide a more complete and physiologically relevant system, capable of providing relevant information for the permeability of compounds, that correlates well with what is observed *in vivo*. Furthermore, this model is a useful tool to study the transcytosis of micro- and nanoparticles, providing information that could be useful for the rational design of delivery systems.

1.9 Aim and Structure of the Thesis

Despite the powerful antioxidant activity of astaxanthin and its promising use as co-ajuvant treatment for Inflammatory Bowel Diseases (IBD) its low oral bioavailability and extreme sensitivity limit its application and are strong justifications for its nano- and microencapsulation. Furthermore, adding the fact that astaxanthin has an increased absorption when co-administered with lipids, NLCs and SLCs could be potential delivery systems to improve the gastrointestinal tract delivery of astaxanthin.

The aim of this thesis was to entrap astaxanthin and shrimp shell extract, rich in astaxanthin, using conventional methods and $scCO_2$ based precipitation methods, in order to improve their stability and bioavailability. Additionally, it aimed to evaluate and compare the permeability and uptake of astaxanthin in the delivery systems in an *in vitro* cell co-culture model, that mimics the intestinal epithelium. Furthermore, it was tested the antioxidant activity of astaxanthin, extract and formulations using cell-based assays, to assess the possible application as co-adjuvant treatment for IBD.

To achieve this goal, the work was divided in four parts:

1. Extraction of astaxanthin from shrimp shells.
2. Development of different delivery systems to entrap astaxanthin and shrimp shell extract to maximize their stability and oral bioavailability.
3. Evaluate the permeability of the formulated astaxanthin using an *in vitro* model system that closely mimics the human intestinal epithelium monolayer.
4. Assess astaxanthin, shrimp shell extract and correspondent formulations for their antioxidant activity in Caco-2 monolayers.

In part 1: Extraction of astaxanthin from shrimp shell

The aim of this task was to extract astaxanthin from shrimp shells, to obtain an extract rich in astaxanthin that could be used in the optimization of the production of the particles. For this it was used a process already optimized, using chloroform.

In part 2: Astaxanthin and shrimp shell extract delivery systems

Taking in consideration that the target was the GIT, it was selected lipid-based formulations as the delivery system of astaxanthin, since this bioactive has an increased absorption when co-administered with lipids.

The aim of this task was to investigate the entrapment of astaxanthin and shrimp shell extract into nanostructures lipid carriers (NLC) using a conventional method, the melt-emulsification method, and into Structure lipid carriers (SLC) using a green precipitation technology, the PGSS® process.

Different techniques were applied to characterize the formulations in terms of morphology, size and thermal behaviour, along with the quantification of entraped astaxanthin.

In part 3: Permeability study in an *in vitro* co-culture model

Prior to the permeability studies, cell-based assays were performed in Caco-2 monolayers to evaluate the cytotoxicity of astaxanthin, shrimp shell extract and formulations. As well as to assess their influence in the mitochondrial integrity.

The permeability studies of pure astaxanthin, shrimp shells extract and respective formulations (NLCs and SLCs) were performed using a Caco-2 monoculture and a Caco-2:HT29-MTX:Raji-B triple co-culture. The integrity of the monolayer and the quality of tight junctions were assessed during the transport studies by monitoring transepithelial electrical resistance (TEER). The amount of permeated astaxanthin was quantified.

In part 4: Antioxidant activity of pure astaxanthin, shrimp shell extract and formulations

Through cell-based assays the antioxidant activity was evaluated by measuring the capacity of astaxanthin, shrimp shell extract and formulations to inhibit ROS production in Caco-2 cells.

2 Experimental Section

2.1 Materials

For the shrimp shells extraction section, shrimp shells were kindly provided by Tejo Ribeirinho Lda.

For the section of the formulation of the bioactive, astaxanthin (>97%), β-carotene (>93%), lecithin (L-α-Phosphatidylcholine, Type X-E, ≥ 40%) and chloroform were purchased from Sigma Aldrich (Portugal). Compritol 888 ato (Glyceryl dibehenate), peceol (Glyceryl monooleate) and precirol ato 5 (Glyceryl distearate) were kindly provided by Gatefossé (France). Olive oil (Azeite virgem extra Clássico- Gallo) obtained from local supermarket (Portugal). Dichloromethane was purchased from LaborSpirit Lda (Portugal). CO_2 (99.95 and 99.998 mol% purity) was delivered by Air Liquide (Portugal)

All cell culture media and supplements, namely FBS, DMEM, MEM NEAA, PS, trypsin/EDTA and HBSS were obtained from Invitrogen (Gibco, Invitrogen Corporation, Paisley, UK). Falcon™ 96-well microplate, tissue-culture treated was purchased from Enzifarma (Portugal).

To perform cells cytotoxicity assays, PrestoBlue purchased from Alfagene (Portugal) and MTS (G3582) from Promega.

To perform the mitochondrial integrity evaluation assay TMRE (Tetramethylrhodamine ethyl ester perchlorate, ≥ 90%) was purchased from Sigma Aldrich (Portugal).

For the Intracellular Reactive oxygen species determination 2′,7′-Dichlorofluorescin diacetate (DCFH-DA) and tert-Butyl hydroperoxide solution (TBHP) were purchased from Sigma Aldrich (Portugal).

For the permeability assays Corning® Transwell® polyester membrane cell culture inserts (12 mm with 3 µm pore polyester membrane insert and 1.12 cm2(CLS3462-48EA)) and Fluorescein sodium salt were purchased from Sigma-Aldrich (Portugal).

Whenever it was necessary to perform sterility tests were performed using tryptone soy broth (TSB, Scharlau, Spain).

2.2 Procedure

2.2.1 Extraction of astaxanthin from shrimp shells

The extraction of astaxanthin was performed, with some modifications, according to the method reported by Hooshmand *et al.* [18]. First, 10 mL of chloroform were mixed with 1 g of grinded lyophilized shrimp shells in a beaker covered by aluminum foil, to protect it from the light. The mixture was stirred for 5 minutes, at room temperature, using a magnetic stirrer. The extract was filtered through vacuum filtration (Vacuum Pump V-700, Buchi, Switzerland). The remaining residues were repeatedly extracted using fresh chloroform, and the filtrates were continuously collected, this procedure was repeated until the filtrate became colorless. Then the extracts were mixed and filtered through a syringe filter (0,22 µm). After that, a known volume of extract was used to measure the absorbance at 488 nm by spectrophotometer (model EPOCH, 219 Bio-Tek, USA). It is worth mentioning that the yield of the carotenoids was calculated as the amount of astaxanthin. The amount of astaxanthin present in the extract was determined using a calibration curve. The calibration curve was obtained by preparing standard samples of astaxanthin in chloroform, in concentrations between 0,5 and 4 µg/mL (R^2=0.99). At last, the organic solvent was evaporated using a Rotary evaporator (Rotavapor R210, Buchi, Switzerland), the final dried extract was collected and weighted.

The yield of the extraction process was determined using the following equation:

$$\textbf{(Eq.1)} \quad \text{Extraction yield (\%)} = \frac{\text{mass of extract}}{\text{mass of residue used}} \times 100$$

The global yield of the carotenoids was determined using the following equation:

(Eq.2) $$\text{Global yield of carotenoids} = \frac{\text{mass of carotenoids in the extract}}{\text{mass of residue used}}$$

Content of carotenoids in the extract was determined using the following equation:

(Eq.3) $$\text{Content of carotenoids in the extract} = \frac{\text{mass of carotenoids in the extract}}{\text{mass of extract}}$$

2.2.2 Extract analysis by High Performance Liquid Chromatography (HPLC)

To determine the amount of astaxanthin present in the extract, HPLC analysis was performed. An Alliance e2695 HPLC model (Waters, Massachusetts, USA), equipped with degasser, autosampler and a PDA detector were used for the analysis of astaxanthin. Chromatographic separation was carried out with a YMC 30 Carotenoid Column (Classical Analytical HPLC Column S-5µm, 250 x 4.6 mm, YMC) coupled with a Guard Cartridges YMC C30 pre-column (5µm, 10x4.0mm, YMC) with mobile phase of Methanol:MTBE (80:20) at 25 °C. The detection wavelength was set at 450 nm and the flow rate was 1 mL/min. A known amount of extract was dissolved in MTBE and filtered through a 0.2 µm filter. The run time for the assay was 45 min and the retention time for astaxanthin was 6.5 min. (Appendix 1 - Figure 6.1)

The amount of astaxanthin present in the extract was determined using a calibration curve. The calibration curve for astaxanthin in MTBE was linear within the range of 1.9 and 15 µg/mL (R^2= 0.99).

The global yield of astaxanthin was determined using the following equation:

(Eq.4) $$\text{Global yield of astaxanthin} = \frac{\text{mass of astaxanthin in the extract}}{\text{mass of residue used}}$$

The content of astaxanthin in the extract was determined using the following equation:

(Eq.5) $$\text{Content of astaxanthin in the extract} = \frac{\text{mass of astaxanthin in the extract}}{\text{mass of extract}}$$

2.2.3 Astaxanthin encapsulation

2.2.3.1 Nanostructured Lipid Carriers (NLC) preparation

NLCs were prepared according to the procedure reported by Tamjidi *et al.* with some modifications [63].

The formulations consisted of 5 wt.% lipid-phase (757 mg of compritol 888 ato or precirol 5 ato, 5 mg of lecithin, 218 mg of olive oil or peceol, 20 mg the bioactive), 2 mL of dichloromethane and 95 wt.% aqueous phase (H_2O) were prepared by melt-emulsification technique. Moreover, the bioactive constitutes 2% of the lipid phase.

The lipid phase was melted in a heating bath at 50 ± 1ºC in a capped flask covered with aluminum foil, to protect it from the light. Simultaneously, the aqueous phase was heated to 75 ± 1ºC. After the lipid phase melted, providing a clear homogeneous phase, it was placed for a few minutes in the same heating bath as the aqueous phase, until it reached 75 ± 1ºC. Afterwards the lipid phase was added to the aqueous phase, and the mixture was homogenized using Ultraturrax (Ultra- Turrax T25 Basic, Ika Werke, Germany) at a certain speed (rpm) for a specified amount of time (see Section 2.2.3.2, Table 2.1 and 2.2). After the O/W emulsion was produced it was immediately place in ice.

2.2.3.2 Optimization of Nanostructured Lipid Carriers (NLC) preparation

Because astaxanthin is very costly (50 mg costs 99.60 EUR from Sigma Aldrich (Portugal)) the optimizations were performed using a model compound, β-Carotene.

For the optimization of the particle size and encapsulation efficiency different conditions (homogenization time) were tested and alterations on the initial formulation were performed.

2.2.3.2.1 Optimization of the formulation composition variables

a) Type of lipid

Two different solid lipids, compritol 888 ato and precirol ato 5, two different liquid lipids, olive oil and peceol, were tested as lipid matrix. The solid lipid and the liquid lipid to be selected for the production of astaxanthin-loaded NLCs are the ones that allow the stability of the dispersion for a longer period.

b) Volume of organic phase

The organic solvent, dichloromethane, was used to solubilize the lipids. It was studied the effect of using or not using organic solvent on the particle size and encapsulation efficiency.

c) Quantity of the bioactive

On the formulation that did not contain organic solvent it was tested different amount of β-carotene in order to improve the process efficacy and encapsulation efficiency.

Table 2.1 summarizes the different formulations tested for the optimization of NLCs.

Table 2.1- Optimization of various formulation parameters for the preparation of nanostructured lipid carriers. The quantity of each component of the formulation is the same as what is reported by Tamjidi *et al* (757 mg of compritol 888 ato or precirol 5 ato, 5 mg of lecithin, 218 mg of olive oil or peceol, 20 mg the bioactive). unless mentioned different. "---" indicates no alterations were performed in comparison to what is reported by Tamjidi *et al.* [63]. All these experiments were performed using the same homogenization time (7 minutes) and speed (21500rpm).

Lipid matrix	Organic Solvent	Quantity of Bioactive
Type of lipid:		
Compritol 888 ato: Olive oil	Dichloromethane	**---**
Precirol ato 5: Olive oil	Dichloromethane	**---**
Compritol 888 ato: Peceol	Dichloromethane	**---**
Volume of Organic Solvent:		
Compritol 888 ato: Olive oil	No organic solvent	**---**
Quantity of Bioactive:		
Compritol 888 ato: Olive oil	No organic solvent	Half of the amount

2.2.3.2.2 Optimization of process variables

a) Homogenization time

For the homogenization it was used Ultraturrax at 21500 rpm (Ultra- Turrax T25 basic, Ika Werke, Germany) and different homogenization times were tested. Table 2.2 summarizes the different experimental conditions tested.

Table 2.2- Optimization of various process parameters for the preparation of nanostructured lipid carriers. The quantity of each component of the formulation is the same as the one reported by Tamjidi *et al.*[63] unless mentioned different.

Lipid matrix	Organic Solvent / Amount of Bioactive	Homogenization time (min)
Compritol 888 ato: Olive oil	Dichloromethane / initial amount of Bioactive	7
Compritol 888 ato: Olive oil	No organic solvent / half the amount of Bioactive	7
Compritol 888 ato: Olive oil	No organic solvent / half the amount of Bioactive	20

2.2.3.3 Encapsulation Efficiency - UV-Vis spectrophotometer

The procedure was performed according to the procedure reported by Tamjidi *et al.*, with some modifications [63]. To determine the total amount of astaxanthin present in the dispersion (M_D), 0.5mL of bioactive-loaded NLCs was mixed with 1 mL of methanol and 2mL of chloroform (for the astaxanthin-loaded and extract-loaded NLCs) or n-hexane (for the β-carotene-loaded NLCs), the mixture was vortexed for 1 minute. Then, the mixture was centrifuged at 6000 g for 5 minutes and two distinct phases were formed. The colored organic phase was collected and diluted with the corresponded organic solvent. To determine the amount of bioactive that was not entrapped (M_{free}), 0.5 mL of bioactive-loaded NLCs dispersion was centrifuged at 10000 g for 15 min and the supernatant was collected. Following this, the same extraction procedure used to determine the total amount of astaxanthin/β-carotene was used to extract the astaxanthin/β-carotene present in the supernatant. Finally, the absorbance of samples was measured by UV-visible spectrometer (model EPOCH, 219 Bio-Tek, USA) at 488 nm for astaxanthin and 450 nm for β-carotene, and the concentration of the bioactive was determined using a calibration curve. The calibration curve was obtained by preparing standard samples of astaxanthin in chloroform, and β-carotene in n-hexane in concentrations between 0.5- 4 μg/mL (R^2=0.99) and 3.4-0.21 μmg/mL (R^2=0.99), respectively.

The encapsulation efficiency was determined according to the respective equation:

(Eq.6) $$\mathrm{EE}(\%) = \frac{\mathrm{M_P}}{\mathrm{M_T}} \times 100\%$$

Where M_T is the total mass of bioactive added (astaxanthin, extract or β-carotene) for the particle production and M_P is the mass of bioactive incorporated in the particles. Furthermore, M_P=M_D-M_{free}, where M_D is the total mass of bioactive in the particle dispersion and M_{free} is the mass of bioactive not entrapped.

2.2.3.4 Dynamic Light Scattering (DLS)

Particle size and polydispersity index (PDI) of the NLCs were measured by dynamic light scattering (DLS) using Zetasizer Nano ZS at 25ºC (Malvern Instruments Ltd., UK).

2.2.3.5 Thermal behavior- Differential Scanning Calorimetry (DSC)

Before SEM and DSC analysis, NLCs formulation was frozen for 24h at -4ºC, then lyophilized (Scanvac CoolSafe, Labogene) and a dry powder was obtained.

Differential Scanning Calorimetry (DSC) was performed in order to study the thermal behavior of the particles, the measurements were carried out on TA instruments Q200 (module MDSC). The particles were weighted (2-5 mg) in an aluminum pan which then was sealed. The probes were heated from -20ºC to 220 at a rate of 10 K/min under nitrogen atmosphere. The results were obtained in terms of heat flow (Joule) vs. temperature (ºC).

2.2.3.6 Particles from Gas Saturated Solutions (PGSS®)

The formulation used was the same as the one used to produce the NLCs (Section 2.2.3.1) with the exception that it was not used H_2O or organic solvent. The formulation consisted in compritol 888 ato, lecithin, olive oil or peceol and the bioactive, the ratio of each component was the same as the ratio used in the formulations of NLCs. The ratio between solid and liquid lipid was 7:2. It is important to mentioned that in all experiments of PGSS® it was used half the initial amount of bioactive (bioactive constitutes of 1% of the lipid phase) relative to what it is reported by Tamjidi *et al.*, the rest of the components of the formulation were in the same quantities as what it is reported [63]. For the particle production optimization, it was used β-carotene.

Structured lipid carriers unloaded and loaded with β-carotene, astaxanthin and shrimp shells extract were produced through PGSS® process in batch mode. The schematic representation of the equipment (FAME UNIT, Separex, France) used to produce the particles is shown in Figure 2.1 and was previously described in the work of V.S.S Gonçalves *et al.* with some modifications [105].

In brief, carbon dioxide was fed by a pneumatic pump (29723-71, Haskel International Inc., CA, USA) to a 50 cm^3 high pressure stirred vessel, electrically thermostated, containing the lipidic mixture to be processed, until the desired working pressure was reached. The mixture and the supercritical CO_2 were kept in contact for 15 min or 30 min, under stirring (150 rpm). After this period, the mixture was depressurized by an automated depressurization valve and atomized through a two-fluid nozzle (d=250 µm) to a cyclone, where it was externally mixed with compressed air (7 Bar). The particles were finally recovered into a collector vessel of 18 L at atmospheric pressure.

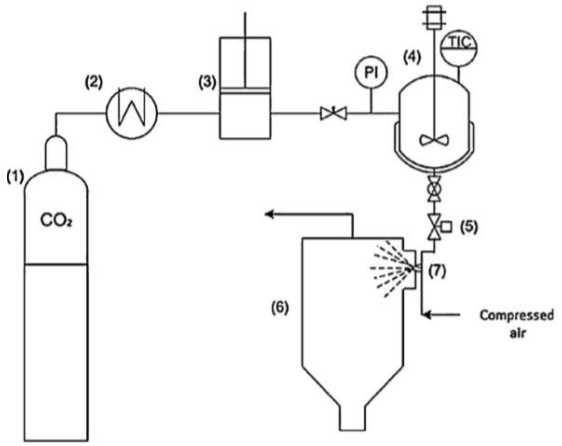

Figure 2.1- Experimental Setup - (**1**) CO_2 cylinder (**2**) cryostat (**3**) pneumatic piston pump (**4**) stirred vessel (electrically thermostated (**5**) automated depressurization valve (**6**) recovery vessel (**7**) nozzle. Adapted from V.S.S. Gonçalves *et al.* [101]

The operating conditions (Temperature and Pressure) were selected according to melting point values of the lipids in the presence of CO_2, previously determined [108].

2.2.3.7 Particle production optimization

Different lipid matrices, and operating conditions such as temperature (T), pressure(P) and contact time with supercritical CO_2 were tested to optimize the particle size, morphology and encapsulation efficiency. The lipid matrix contact time with supercritical CO_2, temperature and pressure values that led to smaller particles with higher encapsulation efficiency were selected. The PGSS® experiments are summarized in Table 2.3.

Regarding the optimization, each experiment was performed in duplicate to evaluate the reproducibility of the process. Because at the time there were not any particles size information the reproducibility was evaluated comparing the experimental load of each experiment in the duplicates, the standard deviation and error were calculated, and statistical analysis were performed.

Table 2.3- Summary of PGSS® precipitation experiments performed testing different lipid matrices (peceol or olive oil) and operating conditions (pressure and contact time with $scCO_2$). The mass ratios between solid and liquid lipid was 7:2.

System	Pressure (bar)	Temperature (ºC)	Contact time
Compritol 888 ato: No liquid lipid	100	70	15
Compritol 888 ato: Peceol	100	70	15
Compritol 888 ato: Peceol	100	70	30
Compritol 888 ato: Peceol	150	70	30
Compritol 888 ato: Peceol	200	70	30
Compritol 888 ato: Peceol	250	70	30
Compritol 888 ato: Peceol	250	70	15
Compritol 888 ato: Olive oil	100	70	15
Compritol 888 ato: Olive oil	250	70	15

2.2.3.8 Encapsulation efficiency - UV-Vis spectrophotometer

The amount of bioactive (β-carotene or astaxanthin) loaded in the microparticles of PGSS® was determined by UV-Vis Spectrophotometer, and for some samples by HPLC analysis. The bioactive was extracted from 3 mg of microparticles using 10 mL of n-hexane (for β-carotene) or 10 mL of acetone (for astaxanthin) in an ultrasound bath for 30 minutes. The suspension was then filtered through a 0.2 µm filter, and the resulting solution was analyzed by UV/Vis spectrophotometer (model EPOCH, 219 Bio-Tek, USA) at 450 nm for β-Carotene and 488 nm for astaxanthin. This analysis was performed under sink conditions and in triplicate.

The amount of bioactive was determined using a calibration curve. The calibration curve was obtained by preparing standard samples of β-carotene in n-hexane and astaxanthin in acetone, in concentrations between 2.7- 13 µg/mL (R^2= 0.99) and 3.4-0,21 µg/mL (R^2=0.99), respectively.

The theoretical load of the bioactive was determined using the following equation:

(Eq.7) $$\text{Theoretical load} = \frac{\text{mass of bioactive initially added}}{\text{total mass (mass of carriers plus bioactive) initially added}}$$

The experimental load of the bioactive was determined using the following equation:

(Eq.8) $$\text{Experimental load} = \frac{\text{mass of bioactive quantified in the particles}}{\text{particles mass}}$$

The encapsulation efficiency was determined using the following equation:

(Eq.9) $$\text{EE}\ (\%) = \frac{\text{experimental bioactive load}}{\text{theoretical bioactive load}} \times 100$$

2.2.3.9 Encapsulation efficiency- HPLC

To further confirm the results obtained for the encapsulation efficiency determined using UV-Vis Spectrophotometer, some samples of β-carotene-loaded particles were analyzed by HPLC analysis. An Alliance e2695 HPLC model (Waters, Massachusetts, USA), equipped with degasser, autosampler and a PDA detector were used for the analysis of astaxanthin. Chromatographic separation was carried out with a YMC 30 Carotenoid Column (Classical Analytical HPLC Column S-5µm, 250 x 4.6 mm, YMC) coupled with a Guard Cartridges YMC C30 pre-column (5µm, 10x4.0mm, YMC) with mobile phase of Methanol:MTBE (80:20) at 25 °C. The detection wavelength was set at 450 nm and the flow rate was 1 mL/min. The calibration curve for β-carotene in MTBE was linear within the range of 9 and 50 µg/mL (R^2= 0.99). The bioactive was extracted from the particles using the same procedure mentioned in Section 2.2.3.8, but once the sample of the disruption of the particles was obtained it was filtered through a 0.2 µm filter and the organic solvent was evaporated in a Rotary Evaporator. The resulting precipitate was resuspended in MTBE. The run time for the assay was 45 min and the retention time for β-carotene was 27,2 min.

The theoretical and experimental load and encapsulation efficiency were determined using the Equations 7 to 9 presented in Section 2.2.3.8.

2.2.3.10 Thermal behavior- Differential Scanning Calorimetry (DSC)

Differential Scanning Calorimetry were performed in order to study the thermal behavior of the microparticles, the measurements were carried out on TA instruments Q200 (module MDSC). The particles of PGSS were weighted (2-5mg) in an aluminum pan which then was sealed. The probes were heated from -20ºC to 230 at a rate of 10K/min under nitrogen atmosphere. The results were obtained in terms of heat flow (Joule) vs. temperature (ºC).

2.2.3.11 Scanning Electron Microscopy (SEM)

Morphology was analyzed by Scanning Electron Microscopy, SEM, (Hitachi S-2400). Before analysis, particles were covered with a gold-platinum film.

2.2.4 *In vitro* cell-based assays

2.2.4.1 Sterilization of the formulations of astaxanthin and shrimp shell extract

Formulations were sterilized using a protocol already described by other authors with some modifications [140]. In short, the microparticles of PGSS® or a certain volume of astaxanthin-loaded and extract-loaded NLCs were placed in direct contact with UV irradiation for 30 min at room temperature in laminar flux chamber. To confirm sterility of the microparticles and NLCs, these were incubated in tryptone soya broth at 37 °C in a humidified atmosphere of 5 % CO_2 to ensure the absence of bacterial contamination (data not shown).

To confirm that the sterilization did not degraded the astaxanthin loaded in the particles the amount of astaxanthin was determined on sterilized and non-sterilized particles.

2.2.4.2 Sample preparation

In the cell-based assays different samples were tested namely, standard astaxanthin, the shrimp shells extract, astaxanthin-loaded and extract-loaded SLCs and astaxanthin-loaded and extract-loaded NLCs.

As for the standard astaxanthin stock solution, astaxanthin (>97%, Sigma Aldrich) was dissolved in DMSO, and depending on the assay it was diluted in culture medium (supplemented with 0.5 % V/V FBS and no antibiotic), PBS or HBSS. The maximum concentration of DMSO to be tested on the cells was 1%. DMSO concentrated solutions of the extracts were not filtered, as DMSO inhibits microorganism growth even when used in small percentages [141].

As for the shrimp shells extract, the extract was dissolved in ethanol, and depending on the assay it was diluted in culture medium (supplemented with 0.5 % V/V FBS and no antibiotic), PBS or HBSS, being 5% the maximum concentration of ethanol to be tested on the cells.

Regarding the microparticles of PGSS® after sterilized, depending on the assay, culture medium (supplemented with 0.5 % V/V FBS and no antibiotic), PBS or HBSS were added and the solution was stirrer in a magnetic stirrer.

Regarding the NLCs samples, these were dispersions of particles in H_2O. Depending on the assay the NLCs sample was diluted in culture medium, PBS or HBSS, being 50% the maximum concentration of H_2O to be tested on the cells.

2.2.4.3 Adherent cells

The human colon adenocarcinoma, Caco-2 cells purchased from Deutsche SammLung von Microorganismen und Zellkulturen (Braunschweig, Germany) and HT29-MTX-E12 (12040401) from European Collection of Authenticated Cell Cultures, were cultured in a standard medium Dulbecco's DMEM supplemented with 10 % (V/V) heat-inactivated FBS, 1 % MEM NEAA and 100 units/mL penicillin and 100 µg/mL streptomycin (1% P-S V/V) and maintained at 37 °C in a humidified atmosphere of 5 % CO_2.

The stock cells were maintained as monolayers in 75 cm^2 cell culture flasks regularly subcultured following trypsinization (0.25 % (w/v) Trypsin-EDTA) when approximately 80-90% confluence was reached.

Cells were maintained in their respective culture medium, but all experiments were performed in culture medium supplemented only with 0,5% FBS and no antibiotic. For every assay, cells were seeded in 96-well TC (tissue culture)-treated microplates at a density of 2 x 10^4 cells/well (Caco-2) and allowed to reach confluence (5-7 days for Caco-2).

2.2.4.4 Non- adherent cells culture

Human Burkitt's lymphoma Raji B (85011429) from European Collection of Authenticated Cell Cultures were grown in a standard DMEM medium supplemented with 10 % heat-inactivated FBS, 1 % MEM NEAA and 1 % PS and maintained at 37 °C in a humidified atmosphere of 5 % CO2. The stocks cells were maintained in suspension in 75cm^2 non-treated cell culture flasks with medium change every three days.

2.2.4.5 Cytotoxicity assay- PrestoBlue®

The cytotoxicity assays were performed on confluent Caco-2 monolayers. After confluence was reached, growth medium was removed, and cells were exposed to several concentrations of samples (100 µL) dissolved in culture medium (supplemented with 0.5 % V/V FBS and no antibiotic) and incubated at 37 °C and 5% CO_2 for 24h (for the pure astaxanthin and shrimp shell extract) or 4h (for PGSS microparticles and NLCs). After these incubation periods, the well content was removed, and cells were washed twice with PBS. Then, 100 µL of PrestoBlue® solution (diluted 1:20 in medium supplemented with 0.5% FBS) was added to each well, and the plate was incubated at 37 °C and 5% CO_2 for 2 hours. After this, the well content was transferred to a black microplate and the fluorescence was measured at 590 nm (with excitation at 560 nm) in FL800 microplate fluorescence reader (Bio-Tek Instruments, Winooski, VT, USA), and cell viability was determined as a percentage of control, after blank subtraction. The PrestoBlue® assay is based on the reduction by viable cells of resazurin to resorufin, a compound that emits fluorescence which can be measured at 590 nm. The amount of resorufin produced is directly proportional to the number of viable cells [142].

Concentrated stock solution of astaxanthin and shrimp shells extract were prepared in DMSO and ethanol, respectively. Regarding the NLCs samples, the stock solution was in H_2O. The concentrations of solvent used in the tested concentration range of the samples did not affect cell viability.

The experiments were performed in at least triplicate with cells between passages 22-46. The experiments were performed in at least duplicate. The results are expressed as % of cell viability obtained for each sample (mol of astaxanthin/mL).

2.2.4.6 Mitochondrial integrity evaluation assay

Mitochondrial integrity evaluation assay was performed by measuring the inclusion of tetramethylrhodamine ethyl ester perchlorate (TMRE), a cell permeable fluorescent dye that specifically stains live mitochondria and accumulates in proportion to mitochondrial membrane potential (MMP). Reduction of the inclusion of TMRE may indicate that there is damage on the mitochondrial membrane potential [54,143].

After confluence was reached, growth medium was removed and cells were exposed to several concentrations of samples (100 µL) dissolved in culture medium (supplemented with 0.5 % V/V FBS and no antibiotic) and incubated at 37 °C and 5% CO_2 for 4h (astaxanthin in DMSO, extract, astaxanthin-loaded and extract-loaded SLCs, astaxanthin-loaded and extract-loaded NLCs). After this period, the well content was removed, and cells were washed twice with HBSS. Subsequently, 100 µL of 2µM TMRE solution (diluted in culture medium, supplemented with 0.5 % V/V FBS and no antibiotic) was added to each well, and the plate was incubated at 37 °C and 5% CO_2 for 30 minutes. Then, the well content was removed, and the plate was washed with HBSS. Fresh HBSS was added once again and the fluorescence was measured at 590nm (with excitation at 560nm) in a FL800 microplate fluorescence reader (Bio-Tek Instruments, Winooski, VT, USA).

The experiments were performed in at least duplicate. The results obtained for each sample (mols of astaxanthin/mL) were expressed in terms of fluorescence emitted in proportion to TMRE inclusion in the mitochondria.

2.2.4.7 Intracellular Reactive Oxygen Species detection

It was evaluated the capacity of astaxanthin, the extract, and the formulated astaxanthin and extract in inhibiting the production of ROS in cells through two different approaches: pre-incubation and co-incubation. In both approaches, 2',7'-dichlorofluorescin diacetate (DCFH-DA) was used as a fluorescent probe. DCFH-DA, a non-fluorescent compound, easily diffuses through the cell membrane and once inside the diacetate moiety is cleaved by cellular esterases producing a more polar and cell membrane-impermeable product, 2',7'-dichlorodidhydrofluorescein ($DCFH_2$). ROS from intrinsic oxidative stress or generated by an oxidative stress inducer diffuse into the cell, where they oxidize $DCFH_2$ to its fluorescent form, DCF. Accumulation of DCF in cells may be measured by an increase in fluorescence at 538 nm (with excitation at 485 nm), which is assumed to be proportional to the amount of ROS. [144]

In the pre-incubation approach, cells were incubated with selected non-toxic concentrations of the samples diluted in culture medium (0.5% FBS) for 4 hours, washed twice with PBS, and then incubated with 25 µM DCFH-DA in PBS for 1 hour. Afterwards the fluorescence was measured in order to evaluate the antioxidant effect of the samples towards intrinsic ROS. DCFH-DA was then removed and sample of TBHP in PBS with concentration insufficient to be considered cytotoxic (4,1mM for Caco-2) was added to the cells. After 1 hour, fluorescence was measured. In the co-incubation approach, cells were first washed twice with PBS and incubated with 25 µM DCFH-DA in PBS for 1 hour. Afterwards, the samples in PBS were added to the plate and the fluorescence was immediately measured in order to have a blank for the samples which color interfere with the fluorescence. Right after the selected concentrations of stress inducer, in PBS, was added and the plate incubated for 1h. After the incubation the fluorescence was again measured. All results were presented as a fluorescence percentage relative to the untreated control, where the same amount stress was induced.

Fluorescence measurements were performed in a FL800 microplate fluorescence reader (Bio-Tek Instruments, Winooski, VT, USA), and fluorescence filters for an excitation wavelength of 485±20 nm and an emission wavelength of 528±20 nm were used.

The samples tested were: astaxanthin in DMSO, the shrimp shell extract, the microparticles of PGSS® and the structured lipid carriers.

The experiments were performed in at least duplicate. The results obtained for each sample (mols of astaxanthin/mL) were expressed in terms of fluorescence emitted in proportion to DCF produced (i.e. in proportion to the ROS produced).

2.2.4.8 Permeability assays: Caco-2 monolayer and Caco-2:HT29-MTX co-culture

2.2.4.8.1 *In vitro* cell models

To obtain the cell models used for the *in vitro* experiments it was used the procedure described by Araújo *et al.* [116] . Monocultures of Caco-2 and a triple co-culture Caco-2:HT29-MTXE12: Raji B with a proportion of 9:1 between Caco-2 and HT29-MTX cells, respectively, were cultured in the apical compartment of a Transwell® inserts with $1x10^5$ cells/cm^2 as the inoculum and maintained for 21 days under a 5 % CO_2 humidified atmosphere at 37 °C.

Caco-2 monolayer and a co-culture of Caco-2:HT29-MTX were maintained under standard incubation conditions for 14 days, with medium change on both, apical (0.5 mL) and basolateral sides (1.5 mL) every two days. Regarding the triple culture model after 14 days it was added Raji-B with 60 000 cell/cm^2 as the inoculum to the basolateral compartment, and these were removed after 4 days [133]. The cell model was maintained the remaining days until the day of the assay in standard incubation conditions.

2.2.4.8.2 Cell monolayer integrity

In order to monitor the formation and integrity of Caco-2 and co-culture monolayers during the 21 days prior to the permeability assay, TEER was measured with EVOM epithelial voltohmmeter equipped with chopstick electrodes (World Precision Instruments, Sarasota, FL, USA). TEER was also measured during the permeability assay to monitor the monolayer integrity. Only monolayers with TEER value higher than 500 Ω cm^2 were used in the permeability assays [116,122].

2.2.4.8.3 Permeability assay

The permeability assays were performed on Caco-2 cell-culture and co-culture of Caco-2:HT29-MTX-E12 after 21 days of culture.

After 21 days of culture, cell medium was removed from apical and basal compartments and both compartments were washed twice with HBSS (pH 7.4), pre-warmed to 37 °C, and the plate was incubated for 1h at 37 °C and 5% CO_2. Then, the HBSS on the apical compartment was replaced by 500 µL of the test samples appropriately diluted in HBSS. The plate was incubated at 37 °C under a 5 % CO_2 humidified atmosphere for 4 hours. At 15, 60, 120, 180, 240 minutes, after the test samples were added, 200 µL from basolateral compartment were collected for chromatographic analyses of astaxanthin and the same volume of HBSS was added to the basolateral compartment. TEER was measured to monitor cells monolayers integrity after samples collection.

After the 4h of incubation, the samples that were on the apical side were collected and stored, to determine the content in astaxanthin, and the HBSS was removed and the plate was washed twice with warm HBSS. For the Caco-2 culture after being washed, culture medium (DMEM, 10% FBS, 1% PS and 1% MEM NEAA) was added to both compartments and the plate incubated, after 24h since the samples were added to the apical side, the TEER was again measured to monitor the monolayer integrity.

For the co-culture after being washed, new HBSS was added to both compartments and the plate was incubated, after 24h since the samples were added to the apical side, 200 µL from basolateral compartment were collected and the TEER was measured. Then, the plate was washed once with culture medium (DMEM, 10% FBS, 1% PS and 1% MEM NEAA), and new culture medium was added, and the plate was again incubated. After 48h since the samples were added, the TEER was measured to monitor the monolayer integrity.

In both cell-models (Caco-2 and co-culture) after being incubated with the culture medium, the medium was removed and the membranes were washed twice with 0.01 M PBS (Sigma-Aldrich, USA). Afterwards, cells were lysed by the addition of 1 % inhibitor of Proteases cocktail for 200 µL of

Cell Lytic. The plate was stirred for 15 minutes at 500 rpm and the lysate centrifuged for 15 minutes at 20 000 xg. The supernatant was stored and analyzed by chromatography to determine the amount of astaxanthin in cell fraction.

The experiments were performed in duplicate. The results obtained for each sample (mols of astaxanthin/mL) were expressed in terms TEER values (Ωcm^2) measured throughout the permeability assay and expressed as astaxanthin cellular uptake (%) and transepithelial transport (%).

2.2.4.8.4 Astaxanthin quantification- HPLC

To quantify the amount of astaxanthin absorbed by the cells the samples that were collected throughout the permeability assay were analyzed by HPLC. Before being analyzed the water from the HBSS buffer was removed by speedvac, and the precipitate was resuspended in dichloromethane. Before being injected in the HPLC they were filtered using a syringe filter (0.2µM).

A Dionex Ultimate 3000 model (Thermo, USA), equipped with degasser, autosampler and a UV-Vis detector were used for the analysis of astaxanthin. Chromatographic separation was performed on reversed-phase column (LiCrospher ® 100 RP-18, 250x4 mm; 5µm; Merck®) with and isocratic mobile phase of Methanol: H_2O (97:3) at 35ºC with injection volume of 20µl. The detection wavelength was set at 474 nm and the flow rate was 1 mL/min. The calibration curve for astaxanthin in dichloromethane was linear within the range 1.95 and 25 µg/mL (R^2= 0,99). The run time for the assay was 20 min and the retention time for astaxanthin was 7 min.

2.2.4.8.5 Statistical analysis

All results are expressed as mean ± standard deviation (SD). Statistical analysis of the results was performed using GraphPad Prism 6 software (GrapghPad Software, Inc., La Jolla, CA). When homogeneous variance was confirmed, results were analysed by one-way analysis of variance (ANOVA), followed by the Tukey test for multiple comparisons. In the case of heterogeneous variances, an appropriate student t-test was performed in order to determine whether means were significantly different. A p-value<0.05 was accepted as statistically significant in all cases.

3 Results and Discussion

3.1 Extraction of carotenoids from shrimp shells using organic solvents

Astaxanthin is known for its high antioxidant and anti-inflammatory activity and is one of the main carotenoids present in crustaceans. Moreover, the processing of crustaceans, such as shrimps, produces large amounts of waste, which still contain valuable components, such as carotenoids. Thus, shrimp waste represents a cheap raw material that could be used to extract carotenoids, particularly, astaxanthin.

Therefore, with the aim of obtaining an extract of astaxanthin, that could be used in the process of optimization of the production of particles and with potential antioxidant activity, extractions of this carotenoid from shrimp shells were performed using chloroform (solid-liquid extraction method).

The extraction process used was based on the method established by Hooshmand *et al.* and optimized in previous works led at the host group [18]. This extraction process is a relatively easy and quick method to obtain an extract with astaxanthin.

Chloroform was selected as the organic solvent to be used, since astaxanthin has a high solubility in this solvent and because it was used in the extraction process optimized in previous works led at the host group. Moreover, polar solvents, such as chloroform, are generally a good extraction media for xanthophylls. Although chloroform is a good solvent to solubilize astaxanthin (its solubility in chloroform is 5 mg/mL, according to Sigma Aldrich for astaxanthin with 97% purity), it will also extract other lipophilic compounds, such as lipids, other carotenoids, and proteins. Thus, the extract obtained besides astaxanthin will also contain other molecules.

Prior to the extractions, the fresh shrimp shells were lyophilized and stored at ambient temperature, protected from the light. At the end of each extraction process, a known volume of extract was used to measure the absorbance at 488 nm, and using a calibration curve the content in carotenoids was determined. Furthermore, the amount of astaxanthin in the extract was determined through HPLC analysis. Also, to determine the extraction yield, the dried extract was weighted after the solvent was evaporated. The extraction yield was calculated using Equation 1, the global yield of carotenoids was calculated using Equation 2, the content of carotenoids in the extract was calculated using Equation 3 the global yield of astaxanthin was calculated using Equation 4, and astaxanthin content in the extract was calculated using Equation 5, presented in in Section 2.2.1.

When using the UV-Vis spectrophotometer to determine the amount of astaxanthin in the extract, it should be noted that the extract is composed by molecules other than astaxanthin, such as other carotenoids and lipids that may also absorb at the wavelength used for the analysis (that was previously established as the maximum absorption wavelength of astaxanthin). Therefore, the UV-Vis spectrophotometer analysis provides information of the content of total carotenoids (and not just astaxanthin) and possibly other molecules present in the extract. Meanwhile, HPLC analysis provides information of the actual content of astaxanthin in the extract. In Table 3.1 it is presented the results obtained for the extraction yield, global yield of the carotenoids, content of carotenoids in the extract, the global yield of astaxanthin and the content of astaxanthin in the extract.

Table 3.1- Shrimp shells extraction: extraction yield, global yield of the carotenoids and content of carotenoids in the extract (results obtained through UV-Vis analysis), the global yield of astaxanthin and content of astaxanthin in the extract (results obtained through HPLC analysis) determined for extractions from shrimp shells using chloroform.

	Extraction yield[a] (% g/g)	Carotenoids global yield[b] (µg/g)	ASX global yield[b] (µg/g)	Carotenoids content in the extract[c] (mg/g)	ASX content in the extract[c] (mg/g)
Shrimp shell extract	4.90	21.66	14.17	0.54	0.36

[a-] In terms of dry weight (%, g/g)
[b-] Total content in the raw material (expressed as µg of ASX or carotenoids/ g of shrimp shell waste)
[c-] Total content in the extract (expressed as mg of ASX or carotenoids/ g of extract)

From the results, the extraction yield was 4.9%, which is very low, but expected considering what was obtained in previous works led at the host group.

It is possible to verify that the results of the global yield of the carotenoids and of the astaxanthin determined through UV-Vis spectrophotometer and HPLC, 21.66 µg/g and 14.17 µg/g respectively, were considerably different. This difference was expected and explained by the fact that the extract, like mentioned, contains carotenoids other than astaxanthin and possibly other molecules that absorb at the wavelength used for the analysis. On the contrary, HPLC is a highly selective and sensitive technique that provided the actual amount of astaxanthin extracted. The results obtained for the global yield of astaxanthin was 14.17 µg/g and the result obtained for the content of astaxanthin in the extract was 0.36 mg/g. As can be verified, the value of the global yield of astaxanthin corresponds to more than half of the value of carotenoids global yield, which indicates that astaxanthin was the major carotenoid extracted.

The extraction of carotenoids from shrimp shells was also reported in several other works. While in this work the global yield of carotenoids was 21.66 µg/g, Dalei *et al.*, who also extracted carotenoids from shrimp shells using chloroform, reported a the yield of 2.14 µg/g [145]. The yield reported by Dalei *et al.* is considerably lower than the yield reported in this work. This difference may be related to the extraction process used by Dalei *et al*, since in that process the raw material was left stirring with the organic solvent for 1 hour, and the process was repeated until the extract became colorless. Since astaxanthin and other carotenoids are very sensitive, in this 1 hour period some might have degraded. Furthermore, the species of shrimps used in both works are different, and possibly the species used in this work might have, naturally, a higher content of carotenoids than the one used by Dalei *et al.* [145]. On the other hand, the same author, also extracted astaxanthin from shrimp shells using other organic solvents, such as acetone, hexane and methanol, and the highest carotenoid yield, 48.64 µg/g, was obtained using acetone [145]. The findings reported by Dalei *et al.* reveal that acetone might be a better solvent to extract carotenoids from shrimp shells than chloroform.

Other authors also reported acetone as the solvent that provided the highest yield of carotenoids. Hooshmand *et al.* obtained the highest carotenoid yield, 61.21 µg/g, using acetone, and the lowest yield, 17.04 µg/g, using n-hexane, from extractions performed on shrimp shells [18]. Similarly, Sindhu *et al.* that used an analogous extraction procedure to the one used in this work, but instead using different organic solvents, obtained the highest the yield of carotenoids, 87.14 µg/g, also using acetone [146].

The extraction of carotenoids using chloroform has not been vastly reported, and the majority of the authors report extraction processes where other organic solvents are used. Studies on the extraction of carotenoids using organic solvents show that acetone is one of the most promising organic solvents used, because it allows the extraction of higher amounts of carotenoids. As a matter of fact, the results reported in the literature for the yield of carotenoids obtained in extractions using acetone are higher than the yield obtained in this work, using chloroform [18,145–147]. Moreover, as already mentioned, the results obtained by Dalei *et al.* can confirm that acetone is a better solvent to extract carotenoids than chloroform. Further studies should be performed to confirm if acetone is, indeed, a better solvent than chloroform to extract carotenoids.

Nonetheless, besides the organic solvent used other factors may also contribute for the low yield of carotenoids obtained, such as (1) the raw material, the shrimp shells used may have had low content in carotenoids or originated from a species of shrimps, which naturally possess low content in these substances; (2) degradation of the carotenoids might have occurred, since the raw material was in storage for some time at ambient temperature instead of being in the freezer.

In this work the content of astaxanthin in the extract was 0.36 mg/g. Meanwhile, other authors stated to have obtained a higher content of this xanthophyll in the extract. Sangsuriyawong *et al.* extracted astaxanthin from shrimp shells using ethanol, and the content of astaxanthin in the extract obtained was 9.00 mg/g [66]. Also, Taksima *et al.* reported a content of astaxanthin in the extract of 1.70 mg/g, using the same extraction method as Sangsuriyawong *et al.* [148]. The low yield of astaxanthin obtained in this work may be related to several factors, such as (1) raw material, perhaps the species of shrimps used may, naturally, contain lower amounts of astaxanthin than other species; (2) degradation of the bioactive, the raw material was lyophilized and stored at ambient temperature for months before being used, and because astaxanthin is very sensitive it may have degraded (which was possible to verify by the color of the shrimp shells, that where displayed a light orange color); (3)

the method of extraction may not be the most efficient, other methods such as supercritical fluids based methods, extractions using vegetable oils, and others, may have allowed a higher yield of astaxanthin; and (4) the solvent used may not be the most suitable to extract astaxanthin.

All in all, a shrimp shell extract containing astaxanthin was obtained, and due to time limitations, no further optimizations on the extraction process were performed. The initial aim for the extraction was to obtain an extract rich in astaxanthin to be used for the optimization of the production of particles. But because the extract obtained had low content in astaxanthin, was hard to work with, since it had a wax-like texture, and because it was not a good representation of the sample intended to be entrapped, since standard astaxanthin was a powder, it was not used for the optimizations of the production of particles. Nevertheless, after the optimizations were concluded the extract was formulated, and, subsequently, the extract and its formulations were tested to assess their antioxidant activity in cell-based assays.

3.2 Astaxanthin Formulation

One of the aims of this dissertations was to formulate astaxanthin, in order to improve its stability and absorption. Since the target was the gastrointestinal tract (GIT), and because the absorption of astaxanthin increases when co-administered with lipids, lipid-based formulations, more specifically NLCs and SLCs, were selected to formulate astaxanthin. For the optimization of the formulation composition and of the process parameters, β-carotene was used as a model compound, since pure astaxanthin is a very expensive compound to acquire commercially. β-carotene was selected since it is relatively similar to astaxanthin, highly hydrophobic and also less expensive.

3.2.1 β-Carotene-loaded NLCs: formulation composition optimization

When developing a delivery system one of the most crucial steps is the optimization of the formulation composition. Generally, a formulation used to produce NLCs is composed by an oil phase and an aqueous phase, being the oil phase composed by a solid lipid, a liquid lipid, a bioactive, an emulsifier and organic solvent, while the aqueous phase may be composed by water, buffers, and may contain surfactants. When developing a formulation it should be noted that the formulation composition is crucial for the efficient production of particles. The lipid phase has an important effect on the properties of NLCs and SLCs, influencing their loading capacity, physical stability, release rate, and ultimately their delivery ability [63]. Moreover, other factors such as size and polydispersity index (PDI) are also influenced by the formulation composition.

Therefore, the aim of this task was to test the initial formulation composition, selected from the literature, and optimized it, in order to optimize the production of NLCs. In the process of optimization, different parameters were tested to assess their influence on the encapsulation efficiency. These included the solid lipid, amount of bioactive and the presence of organic solvent.

Due to time constraints a completely new formulation composition to entrap astaxanthin was not developed, instead it was used a similar formulation composition to the one already established to encapsulate this bioactive, developed by Tamjidi *et al.* [63]. The author performed a lipid screening to determine which liquid lipid solubilized the highest amount of astaxanthin and then tested different solid lipids to evaluate which lipid, when mixed with the liquid lipid, allowed the production of particles with highest physical stability. Compritol 888 ato and oleic acid were the lipids selected [63].

The formulation composition used in this work, as already mentioned, was identical to the one reported by Tamjidi *et al.*, but with some modifications [63]. Nonetheless, the ratio of lipid phase to aqueous phase was unaltered (with 5% of lipid phase). These modifications included the liquid lipid used, in this work it was used olive oil instead of oleic acid, and the aqueous phase, which in this work consisted of distilled water. Generally, olive oil is composed by oleic acid (the major constituent), linoleic acid, palmitic acid, fatty acids and traces of phenolics, such as α-tocopherol, which possess antioxidant activity and may help preserve the antioxidant activity of astaxanthin [145]. Furthermore, Tamjidi *et al.* stated that the use of α-tocopherol in the NLCs formulation improved the chemical stability of the astaxanthin-loaded NLCs [85,149].

During optimizations, alterations on the initial formulation composition (Compritol 888 ato, olive oil, DCM) were performed. It was tested: two different solid lipid, compritol 888 ato and precirol ato 5; the amount of bioactive used, initial amount and half the initial amount and presence of organic

solvent. It should be mentioned that the lipids used, compritol 888 ato, precirol ato 5, olive oil and the emulsifier, lecithin, are generally recognized as safe (GRAS) by FDA.

For the different formulations the particles were produced through melt-emulsification using the same homogenization time (7 minutes) and speed (21500 rpm).

To assure the reproducibility of the production process, statistical analysis was performed for the particle size and encapsulation efficiency, and in all cases the results were found to be not significantly different (p-value>0.05) between the experiments.

The different formulations produced were evaluated in terms of the encapsulation efficiency, particle size and polydispersity index (PDI). In Table 3.2, it is presented the different formulations composition tested as well as the encapsulation efficiency, particle size and PDI of the formulations produced.

Table 3.2- Optimization of the formulation composition for the production of NLCs: Different formulations composition tested for the production of the NLCs. Particle size, PDI and encapsulation efficiency (EE(%)) of β-carotene-loaded NLCs produced.

Formulation	Formulation composition	Particle size (nm)	PDI	EE (%)
F1	Compritol 888 ato; Olive oil; w/ DCM	397.74 ± 2.38	0.43 ± 0.01	20.40 ± 3.85
F2	Precirol ato 5; Olive oil; w/ DCM	a)*	a)*	a)*
F3	Compritol 888 ato; Olive oil; no DCM	408.67 ± 3.36	0.45 ± 0.03	9.38 ± 2.74
F4	Compritol 888 ato; Olive oil; no DCM; and half of the amount of bioactive	407.60 ± 4.67	0.40 ± 0.052	15.43 ± 2.22

N.B: The quantity of each component of the formulation is the same as the one reported by Tamjidi et al. (with 5% of lipid phase), unless mentioned different [63]. Furthermore, the mass ratio between solid and liquid lipid was the same in all cases and was 7:2. All these experiments were performed using the same homogenization time (7 minutes) and speed (21500 rpm). The EE(%) for the β-carotene-loaded NLCs was determined through UV-Vis spectrophotometer analysis. Values are mean ± standard deviation from, at least, two independent experiments performed in triplicate. One- way ANOVA and Tukey's multiple comparisons test was performed using the results obtained for the encapsulation efficiency, particle size and PDI ,of each experiment.
a)* the emulsion produced was not stable and phase separation occurred.

Precirol 5 ato was tested has a solid lipid for the production of NLCs, since it has a lower melting point (50-60ºC) than compritol 888 ato (65-77ºC). Thus, by using precirol ato 5 the risk of degradation of the bioactive, caused by the high temperature used during the production of the particles, would be reduced. However, the emulsion produced was unstable and coalescence occurred. Soon after being prepared, visible aggregates that were more deeply-colored (orange-red) were observed close to the top of the emulsion. So, the particle size and PDI were not determined, and neither was the encapsulation efficiency (EE(%)).

Polydispersity index (PDI), is a measure of the particle size distribution, and ranges from 0 to 1. The PDI should be the lowest possible for the long- term stability of the dispersion. Values between 0.1- 0.25 for PDI indicate a narrow size distribution, while PDI values above 0.5 indicate a very broad distribution [63].

The results presented in Table 3.2 for the formulations F1, F3 and F4 indicate that the bioactive was incorporated into the particles, as can be demonstrated by the EE(%) and orange color of the emulsion (F1) and dispersions (F3 and F4) produced (Appendix 2 - Figure 6.2). Also, particles were produced, as can be verified by the average particle size, which ranged between 397.74 and 408.67 nm, and, additionally, by their PDI which was below 0.5, indicating that there was not a broad size distribution. Moreover, the particles produced in F1, F3, and F4 had very close particle sizes (p-value>0.05) and PDIs values (p-value>0.05), being the EE(%) the main difference. These results indicate that the alterations on the formulation composition did not influence the particle size and PDI.

The initial formulation, F1, was the formulation with highest EE(%), 20.40 ± 3.85%. This can be attributed to the presence of the organic solvent, since β-carotene has a high solubility in dichloromethane (DCM). Thus the presence of the solvent might have improved the solubility of the bioactive in the formulation. Furthermore, the particles produced had a particle size of 397.74 ± 2.38 nm, and a PDI of 0.43 ± 0.01, thus revealing that the size distribution was not broad.

In F3 it was tested the possibility of producing NLCs without using organic solvent. The results confirm that NLCs can be produced without using organic solvent, and the average particle size and PDI of the resulting particles were 408.67 ± 3.36 nm and 0.45 ± 0.03, respectively (Table 3.2). Nonetheless, because no organic solvent was used the oil phase was more viscous, additionally since compritol 888 ato has a high melting point, a small variation in the temperature resulted in the solidification of the lipid phase. In addition, because ultraturrax was used for the homogenization, the lipid phase had to be added to the aqueous phase and the reverse was not possible, since the dispersing element of the equipment has to be completely submerged. Thus, in the step of adding the lipid phase (where the bioactive is present) to the aqueous phase, solidification of the lipid phase occurred, and thus a portion of it was lost. This could be an explanation for the low EE(%), of 9.38 ± 2.74%.

In F1 and F3, during the homogenization, precipitation of the bioactive occurred. This could have happened due to saturation of the bioactive in the carriers (solid and liquid lipids), that is, the capacity of the carriers to solubilize the bioactive was exceed and the lipids were not able to solubilize all the molecules of β-carotene present. Hence, precipitation occurred, since β-carotene is not soluble in the aqueous phase. This precipitation might have occurred, since the formulation established by Tamjidi *et al.* was optimized using an extract where 40% consisted of astaxanthin, while in this work it was used a sample where 93% consisted of β-carotene. Thus, the amount of carriers (solid and liquid lipids) described in the formulation composition established by Tamjidi *et al.* (Section 2.2.3.1), and that was able to solubilize the 40% of astaxanthin present in a specific amount of extract (20 mg), may not be adequate to solubilize 93% of bioactive present in the 20 mg of the study sample added [63].

To overcome the precipitation of the bioactive during the homogenization step, the production of NLCs using half of the initial amount of bioactive was tested in F4. It should be noted that this formulation did not contain organic solvent. With this alteration, the EE(%) increase to 15.40 ± 2.22%, whilst before (F3), with the initial amount of bioactive, it was 9.38 ± 2.74%. (this increase was significant, p-value<0.01). Additionally, no noticeable precipitation was observed during homogenization, and the amount of bioactive, present in the dispersion, that was not incorporated into the particles was very low, thus indicating that the amount of β-carotene added was not in saturation. However, lipid phase loss still occurred, when adding this phase to the aqueous phase, this could explain the low encapsulation efficiency.

When comparing F1, where dichloromethane was used, with F4, where no dichloromethane was used, plus it was used half the initial amount of bioactive, it is possible to verify that F1 still had higher EE(%) than F4 (p-value<0.05). This might be explained by the fact that β-carotene has a high solubility in dichloromethane. Thus the presence of the solvent might have improved the solubility of the bioactive in the formulation. But, most importantly, even if oil phase solidification occurred in F1 it was not as severe as in the experiments where no organic solvent was used, hence in F4 a bigger portion of lipid phase was lost, thus resulting in a lower EE(%) in F4.

The EE(%) reported by Tamjidi *et al.* was 72%, whereas in this work the highest EE(%) obtained was 20.40 ± 3.85% (F1) [63]. This difference may be explained by several factors, one of which, and probably the major contributor for the low EE(%), is the fact that a portion of the lipid phase was lost when the oil phase was added to the aqueous phase. Also, it is logical to suspect that since β-carotene was used for the optimizations, while the formulation was developed to encapsulate astaxanthin, that perhaps this low EE(%) was caused by the potential low solubility of β-carotene in the lipid phase. But since the molecules are similar, both carotenoids, both hydrophobic and soluble in lipids, their solubility in the lipid phase should not be too different or at least not different enough to explain such a drastic decrease in the EE(%). On the other hand, Tamjidi *et al.* used oleic acid as the liquid lipid, since it solubilized the highest amount of astaxanthin, but in this work it was used olive oil instead. Tamjidi *et al.* tested the solubility of astaxanthin in different liquid lipids, and while the solubility of astaxanthin in oleic acid was 1.96 mg/mL, in olive oil it was 1.77 mg/mL [63]. Thus, olive oil

solubilizes a smaller amount of astaxanthin than oleic acid, and the same could happen for β-carotene.

All in all, the combination of all discussed above might explain these low EE(%) obtained. Especially the limitation associated with using ultraturrax (the fact that the dispersing element needs to be submerged, and thus forcing the oil phase to be added to the aqueous phase), since it led to the loss of a portion of lipid phase, where the bioactive was present. Moreover, because no other equipment, that allows the production of particles with reduced size, were available, ultraturrax had to be used, hence, in this work, this limitation restricted the production of the particles. Thus, the NLCs produced in this work were expected to have low EE(%).

Furthermore, even after reducing the amount of bioactive (β-carotene) in F4, the EE(%) was still lower than the one reported by Tamjidi *et al.* [63]. This lower EE(%) could be explained by the reasons mentioned above, plus the absence of the organic solvent and the fact that a larger portion of the lipid phase was lost when no organic solvent is used.

Due to the limited time, no further optimizations on the formulation composition were performed and the most promising formulation was used to produce astaxanthin loaded-NLCs, after the process parameters were optimized. In future studies, a lipid screening should be performed to ascertain that the lipids used were the most suitable to entrap a sample with high content of astaxanthin (97% purity), and which quantities of carriers should be used. Also, instead of using ultraturrax it should be used a different homogenization technique that does not result in a loss of the lipid phase.

Even though F1 seemed to be the most promising formulation, since out of every formulation tested it allowed the production of particles with highest EE(%), it also possessed a major disadvantage, which was the use of organic solvent.

Pharmaceutical industries always strive to avoid using of organic solvents, because these are known to be toxic and possibly carcinogenic. Also, since in this work the formulations were going to be tested in cell models, the use of organic solvents should be avoided, because even the smallest amount may reveal to be toxic for the cells. Additionally, the use of organic solvents implicates the addition of another step to the production process, which is the extraction of the solvent. The addition of another step to the process will limit its scalability and introduce more variables. Thus increasing the complexity of the process, which is always a disadvantage since it limits its application in the industry and increases the process cost and processing time.

Nonetheless, it was demonstrated that NLCs can be produced without using organic solvents and if another homogenization technique is used, that does not result in a loss of the lipid phase, then the EE(%) obtained for this formulation is expected to increase. Additionally, even if in this work, the EE(%) was lower when no organic solvent was used, the production process was still much more beneficial. When no organic solvent is used in the formulation, the complexity and cost of the production process is reduced. Also, the presence of organic solvents residues in the finished product is avoided, thus reducing possible toxic effects and environmental issues. So, considering all the issues associated with the use of organic solvents in the production of delivery systems, and the fact that NLCs can be produced without their use, the formulation that did not contain organic solvent was a better option to produce astaxanthin- and extract-loaded NLCs. Furthermore, this formulation is much more promising in an industry standpoint.

Therefore, in this work no organic solvent was further used to produce the NLCs. So, the formulation that was further studied and optimized was formulation F4, with half the initial amount of bioactive and no organic solvent.

3.2.2 β-Carotene-loaded NLCs: process parameters optimization

Particle size is a critical factor for all drug delivery systems, influencing their distribution in the organism, by influencing their capacity to cross barriers. Furthermore, it affects the kinetics of drug release and the ability of the drug delivery system to be taken up by cells and to undergo paracellular transport. Hence, for oral administration it is desirable to obtain particles as small as possible and with low PDI, to ensure the efficient delivery of the bioactive to the intestinal cells, and to obtain a higher surface area to enhance the dissolution rate [71,75].

Generally, the size of an emulsion droplet, formed by homogenization, is determined by the interplay between droplet breakup and droplet coalescence. Droplet break up is controlled by the type and amount of shear force applied to the droplets [150]. Therefore, in this task the aim was to test

different homogenization times to assess their influence on the particle size and size distribution. However, due time constraints, it was only performed a limited number of experiments, and only two different homogenization times (7 and 20 minutes) were tested. The homogenization time that led to the production of smaller particles, with reduced size distribution and higher encapsulation efficiency was selected to produce astaxanthin- and shrimp shell extract-loaded NLCs.

The formulation composition that was, previously, selected as the most promising one (Section 3.2.1), F4, which did not contain organic solvent and contained half the initial amount of bioactive, was the formulation that was used in these optimization experiments, and, subsequently, to produce the astaxanthin- and extract-loaded NLCs. Additionally, for the process optimization it was used β-carotene.

To assure the reproducibility of the production process, statistical analysis was performed for the particle size and encapsulation efficiency, and in all cases the results were found to be not significantly different (p-value>0.05) between the experiments.

Table 3.3 summarizes the optimization experiments performed for the preparation of β-carotene-loaded NLCs, the speed and the homogenization time, together with the encapsulation efficiency (EE(%)), particle size and PDI of the particles produced.

Table 3.3- Optimization of the NLCs production process: Process parameters tested for the production of NLCs. Particle size, PDI and encapsulation efficiency (EE(%)) of the β-carotene-loaded NLCs produced.

System	Experiment	Speed (rpm)	Homogenization time (min)	EE (%)	Particle size (nm)	PDI
Compritol 888 ato: Olive oil (7:2)	F4	21500	7	15.43± 2.22	407.60± 4.67	0.40± 0.05
Compritol 888 ato: Olive oil (7:2)	H1	21500	20	14.52± 0.23	358.46± 1.31	0.23± 0.08

N.B: The formulation composition used was F4, which contained half the initial amount of bioactive and did not contain organic solvent. The quantity of each component of the formulation is the same as the one reported by Tamjidi *et al.* (with 5% of lipid phase), unless mentioned different [63]. Furthermore, the mass ratios between solid and liquid lipid was 7:2. The EE(%) for the β-carotene-loaded NLCs was determined through UV-Vis spectrophotometer analysis. Values are mean ± standard deviation from two independent experiments performed in triplicate. One- way ANOVA and Tukey's multiple comparisons test was performed using the results obtained for the encapsulation efficiency, particle size and PDI of each experiment.

It is worth mentioning, that contrary to the works of other authors where it is used high energy techniques, such as high-pressure homogenizer or ultrasonicator for the emulsion homogenization and droplet-size reduction, in this work, it was only used a mechanical homogenizer, ultraturrax, since the other equipments were not available. Ultraturrax is a rotor-stator generator homogenizer and one of the most economical, easiest to operate and maintain mechanical homogenizer [150]. Generally, ultraturrax is used to obtain a coarse emulsion, and then a high-pressure homogenizer or a ultrasonicator is used for the droplet-size reduction, allowing the formation of nanoparticles. Although ultraturrax is efficient in producing emulsions, these are normally microemulsions, and droplet-size reduction is very restricted, thus limiting the production of particles in the nanoscale.

Therefore, in this work, it was not expected that the particles produced would be in the size range established for a nanomaterial, between 1-100nm, instead particles with larger sizes were expected. Then again, the pharmaceutical field considers nanoparticles as particles with sizes below 1000 nm (=1 µm) [73,151]. So, in this work the author refers to nanoparticles as particles with size below 1000 nm. Additionally, it is common to find in the literature reports considering NLCs with sizes above 100 nm as nanoparticles [152–154].

In both cases, the production of particles was successful in obtaining particles with sizes below 600 nm, so according to Tamjidi *et al.*, they might have similar permeability abilities in the human GIT as nanoparticles (<100 nm) [71]. Moreover, in both cases the PDI was below 0.5, thus indicating that there was not a broad size distribution.

From the results presented in Table 3.3, it is possible to verify that with the increase of homogenization time there was a significant decrease (p-value≤ 0.01) of the particle size. In H1, where it was used 20 minutes as the homogenization time, the particle size was 358.47 ± 1.30 nm, while in F4, where it was used 7 minutes as the homogenization time, the particle size was 407.60 ± 4.67 nm. This size reduction with the increase of homogenization time was expected, since the emulsion undergoes high speed mixing for longer periods, thus more droplet break up occurs.

Regarding the PDI, there was a significant decrease (p-value<0,01) on the value with the increase of the homogenization time. Nevertheless, both results were below 0.5, which indicates that the dispersion of particles produced did not have a broad size distribution. Still the decrease verified in H1 is related to the production of particles with a narrower size distribution.

While in this work the smallest particle size obtained was 358.47 ± 1.31 nm, and the lowest PDI was 0.20 ± 0.08 , the NLCs produced by Tamjidi *et al.* had an average particle size between 85.10 and 138.30 nm, and PDI values between 0.20 and 0.30 [63]. Although the particles produced in this work had a higher particle size than those reported by Tamjidi *et al.*, the PDI was in the range reported. In the study reported by Tamjidi *et al*., particles with smaller sizes were obtained due to the use of a bath sonicator and a probe- type sonicator, which allow particle size reduction and production of more uniform sized particles. In addition, Afshin *et al.* studied the effect of the sonication treatment on the particle size reduction, and demonstrated that it had a significant effect on particle sizes reduction, when comparing with mechanical stirring [155]. However, the use of sonication techniques also present disadvantages, such as cavitation, which causes high temperatures, metal contamination and oxygen entrance. Moreover, it was demonstrated that, ultrasound waves degrade astaxanthin into colorless compounds [63].

Nonetheless, there are many authors who reported the production of particles with particle size close to the sizes obtained in this work. Oliveira *et al.,* using a solvent injection method, obtained β-carotene-loaded NLCs with the lowest average particle size of 500 nm [152]. Leijao *et al.,* using the method of emulsion evaporation at high temperature and solidification at low temperature, obtained silybin-loaded NLCs with the lowest average particle size of 232.10 nm [153]. Similarly, Doktorovová *et al.,* using a microemulsion method, produced fluticasone propionate-loaded NLCs with the lowest average particle size of 316 nm [156]. In addition, Frias *et al.* using high-shear homogenization and ultrasonication technique obtained NLCs and SLNs with average size ranging from 300 to 400 nm [154].

Moreover, as can be observed from the results presented in Table 3.3, when comparing F4 with H1, the EE(%) was not affected with the increase of the homogenization time (p-value>0.05).

It should be mentioned that, for at least 3 weeks after the preparation, no phase separation was observed in F4 and H1, thus indicating that both were stable during that period. Due to time limitations, no stability studies were performed.

All in all, the process conditions tested in H1, 20 minutes as the homogenization time, allowed the production of smaller particles and with narrower size distribution, furthermore, the encapsulation efficiency was not affected by the operating conditions. Thus, these operating conditions were used for the subsequent production of astaxanthin- and extract-loaded NLCs.

3.2.3 Production of astaxanthin-loaded NLCs and shrimp extract-loaded NLCs

The formulation composition and the process conditions, that led to the production of smaller particles and with narrower size distribution were selected for the subsequent production of nanostructured lipid carriers loaded with astaxanthin and with the shrimp shell extract (Section 3.1).

The astaxanthin and extract-loaded NLCs were produced using the formulation composition of F4, selected as the most promising formulation (Section 3.2.1), and the process conditions used in H1 (Section 3.2.2).

To assure the reproducibility of the production process, statistical analysis was performed for the particle size and encapsulation efficiency, and in all cases the results were found to be not significantly different (p-value>0.05), between the experiments.

Table 3.4 summarizes the formulation and process conditions used to produce astaxanthin and extracted-loaded NLCs, as well as the particle size, PDI and encapsulation efficiency (EE(%)).

Table 3.4- Production of astaxanthin-loaded and extract-loaded NLCs: Process parameters used and particle size, PDI and encapsulation efficiency (EE(%)) obtained for astaxanthin-loaded NLCs and extract-loaded NLCs.

System	Speed (rpm)	Homogenization time (min)	EE(%)	Particle size (nm)	PDI
Astaxanthin-loaded NLCs	21500	20	10.02 ± 0.22	365.43 ± 2.10	0.15 ± 0.11
Extract-loaded NLCs	21500	20	6.85	365.50 ± 3.70	0.26 ± 0.11

N.B: The quantity of each component of the formulation is the same as that reported by Tamjidi et al., with 5% of lipid phase, unless mentioned different [63]. The mass ratios between solid and liquid lipid was the same in all cases and was 7:2. EE(%) for astaxanthin-loaded NLCs was determined through UV-Vis spectrophotometer analysis and the EE(%) for extract loaded-NLCs was determined in terms of astaxanthin incorporated, through HPLC analysis. Values are mean ± standard deviation from two independent experiments performed in triplicate. One- way ANOVA and Tukey's multiple comparisons test was performed using the results obtained for the encapsulation efficiency of each experiment.

From the results presented in Table 3.4, the EE(%) of astaxanthin-loaded NLCs was found to be 10.02 ± 0,22%, and of extract-loaded NLCs it was found to be 6.85%. These results were lower than those obtained for β-carotene-loaded NLCs (experiment H1, Section 3.2.2). Regarding astaxanthin-loaded NLCs (Appendix 2 - Figure 6.3), the EE(%) was significantly lower (p-value≤0.01) than the one obtained for β-carotene-loaded NLCs (experiment H1). This might be explained, if astaxanthin has lower solubility in the lipid phase (compritol 888 ato and olive oil) than β-carotene. As for the extract-loaded NLCs, the EE(%) was much lower than the result obtained for the β-carotene-loaded NLCs (experiment H1, Section 3.2.2). This may be explained by the fact that the extract was very hard to work with, since it had wax-like texture and it was difficult to melt and solubilize with the melted lipid matrix.

Concerning the particle size and PDI, both astaxanthin-loaded NLCs and extract-loaded NLCs presented similar results (p-values>0.05). The particle size of astaxanthin-loaded NLCs was 365.43 ± 2.10 nm and the PDI was 0.15 ± 0.1, whereas, the particle size of extract-loaded NLCs was 365.50 ± 3.70 nm and the PDI was 0.26 ± 0.11. Both astaxanthin-loaded NLCs and extract-loaded NLCs had narrow size distribution (i.e. low PDI). Furthermore, according to Tamjidi *et al.* these particles could have similar permeability abilities in the human GIT as nanoparticles (<100nm) [71]. The particle size and PDI of both astaxanthin-loaded and extracted-loaded NLCs was very similar do the particle size and PDI obtained for the β-carotene-loaded NLCs (experiment H1, Section 3.2.2). When comparing with the astaxanthin-loaded NLCs produced by Tamjidi *et al.,* the particles obtained in this work had larger particle size, but their PDI value was in range reported [63].

3.2.4 Astaxanthin-loaded NLCs: Thermal behavior

Differential Scanning Calorimetry (DSC) is a technique use to study the thermal behavior of a material, providing information about its the melting, recrystallization, glass and polymorphic transitions, as well as information about the interaction between the carriers and the encapsulated material. This technique is frequently used to evaluate the glass transition temperature of non-crystalline and semi-crystalline materials and to determine the melting point of a material. The determination of the melting point of particles provides information about the purity, particle size and alterations in the crystallinity of the study sample [99,157–160].

DSC measurements were performed on bulk compritol 888 ato and astaxanthin-loaded NLCs (after being lyophilized), in order to evaluate their thermal behavior (Figure 3.1).

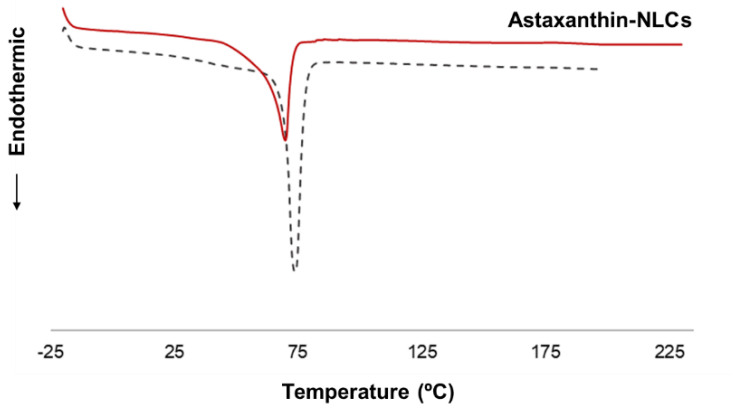

Figure 3.1- **DSC thermograph of astaxanthin-loaded NLCs**. Dotted line represents unprocessed compritol 888 ato.

The thermograph of astaxanthin-loaded NLCs presented a single endothermic peak correspondent to pure compritol 888 ato. As can be observed, this endothermic peak is slightly shifted to a lower melting temperature and has a lower height than the endothermic peak of pure compritol 888 ato. This might indicate lower crystallinity and massive crystal order disturbance (i.e. lattice defects) [63]. This observation should be confirmed through X-ray diffraction (XRD), which assess the crystalline order of the particles. The formation of lattice defects is related to the fact that the addition of the liquid lipid leads to the formation of less-ordered matrices, containing imperfections in their structures and these prevent bioactive expulsion [89,92].

Furthermore, crystalline astaxanthin was not detected in the astaxanthin-loaded NLCs, as can be demonstrated by the absence of the peak correspondent to astaxanthin, which was expected at 222°C [161]. This finding indicates that the bioactive might have been in an amorphous or disordered-crystalline phase [159,160]. When the bioactive is in the amorphous state or in the disordered crystalline phase it can easily diffuse through the lipid matrix, leading to its sustained release [159,160]. This finding should be confirmed through X-ray diffraction (XRD).

After being produced and characterized the astaxanthin-loaded and extract-loaded NLCs were further analyzed through cell-based assays to evaluate possible cytotoxicity, antioxidant activity, and to assess the influence of the delivery system on the improvement of the uptake and permeability of astaxanthin in *in vitro* cell models. It is important to mentioned that before testing the NLCs in cell-based assays, these were sterilized like described in Section 2.2.4.1, and their encapsulation efficiency was evaluated before and after being sterilized and no significant decrease was verified (data not shown).

3.2.5 Development and optimization of β-carotene-loaded SLCs through PGSS® precipitation

Particles from Gas Saturated Solutions (PGSS®), a supercritical fluid-based precipitation process, allows the micronization of lipophilic and thermo-labile compounds without the use of organic solvents and under mild operating conditions.

In this task it was intended to optimize the production of β-carotene-loaded SLCs, for the subsequent production of astaxanthin and extract-loaded SLCs. Different lipid matrices, and operating conditions, such as pressure (P) and contact time with supercritical CO_2 ($scCO_2$), were tested to evaluate their influence on the particle size and encapsulation efficiency (EE%). The lipid matrix, contact time with $scCO_2$, temperature (T) and pressure (P) values that led to the production of smaller particles with higher encapsulation efficiency were selected to produce astaxanthin and shrimp shell extract-loaded SLCs.

Considering that, in this work, the delivery abilities of NLCs and SLCs were intended to be compared, both delivery systems should have the same formulation composition. Thus, the formulation composition that was found to be the most promising one to produce NLCs, F4, was tested to produce SLCs (Section 3.2.1). Although to produce SLCs, through PGSS® process, none of the formulations tested were composed by an aqueous phase. On the other hand, another lipid matrix was also tested, one that was very similar to that of F4, but instead of containing olive oil it contained peceol. Peceol was tested as a liquid lipid since it is reported to have mucoadhesive properties and capacity to inhibit P-glycoproteins [105]. Moreover, peceol and compritol 888 ato have similar hydrophilic-lipophilic balance (HBL), 3 and 2, respectively, this small difference will allow a better mixture between the compounds, which may lead to the production of fine SLCs and with narrow size distribution [105]. Thus, the formulation composition tested to produced SLCs consisted in compritol 888 ato, olive oil or peceol, lecithin and the bioactive, it should be mentioned that the ratio of each component in the lipid matrix was the same as their ratio in the formulations of NLCs (F4), being the ratio between solid and liquid lipid 7:2. Solid lipid microparticles (SLM) were also produced to evaluate the influence of the presence of liquid lipid on the EE%. These were produced using the same formulation composition as the SLCs but without liquid lipid (the formulation was composed by compritol 888 ato, lecithin and the bioactive).

The operating conditions (T and P) used for the production of the particles were selected according to the melting point depression of compritol 888 ato in the presence of CO_2, to ensure the liquid state of the lipid mixture prior to its atomization. These were selected based on to the melting point depression of compritol 888 ato, since it was the major constituent of the lipid matrix and the lipid with highest melting point. Moreover, these conditions were selected based on the results previously reported by Sampaio de Sousa *et al.* [108]. The melting point of compritol 888 ato decreases slightly with the increase of the pressure, and the CO_2 solubility in the solid lipid increases with temperature and pressure [108]. Different pressures and different contact times with $scCO_2$ were tested to evaluate their influence on the particle size and encapsulation efficiency.

To assure the reproducibility of the production process, statistical analysis was performed for the experimental load and in all cases the results were found to be not significantly different (p-value>0.05), between the experiments.

Table 3.5 summarizes the PGSS® precipitation experiments performed for the preparation of β-carotene-loaded SLCs, together with the theoretical load, experimental load and the encapsulation efficiency.

Table 3.5- Summary of PGSS® co-precipitation experiments. Parameters tested to optimize the production of SLCs: Lipid matrix, pressure (P), temperature (T) and contact time with $scCO_2$. As well as, the results obtained in each experiment for: Theoretical load, experimental load, and encapsulation efficiency (EE(%)).

Lipid matrix	Experiment	P (bar)	T (ºC)	Contact time (min)	T. Load (mg/g)	E. Load (mg/g)	EE% (%)
Compritol 888 ato: No liquid lipid	**E.1**	100	70	15	10.13	8.21 ± 0.27	81.05 ±2.07
Compritol 888 ato: Peceol	**E.2**	100	70	15	10.04	11.14 ± 0.43	112.30 ±4.30
Compritol 888 ato: Peceol	**E.3**	100	70	30	10.07	11.88 ± 0.42	117.96 ±4.21
Compritol 888 ato: Peceol	**E.4**	150	70	30	10.03	10.29 ± 0.94	102.49 ±9.23
Compritol 888 ato: Peceol	**E.5**	200	70	30	10.03	9.96 ± 1.02	99.26 ±4.02
Compritol 888 ato: Peceol	**E.6**	250	70	30	10.06	12.16±1,00	120.65 ±6.60
Compritol 888 ato: Peceol	**E.7**	250	70	15	10.03	12.16±0.67	121.17 ±6.65
Compritol 888 ato: Olive oil	**E.8**	100	70	15	10.06	11.84±0.44	116.65 ±4.41
Compritol 888 ato: Olive oil	**E.9**	250	70	15	10.03	12.16±0.67	121.17 ±6.65

N.B: All the components are in the same ratio as the components in the NLCs formulation. The mass ratios between solid and liquid lipid was the same in all cases and was 7:2. The content of β-carotene incorporated in the particles was determined through UV-vis spectrophotometer analysis. Values are mean ± standard deviation from two independent experiments performed in triplicate. One- way ANOVA and Tukey's multiple comparisons test was performed using the results obtained for the experimental load.

Since olive oil contains traces amounts of carotenoids, blank-SLCs were produced using the formulation containing olive oil, to assess the possible interference of the carotenoids present in this liquid lipid on the determination of the amount of β-carotene incorporated into the particles. The presence of carotenoids from the blank-SLCs was not detected through UV-Vis spectrophotometer analysis. Thus, the carotenoids present in the olive oil did not interfere with the determination, through UV-Vis spectrophotometer analysis, of the content of β-carotene incorporated into the particles. (data not shown)

From the results summarized in Table 3.5, it is possible to verify that the EE(%) obtained in the majority of the experiments is above 100%. As can be observed the experimental load of the bioactive was higher than the theoretical load, and generally the reversed is observed. In these experiments what might have occurred was a preferentially loss of the carriers, most probably compritol 888 ato, relative to the bioactive. That is, the amount lost of each component of the formulation was not proportional and a higher amount of carriers was lost in comparison to the amount of bioactive lost, thus the initial ratio of bioactive/carriers is not the same as the final ratio, being the final ratio higher. This phenomenon might be explained by limitations associated with the way PGSS® is designed, and which restrict the production efficiency greatly. During the PGSS® process when depressurization occurs the lipid mixture saturated by $scCO_2$ instead of being immediately expanded through the nozzle into the recovery/expansion vessel, where the atomization occurs, the saturated solution, that was in the stirred vessel at high temperature, will first have to go through a path before arriving to the nozzle, where it will be expanded to ambient temperature. This path that the lipid mixture was to go through might be at a lower temperature that the stirred vessel, causing the solidification of the lipids.

So, in this work what might have occurred was: since compritol 888 ato has a high melting temperature, even in the presence of $scCO_2$, (e.g. at 100 bar the melting temperature is 67ºC), when depressurization occurs and the lipid mixture has to go through the path before arriving to the nozzle,

because this path might have been at a lower temperature than the melting point of compritol, this lipid might have solidified. Thus compritol stayed behind in the circuit and not expanded through the nozzle together with CO_2 and the rest of the components of the lipid matrix [108]. This phenomenon might explain how the experimental load can be higher than the theoretical load.

If a different PGSS® equipment was to be used, one that does not have the design limitations of this PGSS®, this phenomenon might have not occurred. Additionally, if a different solid lipid was used, one with lower melting temperature than compritol 888 ato, this may have not occurred. But since in the optimization of the formulation, in Section 3.2.1, compritol 888 ato was the only solid lipid tested that allowed the production of stable dispersions of NLCs, this lipid continued being used to produce the SLCs, so that both delivery systems could be compared in terms of their delivery ability. In the future, these experiments should be repeated using a different PGSS® equipment, without the design limitations.

Furthermore, the fact that the experimental load of the bioactive was higher than the theoretical load may be advantageous, since the delivery system is able to deliver a high dose of the bioactive without the presence of large amounts of excipients, which may cause undesirable side effects [162].

To confirm the results obtained for the EE(%), determined through UV-Vis spectrophotometer analysis, HPLC analysis was performed on a selected number of experiments (E.2, E.8, E.7 and E.9), and the results obtained are summarized in Table 3.6.

Table 3.6- Summary of PGSS® co-precipitation experiments: Parameters tested to optimize the production of SLCs: lipid matrix, pressure, temperature, contact time with $scCO_2$. As well as, the results obtained in each experiment for: Theoretical load, experimental load, and encapsulation efficiency (determined through HPLC analysis).

System	Experiment	P (bar)	T (ºC)	Contact time	T. Load (mg/g)	E. Load (mg/g)	EE% (%)
Compritol 888 ato: Peceol	**E.2**	100	70	15	10.04	11.35	113.02
Compritol 888 ato: Olive oil	**E.8**	100	70	15	10.06	11.71	116.34
Compritol 888 ato: Peceol	**E.7**	250	70	15	10.03	12.11	120.72
Compritol 888 ato: Olive oil	**E.9**	250	70	15	10.03	12.66	126.13

N.B. All the components are in the same ratio as the components in the NLCs formulation. The mass ratios between solid and liquid lipid was the same in all cases and was 7:2.

The results obtained for the EE(%) through HPLC analysis confirmed the results obtained through UV-Vis analysis (Table 3.6). Also, the results obtained using both techniques were very similar.

Because the encapsulation efficiencies obtained were above 100%, in this work the different experiments will be analyzed in terms of the experimental load of the bioactive. One-way ANOVA and Tukey's multiple comparisons test were performed on the experimental load obtained for each experiment (Table 3.5), and the results are presented in Appendix 3 - Table 6.1.

As expected, E.1, whose lipid matrix was not composed by liquid lipid, was the experiment with the lowest experimental load. When comparing this experiment with the other experiments where the same operating conditions were used, but whose lipid matrix contained liquid lipids, E.2 and E.8, it is possible to verify that the experimental load obtained in E.1 was significantly lower than the loads obtained in E.2 and E.8 (for E.2 P-value ≤ 0.0001 and for E.8 p-value ≤ 0.0001) (Appendix 3 - Table 6.1). This was expected, since the presence of the liquid lipid might improve the solubilization of the bioactive, plus creates more imperfections in the lipid matrix allowing for a higher incorporation of the bioactive [105]. Additionally, the powder of particles obtained in E.1, after a few days since being prepared, started to lose color and after 2 weeks it was almost colorless (data not shown). This loss of coloration might be explained if the number of imperfections in the structure of the particles was reduced, due to low-energy modifications that resulted in a more ordered structure, and that consequently led to bioactive expulsion [105].

Concerning the experiments performed for the formulation containing olive oil, E8 (100 bar) and E.9 (250 bar), the experimental load obtained, in each experiment, revealed not to be significantly different (p-value>0.05) from each other (Table 3.5). These results indicate that the increase of the pressure did not influence the experimental load. However, a visible difference on the powder of particles produced was observed, the one obtained in E.9 was finer than the one obtained in E.8. This observation is related to the particle size of the particles produced, indicating that perhaps the particles obtained in E.9 had smaller particle size.

Regarding the experiments performed for the formulation containing peceol, E.2 to E.7. The experimental load obtained in E.4 and E.5 revealed to be significantly lower than the loads obtained in the other experiments, this indicates that the 150 and 200 bar had a negative influence on experimental load (p-values obtained presented in Appendix 3 - Table 6.1). When comparing E.2 with E.3 and E.6 with E.7, where the only difference was the contact time with $scCO_2$ (E.2 and E.7 it was tested 15 min and E.3 and E.6 it was tested 30 min), the results obtained for the experimental load, in each experiment, revealed not to be significantly different between each other (p-value>0.05). Thus the contact time with $scCO_2$ did not influence the experimental load. Furthermore, when comparing E.2 with E.6 and E.3 with E.7, where the only difference was the pressure used (E.2 and E.3 it was tested 100 bar, and E.6 and E.7 it was tested 250 bar), the results obtained for the experimental load, in each experiment, revealed not to be significantly different between each other (p-value>0.05). Thus, the pressure did not influence the experimental load. However, once again, a visible difference on the powder of particles produced was observed, the ones obtained in experiments using 250 bar were finer than the ones obtained in experiments using 100 bar, this indicates that the pressure might influenced the particle size (Table 3.5).

When comparing E.3 with E.8 and E.7 with E.9, where the only difference was the liquid lipid used (E.3 and E.7 it was used peceol and in E.8 and E.9 it was used olive oil) the results obtained for the experimental load, in each experiment, revealed not to be significantly different between each other (p-value>0.05). These findings indicate that the liquid lipid used did not influence the experimental load (Table 3.5).

All in all, the contact time with $scCO_2$ and the liquid lipid used did not influence the experimental load of the bioactive, in any of the experiments performed. The highest experimental loads were obtained in the experiments using 100 and 250 bar, for both lipid matrix where liquid lipid was used. Moreover, when comparing the experiments where 100 bar and 250 bar were used the pressure did not influence the experimental load, but perhaps influenced the particle size. Notwithstanding, the experiments where 150 bar and 200 bar were tested, reveal that these pressures decreased the experimental load. This might be related to the solubility of the bioactive in the $scCO_2$, at these pressures.

In this work, the content of β-carotene obtained in the microparticles ranged from 8.21 to 12.16 mg/g. De Paz *et al.* also produced β-carotene-loaded microparticles through PGSS® process, but obtained a much lower content of β-carotene in the microparticles. The author formulated β-carotene with poly-(ε-caprolactone), and the highest content of β-carotene incorporated into the microparticles was 0.34 mg/g, when using 70ºC and 150 bar. Also the author verified that with the increase of the pressure the amount of β-carotene entrapped in the particles increased [163].

Since positive results using peceol, in the lipid matrix for the production of SLCs were obtained, it was also tested its use in the production of NLCs. If positive results were achieved using this lipid in the production of the nanoparticles, then the formulations (SLCs and NLCs) where peceol was used would also be tested to assess their delivery ability in *in vitro* cell models. However, when producing the NLCs using peceol it was not obtained a dispersion or an emulsion, instead it was obtained a stiff and gel like solution, and in some cases phase separation was also observed(this procedure was repeated at least 3 times to confirm results). This occurred since peceol when in contact with water spontaneously swells, forming this highly viscous and gel like solution [164]. Nielsen *et al.* stated that peceol (GMO), when in an aqueous medium will absorb the surrounding water and spontaneously swell, forming a cubic phase. When in cubic phase the lipid has a stiff, highly viscous, and gel-like appearance, which confer the carrier its mucoadhesive property [164]. Therefore, this attempt to use peceol, as a liquid lipid, to produce NLCs was not successful, since it was obtained a solution with undesirable characteristics, highly viscous and gel like, for the application intended, oral administration. As a result, since the ability of NLCs and SLCs in improving the cellular uptake of the

bioactive was intended to be compared, both systems should have the same formulation, thus peceol was not be further used to produce SLCs and NLCs, nor was it further analyzed.

3.2.5.1 β-carotene-loaded SLCs stability: Color evaluation

After each experiment a yellow powder of particles was produced. From Figure 3.2-A, it is possible to observe that the powder of SLCs obtained for both formulations, where olive oil and peceol were used, exhibited a similar yellow color. Nonetheless, from the Figure 3.2-B, it is observed that after 4 months, the powder obtained for the formulation containing peceol was no longer yellow, but pink, while the SLCs obtained for the formulation containing olive oil remained yellow. This pink color of the powder of particles may be an indication of the degradation of β-carotene. Incidentally, many authors have reported a loss of color of formulated products due to the oxidation and degradation β-carotene, during storage [165,166]. This degradation, observed in the formulation containing peceol, might be caused by the oxidation of the fatty acids of the lipid, which produce free radicals that will react with β-carotene [167]. Possibly, the antioxidants present in the olive oil, such as α-tocopherol and other carotenoids, might have protected β-carotene from oxidation [85].

It is important to mention that both samples were stored at -20ºC, in falcons with a N_2 atmosphere and protected from the light with aluminum foil.

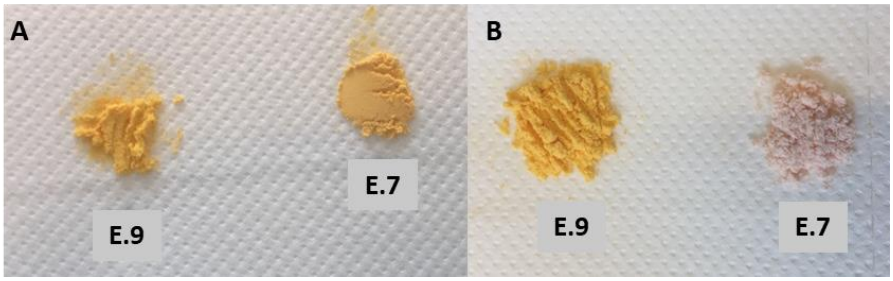

Figure 3.2- β-Carotene-loaded SLCs produced through the PGSS® process: **A**- SLCs after being prepared; **B-** SLCs 4 months after being prepared; Experiments E.9 (with olive oil) and E.7 (with peceol) were performed at 70ºC, 250bar, with 15 min as contact time with $scCO_2$.

3.2.5.2 β-Carotene-loaded SLCs: Physical-chemical characterization

The particles produced in the experiments whose formulation composition contained olive oil (E.8 and E.9) were further characterized to assess their size, morphology, and thermal behavior.

3.2.5.2.1 Size and morphology

Particle size is a critical factor for all drug delivery systems, being one of the factors that controls the kinetics of drug release and influences the target capacity of the delivery system. For oral administration it is desirable to obtain particles as small as possible to obtain a higher surface area to enhance the dissolution rate [103,168].

When comparing the resulting powders of particles obtained for the experiments where 100 bar was used, to the powders obtained in the experiments where 250 bar was used, it was visibly noticeable that the powders obtained for the experiments using 250 bar were finer and drier than the ones obtained using 100 bar. This observation indicates that 250 bar might have allowed the production of smaller particles, than those produced using 100 bar. This was observed in the two different formulations, where olive oil and peceol were used.

Considering that it was decided that peceol was not going to be further used to produce SLCs, since it was not suitable to produce NLCs, only the experiments where olive oil was used were further analyzed.

The resulting particles of the experiments whose formulation contained olive oil, E.8 and E.9, performed at the same temperature, 70ºC, with the same contact time with $scCO_2$,15 minutes, but at different pressures, at 100 bar for E.8 and 250 bar for E.9, were analyzed through SEM, to investigate the effects of the pressure on the size and morphology of the particles (Figure 3.3).

It is important to mention that it was not possible to obtain more precise information about the particle size and particle size distribution, since the equipments that were going to be used to analyze de particles, Laser Diffraction (Malvern Mastersizer 2000) and Morphologi G3 (Malvern), were both unavailable. In the future, the particle size and particle size distribution of the resulting particles of the PGSS® experiments should be determined with higher precision using Laser Diffraction (Malvern Mastersizer 2000) or Morphologi G3 (Malvern). Nevertheless, in this work, the particle size range was obtained from SEM analysis. The particle size is obtained by measuring the particles using the scale present in each micrograph. However, only a limited number of particles is measured, thus the particle size range is not very precise.

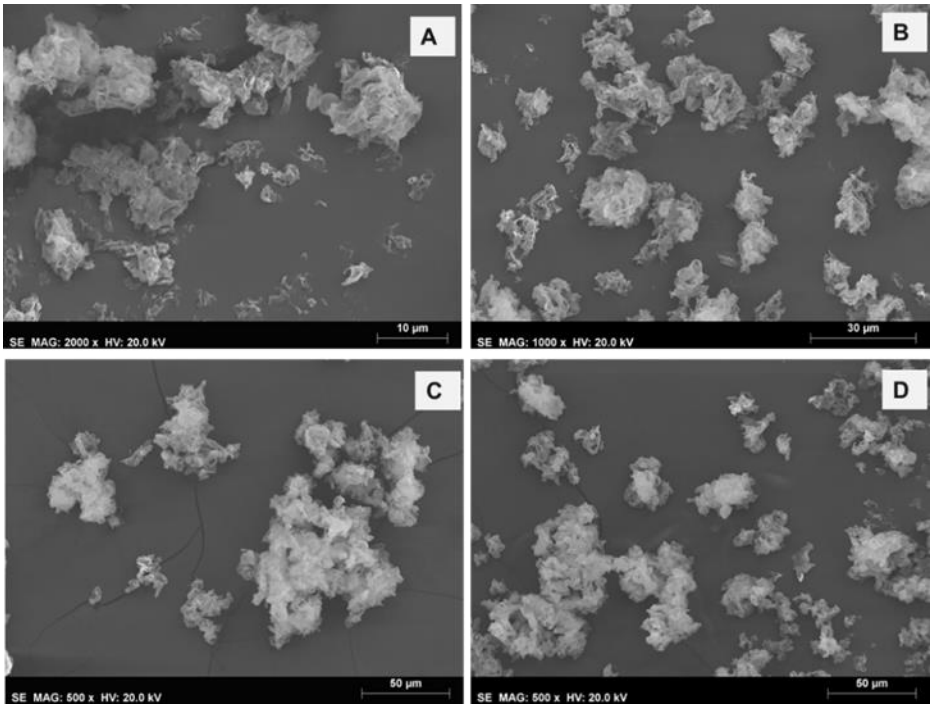

Figure 3.3- **SEM micrographs of β-Carotene-loaded SLCs**. β-Carotene-loaded SLCs produced using a formulation containing olive oil, through PGSS® process (nozzle diameter d=250µm) at 70ºC, with 15 minutes as a contact time with $scCO_2$ and using different pressures; **A)** E.9, β-Carotene-loaded SLCs produced at 250 bar, at 2000x magnification and **B)** at 1000x magnification; **C)** E.8, β-Carotene-loaded SLCs produced at 100 bar, at 500x magnification and **D)** at 500x magnification.

From the SEM micrographs (Figure 3.3), it is possible to observe that the microparticles, obtained in both experiments, exhibited an irregular shape, which is a very common characteristic of particles obtained through PGSS® process. Additionally, the SLCs obtained in E.9 (250 bar) had a more irregular shape than those obtained in E.8 (100 bar), this irregular shape obtained was a result of the high pressure used (250 bar). Furthermore, the microparticles obtained in E.9 were porous. These type of particles are obtained when the solidification is fast, and the pores are produced by the release of CO_2 during depressurization [105]. At high pressures, large amounts of CO_2 are dissolved in the melted lipid matrix, and more CO_2 gas bubbles are formed increasing the cooling rate, which produces porous particles since the gas cannot diffuse out of them before they solidify, thus as the gas diffuses out of the particles it perforates the particle surface [99].

Moreover, it is known that the more CO_2 is solubilized in the melted lipid matrix, less viscous will the lipid mixture be, making it easier to break up the mixture into smaller particles during the atomization step [105]. Since the solubility of CO_2 in compritol 888 ato increases with the increase of pressure and temperature, it was expected that smaller particles would be produced at higher pressures and temperature values [108]. Also, when high pressure is used it causes a high drop in the pressure during depressurization, the higher is the pressure drop the smaller are the particles produced [99].

From the SEM micrographs, the particle size of the SLCs produces in E.9 were between 2.5 to 20 µm, while the SLCs obtained E.8 ranged from 10 to 100 µm. As expected, smaller particles were produced in the experiment where higher pressures were used. Furthermore, in E.8 (100 bar) there was a broader size range, when compared to E.9 (250bar). Particle aggregation is a major contributor to a broader size distribution, and it is possible to observe particle aggregation in E.8 and E.9 [107]. The increase in aggregation in PGSS-processed microparticles is related to the processing temperature and surface oil [107]. Moreover, particle aggregation decreases when the working temperature is close to melting temperature of the lipid matrix, since it leads to faster cooling and crystallization, in the expansion chamber [105].

The results obtained for the particle size range revealed that the ideal conditions to produce the particles with the smallest sizes were the conditions used in E.9. In addition, these conditions allowed the production of microparticles with one of highest experimental loads. Thus, these conditions were used for the subsequent production of astaxanthin and extract-loaded SLCs.

3.2.5.2.2 Thermal behavior

As previously mentioned in Section 3.2.4, Differential Scanning Calorimetry (DSC) is a technique used to study the thermal behavior of a material, providing information about its the melting, recrystallization, glass and polymorphic transitions, as well as information about the interaction of the drug with the lipid matrix. This technique allows to detect alterations in the crystallinity of the sample being analyzed, thus providing information about the possible formation of lattice defects in the lipid matrix of the particles [99,157–160].

DSC measurements were performed for pure compritol 888 ato and β-carotene-loaded SLCs (E.8 and E.9) in order to characterize their thermal behavior, as presented in Figure 3.4.

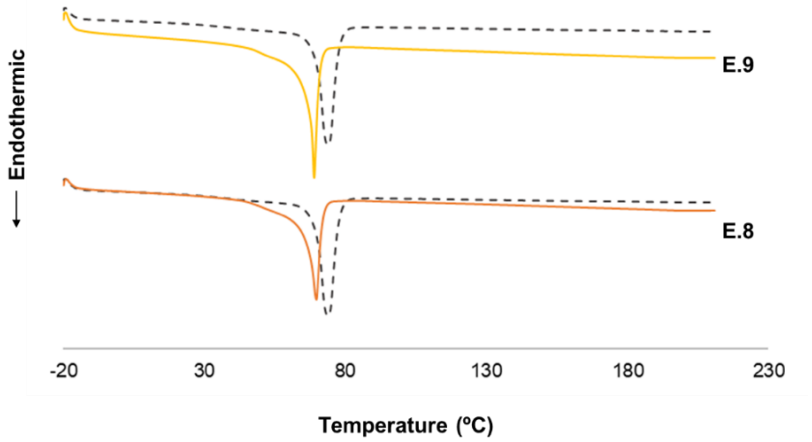

Figure 3.4- DSC thermograph of β-carotene-loaded SLCs. β-Carotene-loaded SLCs produced using a formulation containing olive oil, through PGSS® process at 70ºC, with 15 minutes as a contact time with $scCO_2$, and using different pressures, 100bar (**E.8**) and 250bar (**E.9**). Dotted line represents pure compritol 888 ato.

Regarding the β-carotene-loaded SLCs (E.8 and E.9), both thermographs exhibited the endothermic peak corresponding to the bulk compritol 888 ato. Additionally, in both graphs obtained, there was a shift of the endothermic peak, correspondent to compritol 888 ato, to lower temperatures, which might indicate the presence of lattice defects (i.e. massive crystal order disturbance) on the particles [152]. These lattice defects might be related to the fact that the addition of the liquid lipid leads to the formation of less-ordered matrices, containing imperfections in their structure, and these prevent bioactive expulsion. These results should be confirmed through X-ray diffraction (XRD), that assess the crystalline order of the particles.

Moreover, the thermographs obtained for E.8 and E.9, do not present any peak corresponding to crystalline β-carotene, which should be observed at 180 °C [163]. This finding indicates that the bioactive might have been in an amorphous or disordered-crystalline phase [159,160]. When the bioactive is in the amorphous state or in the disordered crystalline phase it can easily diffuse through the lipid

matrix, leading to its sustained release [159,160]. This finding should be confirmed through X-ray diffraction (XRD).

3.2.6 Production of astaxanthin-loaded SLCs through PGSS® precipitation

The lipid matrix, contact time with $scCO_2$, temperature and pressure values that led to the production of smaller particles with higher experimental load, in the optimization experiments, were selected for the subsequent production of structured lipid carriers loaded with astaxanthin and with the shrimp shell extract, previously obtained (Section 3.1).

The lipid matrix already optimized to produce β-carotene-loaded SLCs, containing olive oil (formulation used in the experiments E.8 and E.9 of Section 3.2.5), was used to produce the SLCs loaded with astaxanthin and with the shrimp shell extract. The operation parameters used were the same as those used in E.9, and were 70ºC, 250 bar and 15 minutes as a contact time with $scCO_2$. De la Fuente *et al.* demonstrated that the solubility of astaxanthin in CO_2 increased with the increase of pressure and temperature [169]. Thus, by using high temperature and pressure values it may be possible to produce of astaxanthin-loaded SLCs with high bioactive load.

The operating conditions used in this study, together with the resulting bioactives experimental load, is presented in Table 3.7.

Table 3.7- Astaxanthin and the shrimp shell extract-loaded SLCs obtained through PGSS® co-precipitation: conditions used (temperature (T), pressure (P) and contact time with $scCO_2$); experimental load and encapsulation efficiency (EE(%)) obtained.

System	T (ºC)	P (bar)	Contact time	E. Load (mg/g)	EE(%)
Astaxanthin-loaded SLCs	70	250	15	9.26 ± 0.80	92.57 ± 7.96
Extract- loaded SLCs	70	250	15	0.003	35.43

N.B: The mass ratios between solid and liquid lipid was the same in both cases and was 7:2. Experimental load for astaxanthin-loaded SLCs was determined through spectrophotometer UV-Vis analysis and the experimental load of the extract loaded-NLCs was determined through HPLC analysis, according to the amount of astaxanthin incorporated in the particles. Values are mean ± standard deviation of a triplicate.

From the results presented in the Table 3.7, the EE(%) of astaxanthin-loaded SLCs was found to be 92.57 ± 7.96% (Figure 3.5). This result was higher than the one obtained by Melgosa *et al.*, that using PGSS® process produced astaxanthin-rich salmon oil-loaded microparticles, using polyethylene glycol-6000 as a carrier, at 50 °C and 250 bar, obtaining 79.20% as EE(%) [170].

Furthermore, the astaxanthin-loaded SLC experimental load was 9.26 ± 0.80 mg/g (Table 3.7). When comparing this result with the one obtained in the optimization experiments where β-carotene and the same operating conditions used to produce astaxanthin-loaded SLCs were used (E.9 of Section 3.2.5), it is possible to verify that the experimental load obtained for astaxanthin-loaded SLCs is significantly lower ($p\text{-value} \leq 0.0001$). This may be related to the different solubility of the bioactives in the $scCO_2$. On the contrary, the result obtained for the astaxanthin-loaded SLCs experimental load was higher than the load obtained by Melgosa *et al.*, whose highest astaxanthin content in the microparticles was 0.04 mg/g [170].

The experimental load obtained for the extract-loaded SLCs was 3 μmg/g. This low load was expected since the amount of astaxanthin presented in the extract is also low (Section 3.1). The encapsulation efficiency was 35.43%.

Figure 3.5- Astaxanthin-loaded SLCs produced using a formulation containing olive oil, through PGSS® precipitation at 70ºC, 250bar and 15 minutes as contact time with $scCO_2$.

3.2.6.1 Astaxanthin- loaded-SLCs: Physical-chemical characterization

3.2.6.1.1 Size and morphology

To assess the size and morphology of the particles, the astaxanthin-loaded SLCs were analyzed through SEM. (Figure 3.6)

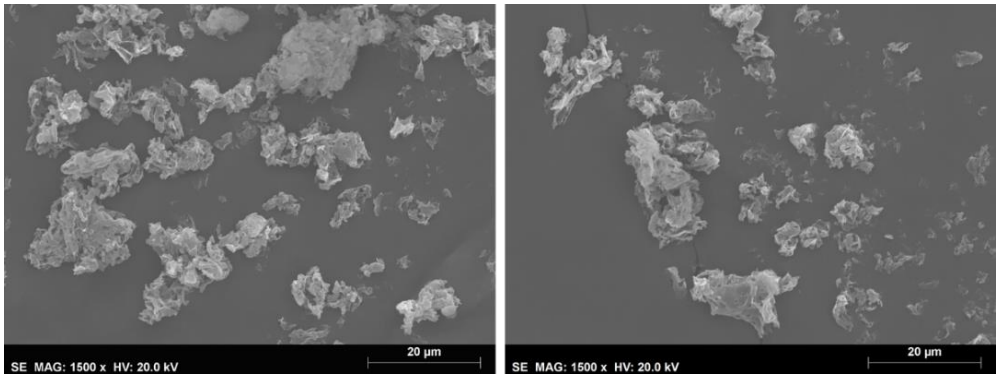

Figure 3.6- SEM micrographs of astaxanthin-loaded SLCs. Astaxanthin-loaded SLCs produced using a formulation containing olive oil, through PGSS® process at 70ºC, 250 bar and with 15 minutes as a contact time with $scCO_2$. Micrographs at 1500x magnification.

From the SEM micrographs, Figure 3.6, it is possible to observe that the particles had irregular shapes and were porous. Like previously mentioned, porous microparticles are obtained when the solidification is fast and produced by the release of CO_2 during depressurization (Section 3.2.5.2.1) [105].

The particle size of the astaxanthin-loaded microparticles was between 1.5 and 20 µm. These results are very close to those obtained for β-carotene-loaded SLCs in E.9, which is expected since the same operating conditions were used (Section 3.2.5.2.1). It is, also, possible to observe, from the SEM micrographs, that aggregation of particles occurred (Figure 3.6).

3.2.6.1.2 Thermal behavior

To evaluate the thermal behavior of pure compritol 888 ato, astaxanthin-loaded SLCs and extract-loaded SLCs, DSC analysis were performed (Figure 3.7).

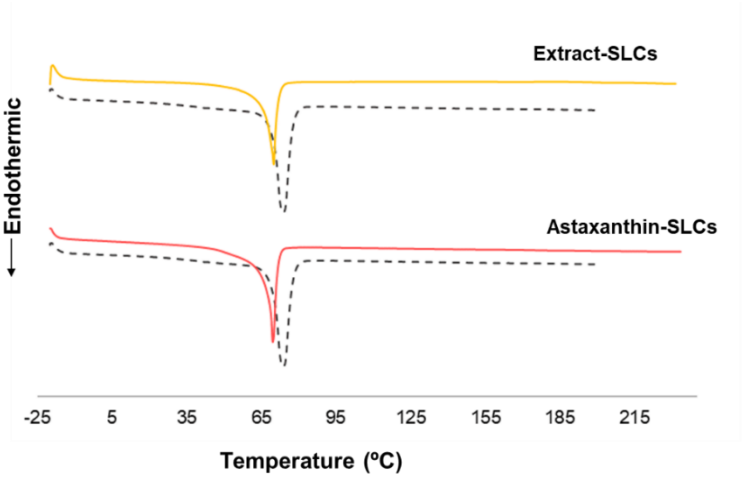

Figure 3.7- DSC thermographs of astaxanthin-loaded SLCs and shrimp shell extract-loaded SLCs produced using the formulation containing olive oil, through PGSS® process at 70ºC and 250 bar and with 15 minutes as a contact time with $scCO_2$. Dotted line represents pure compritol 888 ato.

Once again, in the thermographs of the astaxanthin-loaded and extract-loaded SLCs the endothermic peak corresponding to pure compritol 888 ato is presented. In both thermographs there was a slight shift of the endothermic peak, correspondent to compritol 888 ato, to lower temperatures, which might indicate the presence of lattice defects (i.e. massive crystal order disturbance) in the particles [152]. This observation should be confirmed through X-ray diffraction (XRD), which assess the crystalline order of the particles.

Moreover, the thermograph obtained for astaxanthin-loaded SLCs does not present a peak corresponding to crystalline astaxanthin, which was expected at 222°C [161]. This finding indicates that the bioactive might have been in an amorphous or disordered-crystalline phase [159,160]. When the bioactive is in the amorphous state or in the disordered crystalline phase it can easily diffuse through the lipid matrix, leading to its sustained release [159,160]. This finding should be confirmed through X-ray diffraction (XRD).

After being produced and characterized, the astaxanthin-loaded and extract-loaded SLCs were further analyzed through cell-based assays to evaluate their possible cytotoxicity, antioxidant activity, and to assess the influence of the delivery system on the improvement of the permeability and uptake of astaxanthin, in *in vitro* cell models. It is important to mentioned that before testing the SLCs in cell-based assays, these were sterilized like described in Section 2.2.4.1. Their experimental load was evaluated before and after being sterilized and no significant decrease was verified (data not shown).

3.3 Cell based assays

During the process of development and optimization of novel drugs and formulated products, for oral administration, it is crucial to predict their human intestinal absorption, bioavailability and cytotoxicity.

Having produced astaxanthin and extract-loaded NLCs (Section 3.2.3) and SLCs (Section 3.2.6), it was assessed their cytotoxicity, antioxidant activity and influence on the mitochondrial integrity. Furthermore, it was evaluated the permeability and uptake of astaxanthin in the formulations in *in vitro* cell models.

3.3.1 Cytotoxicity evaluation

Cytotoxicity evaluation is a crucial step when developing a nutraceutical or a drug delivery system, having to be carried out before the permeability studies. Thus, the cytotoxicity of astaxanthin, shrimp shell extract and respective formulations (NLCs and SLCs) was evaluated in the human

adenocarcinoma cell line (Caco-2), using the Prestoblue® reagent, in order to select nontoxic concentrations for further studies.

Several concentrations of each sample (astaxanthin, shrimp shell extract and formulations) were tested in terms of mols of astaxanthin per milliliter of solution, in culture medium with 0.5% FBS. The cytotoxicity was evaluated for incubation times of 24h, for pure astaxanthin and shrimp shell extract, and 4h, for blank-SLCs and for astaxanthin-loaded and extract-loaded NLCs and SLCs. It is more correct to perform the assays using 4h of incubation, since the average human intestinal transit time is around 4h ±1.4h [171]. Although, due to time constraints, the cytotoxicity assays of pure astaxanthin and shrimp shell extract could not be repeated using 4h as the incubation time. Nevertheless, if the compounds do not display cytotoxicity when incubated for 24h with the cells, then they will not display cytotoxicity when incubated for 4h with the cells, either [172].

The concentrations of the samples were considered cytotoxic according to the definition of cytotoxicity proposed by the International Organization for Standardization (ISO 10993-5), which states that a reduction in cell viability by more than 30% is considered a cytotoxic effect [173].

The results of these studies are presented in Figure 3.8 for pure astaxanthin, and astaxanthin-loaded NLCs and SLCs and in Figure 3.9 for shrimp shell extract and extract-loaded NLCs and SLCs and empty SLCs.

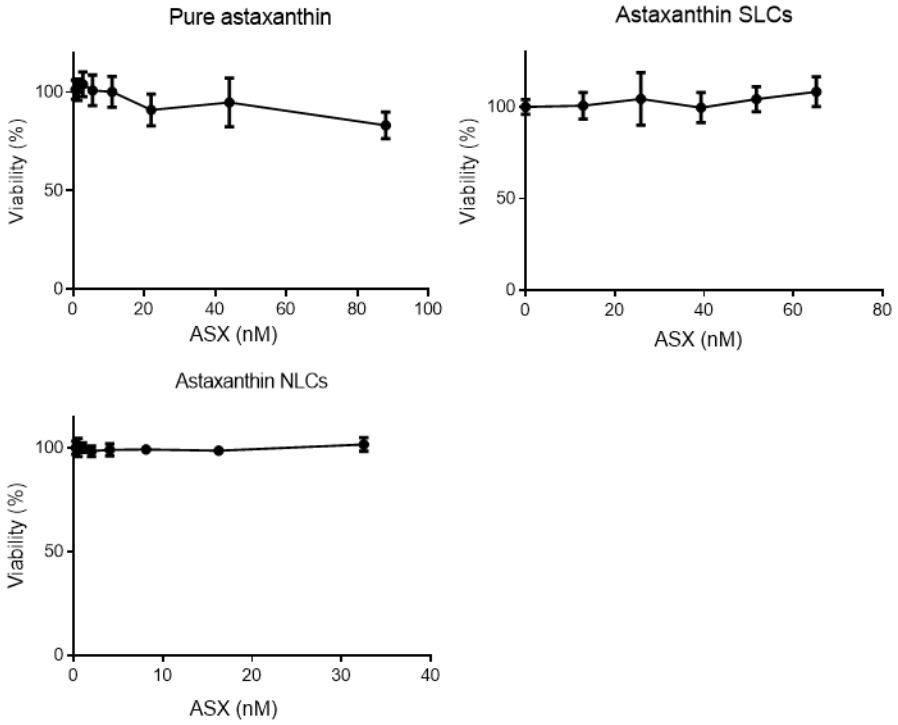

Figure 3.8- Cytotoxicity screening in Caco-2: pure astaxanthin (0.69 - 87.96 nM, 24h incubation); astaxanthin-loaded SLCs (0.25 - 32.50 nM; 4h incubation); astaxanthin-loaded NLCs (12.93 - 65.14 nM, 4h incubation). Results were obtained from at least three independent experiments performed in triplicate.

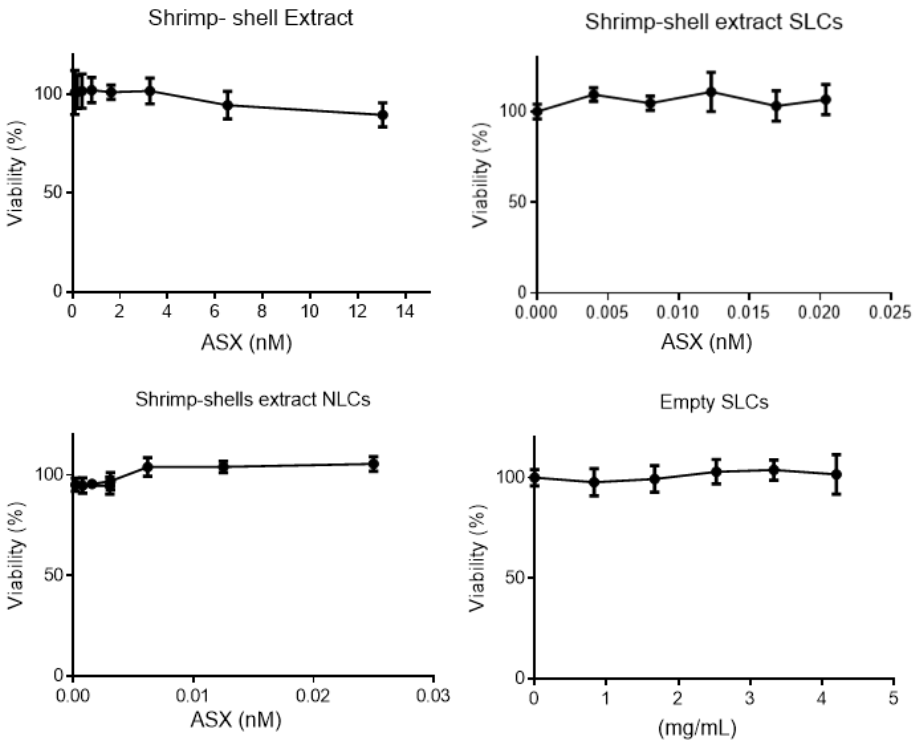

Figure 3.9- **Cytotoxicity screening in Caco-2:** shrimp shell extract (0.10 - 13.050 nM, 24h incubation); extract-loaded SLCs (4,00 pM - 0.02 nM, 4h incubation); extract-loaded NLCs (0.2 pM - 0.025 nM, 4h incubation); and blank-SLCs (0.82 - 4.2 mg/mL; 4h incubation). Results were obtained from at least three independent experiments performed in triplicate.

Pure astaxanthin (standard) was tested between 0.687- 87.96 nM, astaxanthin-loaded NLCs were tested between 0.25 - 32.50 nM, while astaxanthin-loaded SLCs were tested between 12.92 - 65.14 nM (Figure 3.8). Pure astaxanthin revealed a slight decrease on the cell viability with the increase of the concentration, but at the highest concentration tested the percentage of cell viability was 83.27%. Thus, it is possible to conclude that none of the concentrations tested of pure astaxanthin exhibited cytotoxicity. Similar results were obtained by Sangsuriyawong *et al.* who evaluated the cytotoxicity of an extract of astaxanthin in Caco-2, using MTT reagent , and the results revealed cell viability higher than 80% [66].

Shrimp shell extract was tested between 0.10 - 13.95 nM, extract-loaded SLCs were tested between 4.00 pM - 0.020 nM, and extract-loaded NLCs were tested between 0.20 pM - 0.025 nM (Figure 3.9). Regarding the shrimp shell extract, it revealed a slight decrease with the increase of the concentration, still, at the highest concentration tested the percentage of cell viability was 89.57%, thus none of the concentrations tested displayed cytotoxicity.

Particle cytotoxicity depends on many parameters, such as size, surface charge and composition, cell type, and incubation time. Regarding astaxanthin-loaded NLCs, none of the concentrations tested revealed to exhibit cytotoxicity, the same was verified for astaxanthin-loaded SLCs (Figure 3.8). Concerning the extract-loaded NLCs and extract-loaded SLCs, in both samples, none of the concentrations tested revealed to display cytotoxicity, furthermore, the cell viability remained close to 100% at the highest concentrations tested (Figure 3.9).

As for the blank-SLCs, which were tested in terms of mg of particles per milliliter of solution in culture medium with 0.5% FBS, the highest concentration tested did not reveal any cytotoxicity (Figure 3.9).

It should be noted that despite the both formulations of astaxanthin and extract not revealing a decrease in cell viability, it was verified that some concentrations tested of astaxanthin-loaded and extract-loaded SLCs led to cell viability above 100%. Similarly, for astaxanthin-loaded and extract-loaded NLCs both samples, with the increase of the concentrations, enhanced cell viability.

An enhanced cell viability can be caused by several factors: (1) the formulations have protective effects on the cells, promoting cell survival/proliferation, (2) interference of remaining particles in fluorescence readings, leading to an overestimation of cell viability, (3) the formulations are inducing production of intracellular ROS, which are known to promote cell proliferation, or (4) presence of remaining microorganisms in the particles due to ineffective sterilization, which may interfere with the Prestoblue® reagent [32,174,175]. It is worth mentioning, that the particles (NLCs and SLCs) revealed to be sterile, since contaminations did not occur in the sterility tests (data not shown).

Since none of the concentration tested of each sample revealed to cause cytotoxicity, the maximum concentrations of each sample will be used in the subsequent experiments.

3.3.2 Mitochondrial integrity evaluation

Oxidative stress can cause mitochondrial dysfunction, which results in functional loss. A major indicator of mitochondrial dysfunction is the disruption of the mitochondrial membrane potential (MMP). As already stated, astaxanthin has ROS scavenging activity and is able to activate antioxidant enzymes. Therefore, by inhibiting oxidative stress in cells, astaxanthin may suppress oxidative stress-induced mitochondrial dysfunction and mitochondrial ROS production.

Having as a future perspective to test the protective effect of astaxanthin against mitochondrial dysfunction in oxidative stress conditions, it was first tested if astaxanthin, the extract and respective formulations influenced the mitochondrial integrity when oxidative stress was not induced.

Thus, in this work, astaxanthin, shrimp shell extract and their respective formulations were tested to evaluate their influence on the mitochondrial function, by monitoring alterations in mitochondrial membrane potential (MMP). The alterations on the MMP were evaluated through mitochondrial inclusion of TMRE. The results of these studies are presented in Figure 3.10 for pure astaxanthin, astaxanthin-loaded NLCs and SLCs, and Figure 3.11 shrimp shell extract and extract-loaded NLCs and SLCs and empty SLCs.

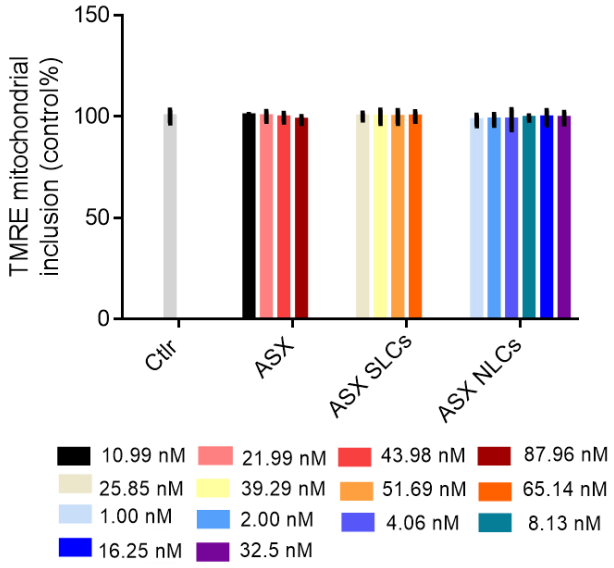

Figure 3.10- Effect of astaxanthin, astaxanthin-loaded NLCs and SLCs on the amount of TMRE incorporated within the mitochondria as a measure of mitochondrial membrane integrity, after 4h incubation. Data are expressed in percentage relative to the control (fluorescence of non-treated cells set to 100%). Results were obtained from at least three independent experiments performed in triplicate. The symbol * indicates significance relative to the control (* p-value<0.05; ** p-value<0.01, *** p-value<0.001, **** p-value<0.0001). The concentrations are expressed as mols of astaxanthin per milliliter of culture medium.

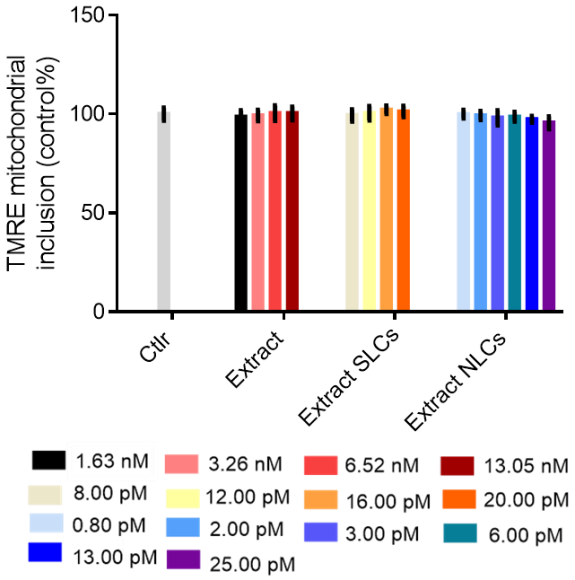

Figure 3.11- Effect of shrimp shell extract; extract-loaded NLCs and SLCs on the amount of TMRE incorporated within the mitochondria as a measure of mitochondrial membrane integrity, after 4h incubation. Data are expressed in percentage relative to the control (fluorescence of non-treated cells set to 100%). Results were obtained from at least three independent experiments performed in triplicate. The symbol * indicates significance relative to the control (* p-value<0.05; ** p-value<0.01, *** p-value<0.001, **** p-value<0.0001). The concentrations are expressed as mols of astaxanthin per milliliter of culture medium.

The results presented in Figure 3.10 and 3.11 reveal that for all the concentrations tested of each sample there was not a significant decrease on the TMRE mitochondrial incorporation relative to the control (p-value>0.05). Thus, astaxanthin, shrimp shell extract and their respective formulations did not alter the mitochondrial membrane potential (MMP), therefore none of the concentrations tested caused mitochondrial dysfunction. Similar results were obtained by Wolf *et al.*, whose results not only demonstrated that astaxanthin did not cause mitochondrial dysfunction but increased MMP. Likewise, Yu *et al.* also tested the mitochondrial inclusion of TMRE, and the results revealed that astaxanthin protected mitochondria from heat induced dysfunction [55,176]

Since there are reported evidences of mitochondrial dysfunction within the intestinal epithelium of patients with IBD, and since oxidative stress, which is known to cause mitochondrial dysfunction, is a sign of these diseases, it would be interesting to test the study samples (astaxanthin, extract and respective formulations) protective role against oxidative stress-induced mitochondrial dysfunction.

Nevertheless, since the mitochondrial function is crucial for the cell survival, this assay also provides an additional information on the toxicity of the samples, but this time on their possible toxic effects towards mitochondrial integrity. As a result, none of the concentrations tested, of each sample, affected the MMP, thus indicating that ATP depletion or decreased metabolic oxygen consumption did not occur. Furthermore, the study samples did not display toxic effects towards mitochondria to result in mitochondrial dysfunction. Thus, it is possible to conclude that none concentrations tested of each sample revealed to display toxicity towards mitochondria. Therefore, the maximum concentrations of each sample will be used in subsequent experiments.

3.3.3 *In vitro* permeability studies: Astaxanthin, shrimp shell extract, astaxanthin-loaded NLCs and SLCs, extract-loaded NLCs and SLCs

The bioavailability of a compound is highly influenced by its cellular uptake and transport across the intestinal epithelium. During process of development of formulated products, it is fundamental to assess their permeability in a model that is a good representation of the *in vivo* settings, in order to better predict its permeability *in vivo*.

Having developed and optimized two delivery systems (NLCs and SLCs) to improve the stability and bioavailability of astaxanthin and having tested the cytotoxicity of the formulations and

their influence on the mitochondrial integrity, the next step was to assess their ability to improve the cellular uptake and transepithelial transport of the entrapped compound, in *in vitro* cell models. The permeability and uptake of pure astaxanthin, astaxanthin entrapped in astaxanthin-loaded NLCs and SLCs, shrimp shell extract, and extract entrapped in extract-loaded NLCs and SLCs was evaluated using the Caco-2 monolayer cell model and the triple co-culture Caco-2:HT29-MTX:Raji-B cell model. The aim was to determine the cellular uptake and transepithelial transport of the free astaxanthin and of the bioactive entrapped in the two delivery systems. Furthermore, to assess the influence of the delivery systems on the uptake of the compound, by comparing the uptake of the free compound with that of the compound entrapped in the delivery systems. Also to assess the influence of the particle size of the delivery system on the permeability and uptake.

The concentrations of each sample tested were previously determined as non-cytotoxic and revealed to not influence mitochondrial integrity. For pure astaxanthin the concentration tested was 87.96 nM, for shrimp shell extract it was 20.00 pM (concentration of astaxanthin in the extract), for astaxanthin-loaded NLCs it was 32.50 nM and 16.25 nM, for astaxanthin-loaded SLCs it was 51.69 nM, for extract-loaded NLCs it was 25.00 pM and 13.00 pM, and for extract-loaded SLCs it was 16.00 pM.

Prior to the experiment, the cultures were equilibrated with HBSS and the transepithelial electrical resistance (TEER) values were stabilized. The measurement of the TEER provides a quantitative measure of the integrity and maturity of a monolayer. Prior, during and after the assay the TEER was monitored to evaluate the monolayer integrity. The TEER is influenced by the cell culture medium in the apical and basolateral compartment, by the membrane of the filter inserts and by the electrode interface. Since the permeability experiments were performed in HBSS, the TEER values tended to decrease relative to the TEER determined when the cells were in culture medium, still before the experiments all wells presented TEER values above 500 Ω cm^2.

The permeability studies were conducted for 4h (240 minutes), since it is known that the average human intestinal transit time is around 4h ± 1.4h [171]. The cells were incubated with the samples for 4h, and after this period the samples were removed. At first, it was used a protocol where after removing the samples new culture medium was added, and the cells were incubated for 24h, to assess if the cell monolayer was able to recuperate the normal TEER values (above 500 Ω cm^2), thus providing information on the integrity of the cell monolayer. However, some alterations were performed on this protocol. The new protocol is very similar to the previous one, the only difference being that after removing the samples, after the 4h incubation, HBSS was added, and the cells were incubated for 24h. The aim was to be able to collect a sample from the basolateral compartment to determine the amount of astaxanthin that had been released by the cells in that period. After this, the HBSS was removed and culture medium was added, and the cells were incubated for 24h, to be able to assess the cell monolayer integrity after the assay, just like performed in the old protocol. However, due to time constraints, these samples collected from the basolateral compartment 24h after the assay had begun were not analyzed by HPLC.

In Figure 3.12, it is presented the TEER values measured during the permeability assay in Caco-2 monocultures (A-B) and co-culture (C-D), to assess the permeability of pure astaxanthin, shrimp shell extract, astaxanthin-loaded SLCs and extract-loaded SLC. In Figure 3.13, it is presented TEER values measured during the permeability assays in the co-culture, to assess the permeability of astaxanthin-loaded NLCs and extract-loaded NLCs.

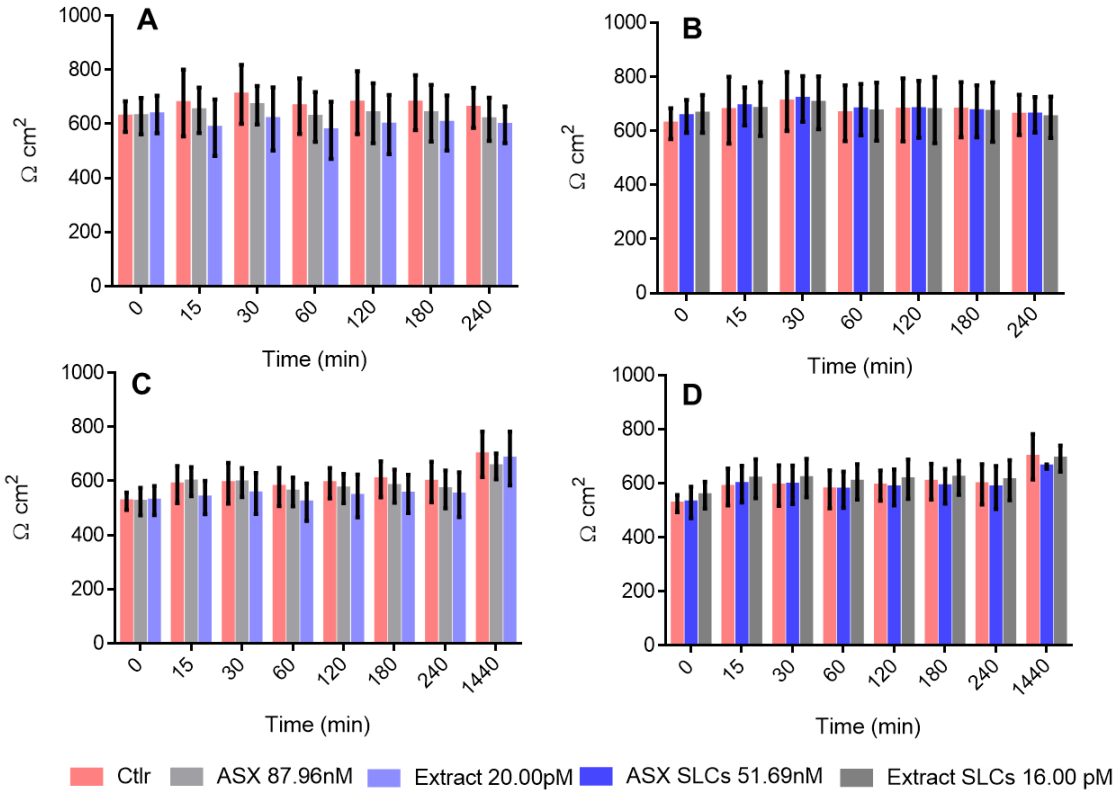

Figure 3.12- TEER values measured during the permeability assay in Caco-2 monoculture (A-B) and co-culture Caco-2:HT29-MTX:Raji-B (C-D). Permeability studies performed to assess the uptake and transport of astaxanthin in pure astaxanthin (87.96 nM), shrimp shell extract (20.00 pM), astaxanthin-loaded SLCs (51.69 nM) and extract-loaded SLC (16.00 pM). The concentrations are expressed as mols of astaxanthin per milliliter of HBSS. The values presented are a mean of 3 measurements per well from, at least, 2 independent experiment.

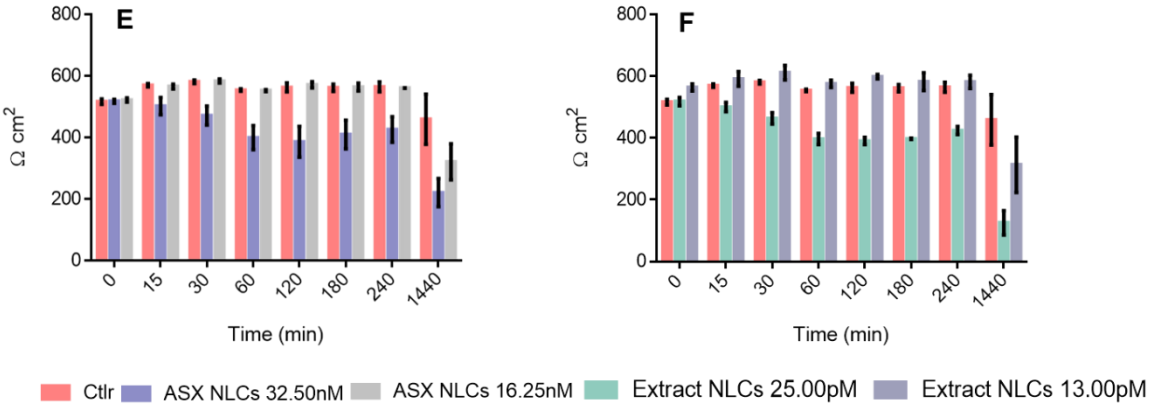

Figure 3.13- TEER values measured during the permeability assay in a co-culture Caco-2:HT29-MTX:Raji-B. Permeability studies performed to assess the uptake and transport of astaxanthin in astaxanthin-loaded NLCs (32.50 nM and 16.25 nM) and extract-loaded NLCs (25.00 pM and 13.00 pM). The concentrations are expressed as mols of astaxanthin per milliliter of HBSS. The values presented are a mean of 3 measurements per well from 2 independent experiment.

The TEER was measured after the permeability studies were concluded, in order to assess the monolayer integrity and assess if during the permeability assay the monolayer was damaged. For the

Caco-2 monoculture it was measured 24h after the assay had begun and for the co-culture it was measured 48h after the assay had begun. Figure 3.14 summarizes the TEER values measured before and after the permeability studies of pure astaxanthin, shrimp shell extract, astaxanthin-loaded SLCs and extract-loaded SLC in Caco-2 (A-B) and in the co-culture (C-D). Furthermore, Figure 3.15 summarize the TEER values measured before and after the permeability studies of astaxanthin-loaded NLCs and extract-loaded NLCs in the triple co-culture.

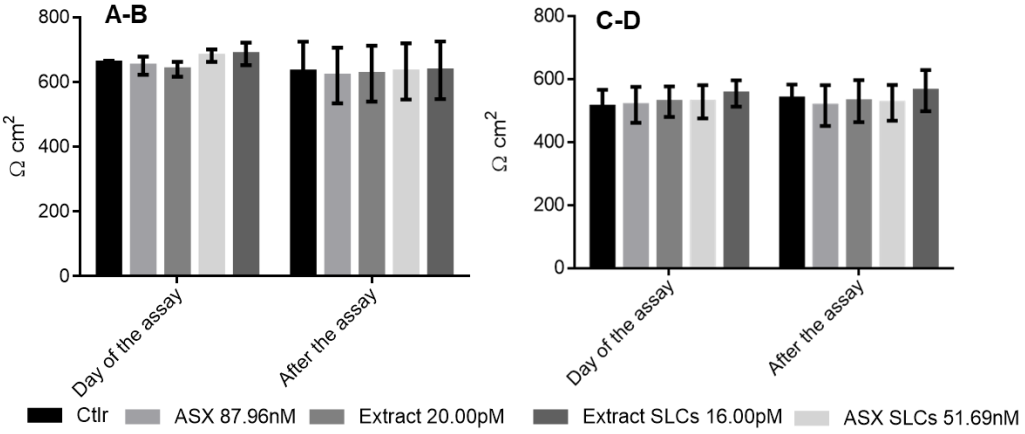

Figure 3.14- TEER values before and after the permeability assay in Caco-2 monoculture (**A-B**) and co-culture Caco-2:HT29-MTX:Raji-B (**C-D**)**.** Permeability studies performed to assess the uptake and transport of astaxanthin in pure astaxanthin (87.96 nM), shrimp shell extract (20.00 pM), astaxanthin-loaded SLCs (51.69nM) and extract-loaded SLC (16.00 pM). The values presented are a mean of 3 measurements per well from, at least, 2 independent experiment.

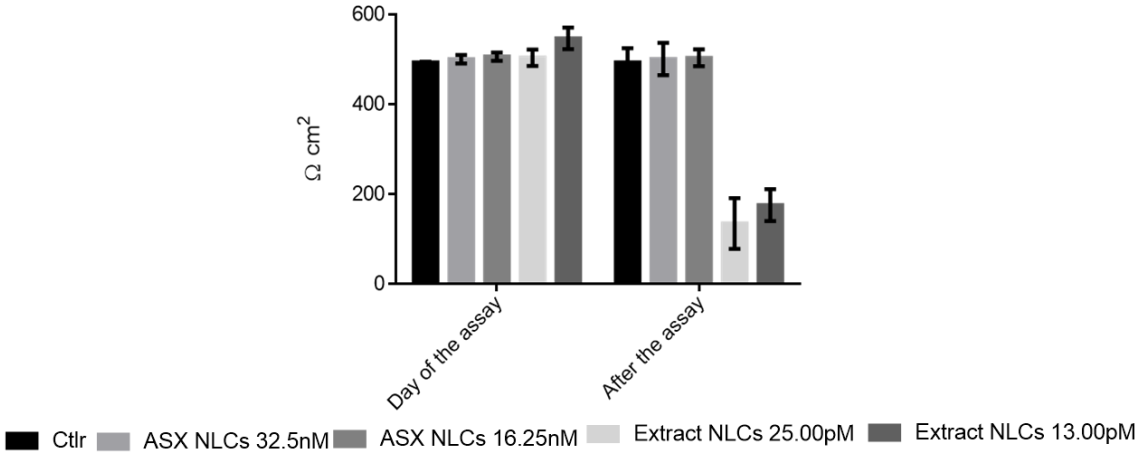

Figure 3.15- TEER values before and after the permeability assay in a co-culture Caco-2:HT29-MTX:Raji-B**.** Permeability studies performed to assess the uptake and transport of astaxanthin in astaxanthin-loaded NLCs (32.5 nM and 16.25 nM) and extract-loaded NLCs (25.00 pM and 13.00 pM). The concentrations are expressed as mols of astaxanthin per milliliter of HBSS. The values presented are a mean of 3 measurements per well from 2 independent experiment.

The TEER values increase with time and reach the highest values after 21 days in culture. One of the limitations of the Caco-2 monoculture model is the fact that the tight junction formed between cells are tighter than the ones found *in vivo* and this tightness limits the paracellular transport. This feature can be detected by the TEER values that tend to be higher than those observed *in vivo* [116,117,122,133]. Meanwhile the co-culture, that is composed by Caco-2, HT29-MTX and M-cells, is a better representation of the tightness found in the intestinal epithelium. The HT29-MTX, that despite being attached to Caco-2 cells through tight junctions, do not form tight junctions as tight as those

formed between Caco-2, hence more intercellular space exists between the cells. Owing to this, the co-culture monolayer reveals to be more permeable than the Caco-2 monoculture, since paracellular transport is not restricted, furthermore, the TEER values tend to be lower than those of the Caco-2 monoculture, and similar to what is found *in vivo* [116,117,122,133]. An increase in TEER values translates into a decrease in epithelial permeability, thus, Caco-2 monolayers should reveal lower permeabilities than the triple co-culture and the intestinal epithelium [116,117,122,133].

From the results presented in Figure 3.12 to 3.15, it is possible to verify that the TEER values measured in the Caco-2 monoculture were higher relative to those measured in the triple co-culture. This was expected since in the Caco-2 monoculture the tight junctions formed are very tight, which translates in a reduced permeability and high TEER values. In contrast, as explained, the tight junctions formed between Caco-2 and HT29-MTX are not as tight as the ones formed between Caco-2, thus translating in higher permeability and lower TEER values.

Concerning the TEER values measured, during the permeability assays, for the wells where pure astaxanthin, extract and the SLCs formulations were tested (Figure 3.12), it is possible to verify that there were no major alterations on the TEER values of each well, in both cell models. It is known that when paracellular transport occurs there is a decrease in the TEER values, since the tight junctions open [116,122]. Although if the transport route is transcellular the TEER values do not decrease.

Regarding the TEER values measured, during the permeability assays, for the wells where the NLCs formulations were tested (Figure 3.13), it is possible to verify that there was a decrease over time of the TEER values in the wells where the highest concentrations of astaxanthin-loaded (32.25 nM) and extract-loaded (25.00 pM) NLCs were tested. This decrease in the TEER values may indicate that paracellular transport occurred. In addition, there was a severe decrease between the values measured at 240 min and 1440 min. Nonetheless, after last the time point, 1440 min, the HBSS was removed and culture medium was added to the cell culture, to analyze the recuperation of cell culture (assess the integrity of the cell monolayer after the assay) (Figure 3.15). From the results, there was not a recuperation of the TEER values on the wells where the extract-loaded NLCs were added, since the final TEER values were much lower than the values measured before the assay, and lower than 500 Ω cm^2. Additionally, when the cell monolayer was observed through the microscope it was verified that the monolayer was not intact, since parts of it were missing, indicating that perhaps cell death occurred. Thus, these findings indicate that extract-loaded NLCs induced stress on the cells and damaged the cell monolayer (Figure 3.15).

Finally, after the permeability study was concluded the TEER was measured in order to assess the integrity of the cell monolayer and to assess if during the permeability study any damage to the cell monolayer had occurred (Figure 3.14 and 3.15). From the results, apart from the wells where extract-loaded NLCs were added and where the final TEER was very low (indicating that the monolayer was not intact), the samples did not damage the cell monolayer, since the final TEER measured was very close to the values obtained before the permeability study and above 500 Ω cm^2, thus indicating that the monolayer was intact (Figure 3.14 and 3.15).

After the permeability studies were concluded, the samples that were collected throughout the experiment were analyzed through HPLC, and the content in astaxanthin was determined. Subsequently, the cellular uptake and transepithelial transport of astaxanthin were determined. The transepithelial transport was determined by analyzing, through HPLC, the samples collected from the basolateral compartment at the end of the experiment (240 min). Due to time constraints and because of the unavailability of equipments (mass spectrometer) the cellular uptake was not determined. Instead it was determined an approximation of the cellular uptake, which was determined by subtracting the initial (0 min) amount of astaxanthin added to the amount present in the samples collected, at the end of the experiment (240 min), from the apical and basolateral compartments. This is only an approximation, since it does not take in account the degradation and metabolization that the study compound can undergo in the media and once inside the cells. Further studies, with an adequate lysis protocol and using a more sensitive quantification method than the one used (HPLC) in this work, should be performed in order to quantity the cellular uptake of astaxanthin.

In Table 3.8, it is presented the results obtained for the estimation of the cellular uptake and transepithelial transport, it is worth mentioning that the results are the mean of at least two independent experiments.

Since the shrimp shell extract had very low amount of astaxanthin in some samples it was not detected any amount of astaxanthin and in others the amount detected was below the detection limit

of the method. Thus, the results regarding the shrimp shell extract, extract-loaded NLCs and SLCs analyzed will not be discussed. In the future, the analysis of these samples should be repeated using a more sensible technique, such as mass spectrometer.

Table 3.8- Astaxanthin, astaxanthin-loaded NLCs and astaxanthin-loaded SLCs permeability studies in Caco-2 monoculture and triple co-culture Caco-2:HT29-MTX:Raji-B: Estimated cellular uptake and transepithelial transport.

	Sample	Initial concentration (nM)	Particle Size	Cellular uptake estimation (%)	Transepithelial transport (%)
Caco-2	Astaxanthin	87.96	---	43.19 ± 1.94	n.d.
	ASX SLCs	51.69	1.50-20.00 µm	54.92 ± 2.15	n.d.
Triple co-culture	Astaxanthin	87.96	---	53.88 ± 1.35	<LOQ
	ASX SLCs	51.69	1.50-20.00 µm	62.87 ± 3.13	<LOQ
Triple co-culture	ASX NLCs	32.50	365.433 ± 12.101 nm	75.08 ± 2.12	<LOQ
	ASX NLCs	16.25	365.43 ± 12.10 nm	76.34 ± 3.83	<LOQ

N.B: The concentrations are expressed as mols of astaxanthin per milliliter of culture medium.
Values are mean ± standard deviation of, at least, 2 independent experiments;
n.d.- not detected; LOQ- Quantification limit of the method

The uptake and transport route of a compound and delivery system depends on several factors such as, size, surface charge and hydrophilicity. Moreover, the presence of M-cells is reported to influence the absorption of nanoparticles. M-cells are regarded as potential portals for particles transcytosis [177].

Regarding the transepithelial transport, it was only detected the presence of astaxanthin on the samples collected from the experiments where the Caco-2:HT29-MTX:Raji-B model was used. Although a small peak was visible at the retention time expected for astaxanthin (Appendix 4 - Figure 6.7) the results obtained were below the quantification limits of the method, thus the content of astaxanthin could not be determined. The fact that it was only detected astaxanthin in samples belonging to the experiments where the triple co-culture was used, imply that the transepithelial transport was higher in the triple co-culture than in the monoculture. This finding may be related to the increased permeability in the triple co-culture, due to the decrease in tight junction stickiness which translate in lower TEER values comparatively to the monoculture and to the presence of M-cells, which are known for their high transcytotic capacity (Figure 3.12).

As already mentioned, the cellular uptake was not determined. Instead, it was performed an estimation of the cellular uptake, it should be noted that no conclusive analysis can be performed using these results, and these are only indicative.

Permeability studies with pure astaxanthin and astaxanthin-loaded SLCs were conducted in Caco-2 and in the triple co-culture Caco-2:HT29-MTX:Raji-B. Although for both samples and in both cell models there was not a decrease in the TEER during the permeability assays, the results from the estimation could indicate that cellular uptake occurred (Table 3.8).

Considering the cellular uptake estimations, the estimated cellular uptake of astaxanthin in the experiments where pure astaxanthin was tested was 10% higher (p-value<0.0001) in the triple co-culture relative to the Caco-2 monoculture. This increase in the cellular uptake might be related to the presence of M-cells, which are known to possess high transcytotic capacity. The increase in permeability, as already explained, is due to the decrease in the tightness of tight junctions, which promotes paracellular transport. The higher permeability was confirmed through the lower TEER values measured in the co-culture, relative to the monoculture (Figure 3.14) [116]. Moreover, these estimated results are corroborated by several other authors, who reported a higher permeability in the triple co-culture relative to the monoculture [116,130,135,178].

In regard to the estimated cellular uptake of astaxanthin in the experiments where astaxanthin-loaded SLCs were tested, the results show that the uptake was significantly higher (p-value< 0.001) than the estimated uptake verified for pure astaxanthin. Indicating that an enhanced cellular uptake of astaxanthin via the SLCs delivery system could occur. This was observed in both cell models. Similar results were obtained in the experiments where astaxanthin-loaded NLCs were tested, where the estimated cellular uptake of astaxanthin increased 21% relative to the experiments where pure astaxanthin was tested. Thus, it could be inferred that the entrapment of astaxanthin into the SLCs and NLCs significantly improves (p-value<0,0001 and p-value<0,0001, respectively) its uptake comparatively to the pure astaxanthin. Results obtained in *in vivo* tests (rats) performed by Meor *et al*. revealed that the encapsulation in microparticles (8.90 μm) and nanoparticles (128 nm) significantly increased astaxanthin bioavailability relative to the free compound [179].

Even though the SLCs had high particle size, between 1.5-20 μm, cellular uptake could still have occurred. Particles up to 10 μm in diameter can only be taken up by phagocytes (macrophages, dendritic cells, and the like) or by M-cells [71,75,112]. In the monoculture model phagocytes were not represented nor were M-cells. Hence, it is hypothesized that only the smaller sized particles were taken up by the cells. Since the size range was not determined precisely (since it was determined through SEM analysis) and a size distribution (PDI) was not provided, it is possible that the powder of microparticles obtained consisted mostly of smaller sized particles and, also, particles smaller than 1.5 μm may exist, but were not observed in the SEM micrographs. The fact that the powder of microparticles might have consisted mostly of smaller sized particles explains the high cellular uptake obtained. Furthermore, Desai *et al.* demonstrated that particles up to 10 μm were taken up by Caco-2 cells [180]. Additionally, the author confirmed that the particle size influences the uptake of particles, since particles with 0.1 μm had significantly higher uptake than particles with 10 μm [180].

Furthermore, it was observed that in the experiments where astaxanthin-loaded SLCs were tested, the estimated cellular uptake of astaxanthin was 8% higher in the co-culture relative to the Caco-2 monoculture. This increase might be related to the presence of M-cells, which are reported to be the main site of uptake of particles. Results reported by Antunes *et al.* regarding the uptake of nanoparticles, showed an increase of the cellular uptake of nanoparticles (550 nm) in the triple co-culture, comparatively to the monoculture [116]. All in all, it is hypothesized that the entrapment of astaxanthin in SLCs could constitute a potential vehicle for the delivery of astaxanthin to the intestinal epithelium.

When comparing the estimated cellular uptake of astaxanthin observed for astaxanthin-loaded NLCs and astaxanthin-loaded SLCs, it is clear that the estimated cellular uptake verified for astaxanthin loaded NLCs is significantly higher (p-value<0,001) than the estimated uptake for astaxanthin-loaded SLCs. There are several explanations for this increase in the uptake with the decrease in the particle size: (1) smaller particles have a larger surface area and may be digested faster by digestive enzymes so that their contents are released and absorbed more easily;(2) smaller particles may penetrate the mucous layer that covers the cell monolayer, thus increasing their residence time and bringing them closer to the site of absorption; (3) smaller particles may directly undergo transepithelial transport through paracellular or transcellular mechanisms; (4) the water solubility of highly lipophilic components increases as the particle size decreases, thus improving their absorption [181]. From the results, while there was a decrease on the TEER values for the astaxanthin-loaded NLCs, which may indicate that paracellular transport occurred, the same was not observed for the SLCs, where no significant decrease was verified (Figure 3.12 and 3.13). This difference in the estimated cellular uptake could be due to paracellular transport occurring for the NLCs sample.

The results obtained for the estimated cellular uptake of astaxanthin-loaded NLCs and SLCs might indicate that the uptake is size-dependent, since smaller particles exhibited a greater cellular uptake of astaxanthin when compared to larger particles. This hypothesis has been demonstrated by many authors. Findings reported by Schimpel *et al.* support this claim, the author tested the permeability of nanoparticles of 50 and 200 nm in Caco-2 monoculture and in the Caco-2:HT29-MTX:M-cells co-culture [135]. First the author verified that the cellular uptake increased in the triple co-culture compared to the monoculture, and then verified that the cellular uptake of nanoparticles of 50 nm was higher than the uptake of nanoparticles of 200 nm [135]. Rieux *et al.* tested the permeability of 200 and 500 nm nanoparticles in Caco-2:M-cells co-culture and verified that the transport of 200 nm nanoparticles was seven times higher than that of 500 nm nanoparticles. Moreover, Anarjan *et al.*

proposed that the large surface area of small particles may allow for efficient digestion and easier absorption [181].

Other authors have reported cellular uptake of astaxanthin and formulations of astaxanthin, but to this author's best knowledge, this is the first work where it is reported the permeability studies of astaxanthin and formulations of astaxanthin in a triple co-culture Caco-2: HT29-MTX:Raji-B [66,68,179,181,182].

All in all, considering this estimated cellular uptake, astaxanthin-loaded NLCs were the system that allowed the highest cellular uptake of astaxanthin and it is possible to presume that the NLCs may be a better delivery system to increase the uptake of astaxanthin in the GIT. Nevertheless, SLCs also demonstrated to be a possible delivery system to increase uptake of astaxanthin in the GIT since they increased astaxanthin estimated uptake comparatively to pure astaxanthin.

Future studies should be performed to confirm these results and the analysis where the estimated cellular uptake was used.

3.3.4 Evaluation of the antioxidant activity of astaxanthin, shrimp shell extract and formulations: cell-based assay

The antioxidant activity of astaxanthin has been widely studied using chemical-based assays, such as TBARs, DPPH radical-scavenging assay, lipid peroxidation inhibition assay, lipophilic α-Tocopherol Equivalent Antioxidant Capacity (α-TEAC) assay, among others [183]. Unlike chemical antioxidant assays, which because of their simplicity have considerable limitations concerning the prediction of the antioxidant activity in a physiological environment, cellular antioxidant assays encompass some of the complexity of biological systems, namely cellular uptake of the tested compounds, subcellular location, and metabolism [184].

Having produced nano and microformulations of astaxanthin and the shrimp shell extract, tested their cytotoxicity, and estimated the cellular uptake of astaxanthin entrapped in the delivery systems, next their antioxidant activity was tested, to assess if the delivery systems enhanced the antioxidant activity of the study sample. Therefore, in this work pure astaxanthin, shrimp shell extract, and the respective formulations (NLCs and SLCs) were tested to assess their antioxidant activity through cell-based assays using the Caco-2 cell line. First the capacity of the samples to inhibit intrinsic ROS production was evaluated. Then, their capacity to inhibit the exogenous ROS, in an oxidative stress situation, was evaluated.

3.3.4.1 Inhibition of Intrinsic ROS Production

The highest concentration and subsequent dilutions of each sample were used in the cellular antioxidant activity assays. Caco-2 were pre-incubated with the samples, and their capacity to inhibit intrinsic ROS production was evaluated. The results obtained for astaxanthin, astaxanthin-loaded NLCs and SLCs are presented in Figure 3.16, while the results of the shrimp shell extract, extract-loaded NLCs and SLCs are presented in Figure 3.17.

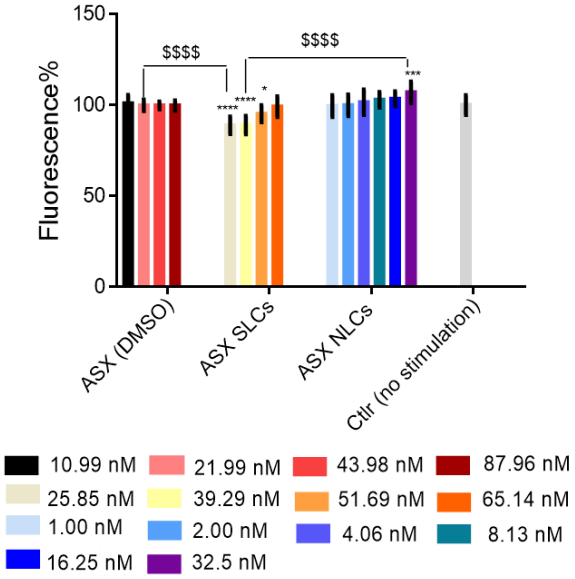

Figure 3.16- Pre-incubation of cells with astaxanthin, astaxanthin-loaded NLCs and SLCs for 4h- effect on intrinsic ROS generation. The symbol * indicates significance relative to the control (* p-value<0.05, ** p-value<0.01, *** p-value<0.001, **** p-value<0.0001). Similar concentrations of different samples were compared and $ indicates significance relative to each other ($ p-value<0.05, $$ p-value<0.01, $$$ p-value<0.001, $$$$ p-value<0.0001). Results were obtained from at least two independent experiments performed in triplicate. The concentrations are expressed as mols of astaxanthin per milliliter of culture medium.

None of the concentrations tested of pure astaxanthin revealed to cause any significant change on the fluorescence relative to the control, these results indicate that the bioactive did not inhibit the production of intrinsic ROS (Figure 3.16). However, contradictory results were obtained by Wolf *et al.* who incubated He-La cells with 800 nM of astaxanthin for 2 days, and whose results revealed that astaxanthin was able to inhibit the production of intrinsic ROS [55]. A possible explanation concerning the results obtained for astaxanthin, in this work, is related to the fact that the highest concentration tested was only 87.96 nM, and perhaps a relevant amount of astaxanthin, to cause a significant decrease in the fluorescence (i.e. decrease in the levels of ROS) relative to the control, was not taken up by the cells.

Regarding astaxanthin-loaded SLCs it is possible to observe that the three lowest concentrations tested (25.85 nM, 39.29 nM and 51.69 nM) revealed to significantly decrease the fluorescence relative to the control (p-value<0.0001 for the two lowest and p<0.05 for 51.69 nM), thus revealing an inhibition of the intrinsic ROS production (Figure 3.16).

When comparing similar concentrations of astaxanthin in the pure astaxanthin sample (21.99 nM) with the astaxanthin-loaded SLCs sample (25.85 nM), the results indicate that the levels of ROS obtained for astaxanthin-loaded SLCs were significantly lower (p-value<0.0001) than those obtained for the pure astaxanthin. These results might reveal that the delivery system allowed astaxanthin to permeate the cell membrane, and once inside the cells, the bioactive was able to inhibit the production of intrinsic ROS. Moreover, lower concentrations of astaxanthin in the formulated astaxanthin sample (e.g. 25.85 nM) were able to significantly inhibit the production of intrinsic ROS, while higher concentrations of pure astaxanthin (e.g. 87.96 nM) did not reveal any alterations relative to the control. According to the estimated cellular uptake determined in the permeability studies, SLCs might have improved the uptake of astaxanthin (Section 3.3.3). Still, this improvement would not justify the fact that the lowest concentration tested of astaxanthin-loaded SLCs (25.85 nM) would decrease the levels of ROS, but the highest concentration tested of pure astaxanthin (87.96 nM) would not.

Nevertheless, a possible explanation for the decrease in the levels of intrinsic ROS when treating cells with astaxanthin-loaded SLCs is that the components of the delivery system, specifically the olive oil, which is known to contain antioxidant molecules, could be exerting antioxidant effects. This theory is supported by findings of Puglia *et al.* and Pinto *et al.*, both authors reported that blank

NLCs exhibited antioxidant activity [185,186]. The first author, Puglia *et al.*, produced blank-NLCs where sesame oil was used [185]. Pinto *et al.* produced NLCs using different vegetable oils, such as olive oil, sunflower oil and oil, and in all cases the blank-NLCs exhibited intrinsic antioxidant activity [186]. Further studies should be performed to assess the antioxidant activity of blank SLCs.

Nonetheless, it is possible to verify that with the increase of the concentration of astaxanthin-loaded SLCs there is an increase in the production of ROS. Still the highest concentration tested did not increase the production of ROS above the control. A possible explanation for this increase is that higher concentrations of the delivery system (its components) might start to induce stress in the cells, and this stress (production of ROS) might start to annul the antioxidant effect of astaxanthin or of the antioxidants present in olive oil (liquid lipid used). Thus, at the highest concentration tested the production of ROS might have overpowered the antioxidant activity of astaxanthin or of antioxidants of olive oil, hence the levels of ROS were not significantly different from the control. Another possible explanation is related to the fact that astaxanthin at high concentrations might be inducing the production of ROS. Indeed, the results obtained by Niu *et al.* showed that astaxanthin can lead to the production of trace amounts of ROS, instead of directly quenching them [38]. Moreover, the author speculated that astaxanthin by producing trace amounts of ROS is activating the antioxidant pathway (Nrf-2/ARE) [38]. Further studies should be performed in order to ascertain the results obtained and to ascertain if the increase in the level of ROS is caused by the delivery system or by the increase of intracellular astaxanthin.

On the contrary, astaxanthin-loaded NLCs increased the levels of ROS instead of decreasing them (Figure 3.16). The lower concentrations of astaxanthin-loaded NLCs tested, might not allow the delivery of relevant amounts of astaxanthin to cause a significant decrease or increase in the level of ROS relative to the control. Furthermore, the highest concentration tested was the only concentration that increased significantly the level of ROS relative to the control. This observation could be explained if the concentrations of astaxanthin-loaded NLCs, although determined as non-cytotoxic, were inducing some stress in the cells. This highest concentration of astaxanthin-loaded NLCs might allow the permeation of an amount of astaxanthin that induces the production of ROS. Also, at this concentration the delivery system might be inducing ROS production. Both theories should be evaluated in future studies.

All in all, since these results were unexpected, considering what it is reported in the literature for the antioxidant activity of astaxanthin, the experiments should be repeated [10,11,14,50,187,188]. Additionally, it should be assessed whether if the intracellular astaxanthin or the delivery systems (or both) are inducing ROS production.

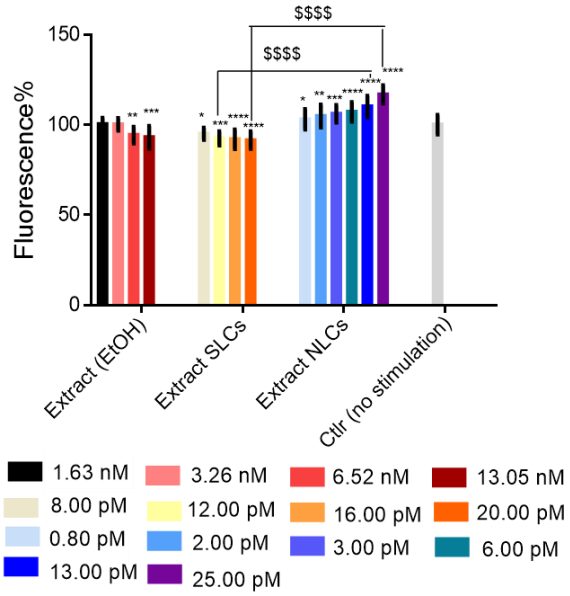

Figure 3.17- Pre-incubation of cells with shrimp shell extract, extract-loaded NLCs and SLCs for 4h-effect on intrinsic ROS generation. The symbol * indicates significance relative to the control (* p-value<0.05, ** p-value<0.01, *** p-value<0.001, **** p-value<0.0001). Similar concentrations of different samples were compared and $ indicates significance relative to each other ($ p-value<0.05, $$ p-value<0.01, $$$ p-value<0.001, $$$$ p-value<0.0001). Results were obtained from at least two independent experiments performed in triplicate. The concentrations are expressed as mols of astaxanthin per milliliter of culture medium.

Regarding the results obtained for the shrimp shell extract (Figure 3.17) there was a decrease in the levels of intrinsic ROS with the increase of the concentration of the extract. Moreover, the two highest concentration tested (6.52 nM and 13.05 nM) revealed a significant decrease relative to the control. These results indicate that the extract is composed of molecules with antioxidant activity that can permeate the cell membrane and inhibit the production of endogenous ROS. The fact that the extract is composed by compounds other than astaxanthin, such as other carotenoids, which are reported to exhibit antioxidant activity, and the fact that these must have a higher cellular uptake than astaxanthin, explains how the extract, that has lower amounts of astaxanthin, exhibited antioxidant activity while the pure astaxanthin sample did not (Figure 3.16).

Concerning the extract-loaded SLCs there was a significant decrease of the levels of ROS with the increase of the concentration (Figure 3.17). Even the lowest concentration tested revealed to significantly lower the levels of ROS relative to the control. At the highest concentration tested the fluorescence percentage was 91.49 ± 4.85%, while for the extract (not formulated) at the highest concentration tested the percentage was 93.05 ± 6.25%. These results display small differences with no significant difference (p-value>0.05). Thus, in the SLCs sample a lower concentration of extract is able to produce the same decrease in the levels of ROS as a higher concentration of extract in the non-formulated sample. This might indicate that there are some molecules in the extract that are not able to permeate the cell membrane, and that the SLCs allow their permeation into the cells, where they will exert their antioxidant activity. Moreover, the extract entrapment might increase its cellular uptake, thus allowing a higher amount of antioxidant molecules to be delivered into the cell. These results showed that the SLCs improve the absorption of the extract, thus improving its antioxidant activity. Nevertheless, as already mentioned the antioxidant molecules present in the olive oil, which composes the SLCs, might also be exerting antioxidant activity, so it is important to test the antioxidant activity of blank-SLCs.

When comparing astaxanthin-loaded SLCs with extract-loaded SLCs, it was observed that the lowest concentrations of astaxanthin-loaded SLCs provided a higher decrease in the levels of ROS (Figure 3.16 and 3.17). Additionally, unlike what was observed for astaxanthin-loaded SLCs, in the experiments where extract-loaded SLCs were tested there was a decrease in the level of ROS with the increase of the concentration. Thus, these findings could indicate that higher concentrations of

particles do not induce stress on the cells, since in both cases the same amount of particles was tested (it is worth mentioning that when testing SLCs, these were weighed and then culture medium was added and for astaxanthin- and extract-loaded SLCs the same amount of particles was weighted). So perhaps in the higher concentrations tested of astaxanthin-SLCs, astaxanthin was, indeed, inducing the production of ROS. Nevertheless, these hypotheses should be confirmed by testing the antioxidant activity of blank-SLCs.

The extract-loaded NLCs increased intrinsic ROS levels instead of decreasing them (Figure 3.17). Even the lowest concentration tested revealed significantly higher (p-value<0.05) percentage of fluorescence relative to the control.

Regarding the increase of the levels of ROS observed in the extract-loaded and astaxanthin-loaded NLCs, this increase might be explained by the fact that even if the NLCs formulations were not found to be cytotoxic or to cause mitochondrial dysfunction they might still induce stress in the cells. The results suggested that the NLCs induced stress by increasing the production of ROS. Actually, one of the toxicity mechanisms of particulate systems is the induction of ROS production through several mechanisms, to a degree depending on inherent characteristics of the particles and cells [32,189,190].

In fact, Doktorovová *et al.* reported that the treatment with solid lipid nanoparticles (SLNs) led to the production of higher levels of ROS but did not decrease the cell viability. Furthermore, the author demonstrated that the treatment with SLNs increased the activity of antioxidant enzymes such as GST and Gpx, which its increase is an indication of oxidative stress [189]. Moreover, similar results were obtained by Shanmugapriya *et al.*, who tested astaxanthin nanoemulsions on HT29 and AGS cell lines and verified that the levels of ROS increased with the concentrations of the sample [81].

On the other hand, DCFH-DA is known to be susceptible to some interferences, being able to undergo auto-oxidation which leads to increased fluorescence intensity of the resulting higher quantity of DCF [189].

Nonetheless, the results obtained in the cytotoxicity studies provide indications that the NLCs might have been increasing the ROS production, since with the increase of concentration of the particles (for astaxanthin and extract) there was an enhancement of the cell viability, which can be attributed to the fact the production of intracellular ROS promotes cell proliferation [173,174]. In addition, in the permeability studies it was confirmed that the two highest concentrations tested of extract-loaded NLCs induced stress on the cells, since the cell monolayer was not able to recuperate the normal TEER values (above 500 Ωcm^2), thus indicating that it was not intact (Figure 3.17). However, the two highest concentrations tested of astaxanthin-loaded NLCs showed to not have damaged the cell monolayer, since the monolayer was able to recuperate the normal values of TEER (Figure 3.17). This can be related to the fact that astaxanthin-loaded NLCs did not increase the levels of ROS as much as the extract-loaded NLCs, as can be observed from Figure 3.16 and 3.17. Moreover, only the highest concentration tested of astaxanthin-loaded NLCs induced ROS production.

It is important to mention that the particles, NLCs and SLCs, were sterilized using UV light, which is known to cause lipid oxidation. Thus, if the lipids that compose the particles were oxidized, radicals were produced, which in turn could react with the cell components. This phenomenon can contribute to the ROS production observed for the NLCs.

Regarding extract-loaded NLCs, perhaps the particulate system of the extract-loaded NLCs was inducing the production of ROS to a higher degree than the particulate system of astaxanthin-loaded NLCs. Moreover, the particles of extract-loaded NLCs and astaxanthin-loaded NLCs might have different surface charge. Possibly the surface charge of the extract-loaded NLCs might be more positively charged than the astaxanthin-loaded NLCs. It is reported that cationic nanoparticles increase the levels of ROS to a higher degree than anionic or neutral particles [32,191].Further studies need to be performed to confirm these theories.

So it is possible to conclude that the NLCs, even though they did not show cytotoxicity (Section 3.3.1) and did not influence the MMP (Section 3.3.2), they were found to exhibit toxicity through the increase of ROS production. The particle size must influence the toxicity of the particles, since the NLCs revealed to exhibit toxicity through the induction of ROS production, while SLCs did not reveal any toxicity.

3.3.4.2 Protection against an Oxidative Stress Inducer – TBHP

In order to assess the protective effects against oxidative stress of astaxanthin, shrimp shells extract and respective formulation towards enterocytes, studies were performed using an oxidative stress inducer tert-Butyl hydroperoxide (TBHP). Unlike H_2O_2, TBHP is more stable and forms more stable radical species. Studies indicate that TBHP can cause lipids peroxidation, alkylation of proteins and DNA and alterations in cellular calcium and glutathione levels [182].

The highest concentration and subsequent dilutions of each sample were used in the cellular antioxidant activity assays.

The effect of the samples against TBHP-induced ROS generation was evaluated in two different conditions: pre-incubation of the cells with the samples prior to addition of the stress inducer (TBHP), and co-incubation of the samples with the stressor. While, pre-incubation might reveal the preventive action of the samples, co-incubation is more representative of a potential therapeutic approach.

Initially, a concentration of TBHP considered non-toxic for the cells was determined through the cytotoxicity studies (data not shown) and concentration 4.10 µM was selected.

3.3.4.2.1 Pre-incubation prior to stress induction

In the pre-incubation approach the cells were incubated for 4h with the samples (astaxanthin, astaxanthin-loaded NLCs and SLCs and shrimp shell extract, extract-loaded NLCs and SLCs) prior to the induction of stress with TBHP (Figure 3.18 and 3.19).

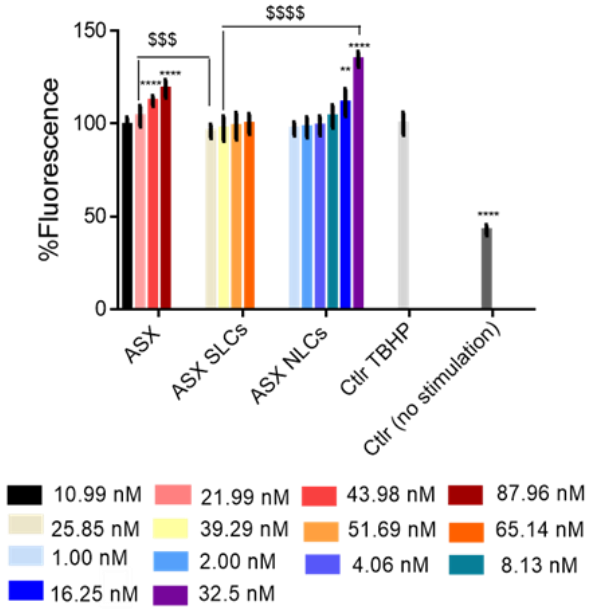

Figure 3.18- Pre-incubation of cells with astaxanthin, astaxanthin-loaded NLCs and SLCs for 4h-effect on total ROS generation. The symbol * indicates significance relative to the TBHP control (* p-value<0.05, ** p-value<0.01, *** p-value<0.001, **** p-value<0.0001). Similar concentrations of different samples were compared and $ indicates significance relative to each other ($ p-value<0.05, $$ p-value<0.01, $$$ p-value<0.001, $$$$ p-value<0.0001). Results were obtained from at least two independent experiments performed in triplicate. The concentrations are expressed as mols of astaxanthin per milliliter of culture medium.

While none of the concentrations tested of pure astaxanthin (Figure 3.18) revealed an inhibition of the production of intrinsic ROS nor did they increase the levels of ROS, the pre-incubation of the cells with astaxanthin prior to addition of the stress inducer revealed that astaxanthin increased the levels of ROS (Section 3.3.4.1). The two highest concentrations tested (43.98 and 87.96 nM) revealed significantly higher (p-value<0.001) levels of ROS comparatively to the TBHP control. Nonetheless, some authors have reported that astaxanthin does not directly scavenge ROS, but instead it acts by

activating antioxidant signaling pathways, such as Nfr-2/ARE pathway. Wolf *et al.* reported that the pre-incubation with astaxanthin prior to stress induction did not decrease the levels of ROS on HeLa and Jurkat cell lines. Furthermore, the author hypothesized that the antioxidant effects of astaxanthin were not due to the scavenging of free radicals but due to the reduction of endogenous oxidative stress and to the maintenance of the mitochondrial membrane potential [55]. Moreover, Wang *et al.* found that the antioxidant effects of astaxanthin were through upregulation of HO-1 expression via the ERK1/2 pathway in SH-SY5Y cells [192]. Likewise, Niu *et al.* proved that astaxanthin produced trace amounts of ROS instead of directly quenching them. The author theorized that the trace amounts of ROS produced by astaxanthin might act as secondary signals to activate the antioxidant pathway, since trace amounts of ROS activate the Nfr-2/ARE signal pathway, which will lead to the expression of phase II detoxifying antioxidant enzymes [38,40]. Furthermore, the results of other authors support the theory that astaxanthin induces the production of trace amounts of ROS to activate the Nfr-2/ARE signal pathway [40,193].

In this work it is hypothesized that perhaps astaxanthin is inducing ROS production in order to activate the Nfr-2/ARE signaling pathway. Thus, with the increase of the concentration of astaxanthin there is an increase in the level of ROS, since more molecules of astaxanthin are producing these molecules. Further studies need to be performed to confirm this hypothesis, to repeat the assays to confirm the results and also to assess if astaxanthin is able to scavenge ROS directly or if its antioxidant effect is only through the activation of antioxidant pathways.

Regarding, the astaxanthin-loaded SLCs none of the concentrations tested showed significant difference relative to the control (Figure 3.18). Thus, astaxanthin-loaded SLCs did not demonstrate protective effects against oxidative stress. But from the experiments to evaluate the inhibition of the production of intrinsic ROS it is known that this sample decreased the levels of endogenous ROS (Figure 3.16). Similar results were obtained by Wolf *et al.* who reported that, while astaxanthin decreased the levels of endogenous ROS, the incubation with astaxanthin prior to stress induction did not decrease the levels of ROS. Additionally, the author speculates that the antioxidant activity of astaxanthin is not through directly quenching ROS, but through the decrease of endogenous ROS [55].

Concerning the astaxanthin-loaded NLCs (Figure 3.18), once again as observed in the inhibition of the production of intrinsic ROS experiment this sample did not reduce the levels of ROS relative to the control, but instead there was an increase in the levels of ROS with the increase of the concentration of the sample (Section 3.3.4.1). As was already explained in Section 3.3.4.1, this increase in ROS production can be attributed to toxicity exhibited by the particulate system and/or to the fact that the NLCs allowed a higher permeation of astaxanthin, and once inside the cells astaxanthin might have induced ROS production. The theory that astaxanthin is inducing ROS production is corroborated by the results obtained for pure astaxanthin, where the increase in the level of ROS is observed with the increase of the concentration of astaxanthin (Figure 3.18). Additional studies should be performed to confirm if the increase is due to the delivery system or if it is astaxanthin who is inducing the production of ROS, or both.

Considering what is reported in the majority of the works published about the antioxidant activity of astaxanthin, the results obtained in this work should be further confirmed [10,11,14,50,187,188].

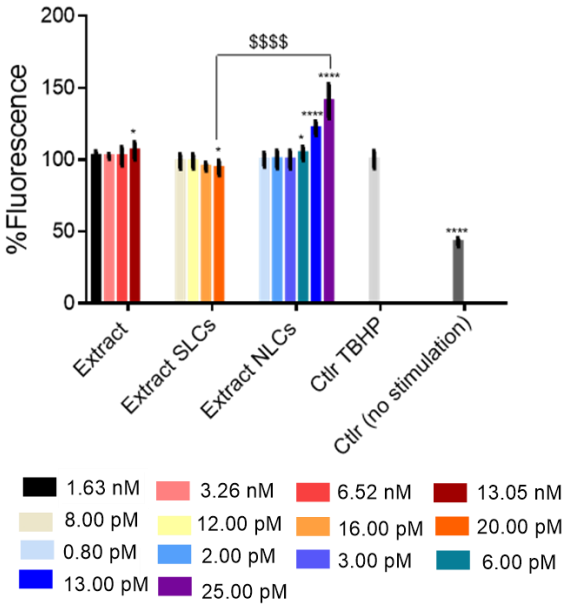

Figure 3.19- Pre-incubation of cells with shrimp shell extract, extract-loaded NLCs and SLCs for 4h-effect on total ROS generation. The symbol * indicates significance relative to the TBHP control (* p-value<0.05, ** p-value<0.01, *** p-value<0.001, **** p-value<0.0001). Similar concentrations of different samples were compared and $ indicates significance relative to each other ($ p-value<0.05, $$ p-value<0.01, $$$ p-value<0.001, $$$$ p-value<0.0001). Results were obtained from at least two independent experiments performed in triplicate. The concentrations are expressed as mols of astaxanthin per milliliter of culture medium.

Concerning the shrimp shell extract (Figure 3.19) none of the concentrations tested revealed to decrease the levels of ROS relative to the control. Instead the highest concentration tested increased significantly the percentage of fluorescence comparatively to the control, thus increased the production of ROS. On the contrary, in the inhibition of the production of intrinsic ROS experiment (Section 3.3.4.1) this highest concentration provided the highest inhibition of the production of endogenous ROS. This contradictory result might be explained by the fact that in an oxidative stress condition (high concentration of ROS) some carotenoids instead of acting as antioxidants, they act as pro-oxidants. β-carotene, for example, in low concentrations of ROS acts as an antioxidant but in high concentrations of ROS it acts like a pro-oxidant and similar behavior is observed for other carotenoids [194]. So, in this experiment some of the antioxidant molecules that previously (Section 3.3.4.1) exhibited antioxidant effects, here they exhibit pro-oxidant effect. Also, this increase was only observed for the highest concentration tested since the other concentrations might have not allowed the permeation of enough amount of pro-oxidant molecules to cause a significant effect.

Regarding the extract-loaded SLCs (Figure 3.19), this was the only sample tested that provided a protective effect against oxidative stress. The highest concentration tested was the only one who exhibited significant difference relative to the control, being able to reduce the levels of ROS, relative to the control. This decrease could be explained by the fact that the SLCs could have allowed the permeation of antioxidant molecules that in the extract were not able to enter the cells, additionally SLCs might have allowed the uptake of higher amounts of antioxidant molecules, who were able to scavenge the ROS generated and overpower the effects of other pro-oxidants molecules. Moreover, the presence of antioxidant molecules from the olive oil could also aid in the scavenging of ROS.

As for the extract-loaded NLCS, the three lowest concentrations tested (0.8, 2.00, and 3.00pM) did not reveal any significant difference from the control, but the tree highest concentrations (6.00, 13.00, 25.00 pM) revealed to significantly increase ROS production (Figure 3.19). As was mentioned previously this increase in ROS production can be attributed to toxicity exhibited by the particles (Section 3.3.4.1). However, in Section 3.3.4.1 all the concentrations of extract-loaded NLCs were found to increase the levels of ROS, while in this approach the increase was only verified for the three highest concentrations. Possibly, the level of ROS produced by the NLCs in the lower concentrations

were masked by the amount of ROS produced by the stress inducer. Further studies should be performed to confirm these results.

3.3.4.2.2 Co-incubation approach

In the co-incubation approach the cells were incubated for 1h with the samples (astaxanthin, astaxanthin-loaded NLCs and SLCs and shrimp shell extract, extract-loaded NLCs and SLCs) and the stress inducer, TBHP (Figure 3.20 and 3.21).

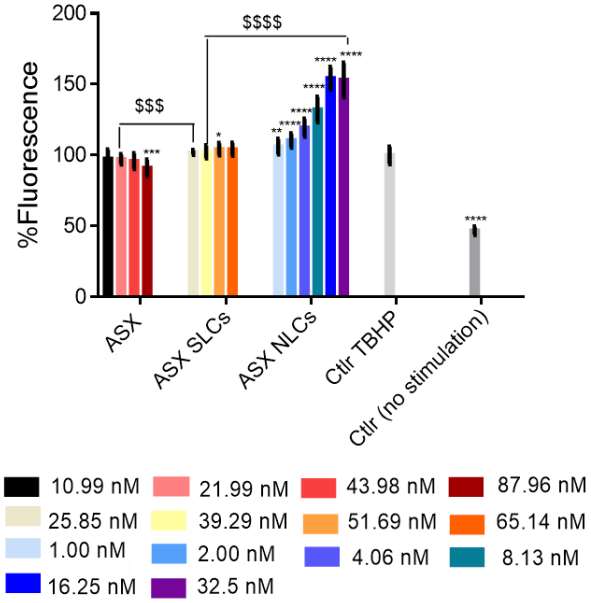

Figure 3.20- Co-incubation of cells with samples (astaxanthin, astaxanthin-loaded NLCs and SLCs) and TBHP for 1h- effect on total ROS generation. The symbol * indicates significance relative to the TBHP control (* p-value<0.05, ** p-value<0.01, *** p-value<0.001, **** p-value<0.0001). Similar concentrations of different samples were compared and $ indicates significance relative to each other ($ p-value<0.05, $$ p-value<0.01, $$$ p-value<0.001, $$$$ p-value<0.0001). Results were obtained from at least two independent experiments performed in triplicate. The concentrations are expressed as mols of astaxanthin per milliliter of culture medium.

Unlike in the other experiments (Section 3.3.4.1 and 3.3.4.2) where astaxanthin did not exhibit antioxidant activity, in this approach astaxanthin demonstrated to exhibit antioxidant effects (Figure 3.20). In the highest concentration tested astaxanthin revealed to significantly decrease (p-value<0,001) the percentage of fluorescence relative to the control, thus it significantly decreased the levels of ROS comparatively to the control. These results, obtained for astaxanthin, are opposite to what was obtained when incubating astaxanthin prior to stress induction, where with the increase of the concentration of astaxanthin there was an increase in the levels of ROS. These findings indicate that, perhaps when intracellularly, astaxanthin will exert its antioxidant activity by inducing the production of ROS to activate the antioxidant pathways (e.g. Nfr-2/ARE), but when extracellularly, where it cannot activate the antioxidant pathways, it will directly scavenge ROS. Furthermore, these results refute the theory that astaxanthin is not able to directly scavenge ROS. Future studies need to be performed to confirm these theories.

Regarding astaxanthin-loaded SLCs, none of the concentration tested revealed any significant alteration relative to the control. Only one of the concentrations tested (51,69nM) was found to significantly increase the levels of ROS relative to the control, a possible explanation is the oxidation of the lipids that compose the particles (Figure 3.20). When comparing these results with those obtained for pure astaxanthin, where there was a decrease in the levels of ROS, the results obtained for astaxanthin-loaded SLCs could indicate that in the 1h incubation (used in the co-incubation approach), astaxanthin was not released from the delivery systems, thus did not exert its antioxidant effect (Figure 3.20).

Concerning the astaxanthin-loaded NLCs, all concentrations tested significantly increased the levels of ROS relative to the control (Figure 3.20). As was verified in the other approaches (Section 3.3.4.1 and 3.3.4.2), the highest concentrations tested of astaxanthin-loaded NLCs increased the levels of ROS, and this increase was hypothesized to be caused by the induction of ROS production by astaxanthin and/or by the particulate system. In this approach the particles are in contact with the stress inducer, TBHP, which could oxidize the lipids that compose the particles [85,167]. TBHP by oxidizing the lipids that compose the particles led to the production of free radicals, thus triggering the propagation of lipid oxidation reactions. Also, as the concentration of astaxanthin-loaded NLCs increases, increases the amount of particles that can be oxidized, thus increasing the amount of ROS produced.

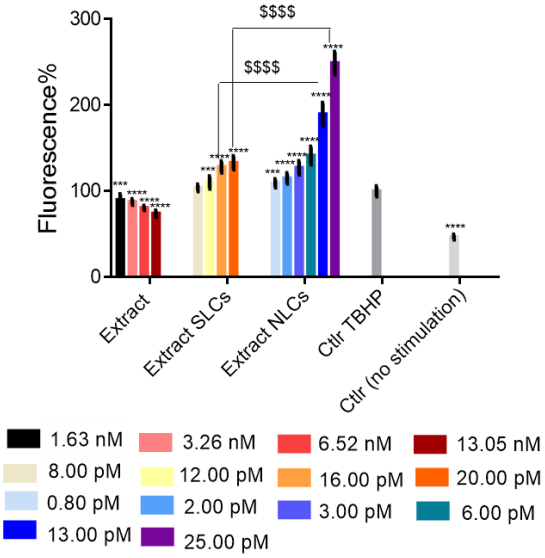

Figure 3.21- Co-incubation of cells with samples (shrimp shell extract, extract-loaded NLCs and SLCs) and TBHP for 1h- effect on total ROS generation. The symbol * indicates significance relative to the TBHP control (* p-value<0.05, ** p-value<0.01, *** p-value<0.001, **** p-value<0.0001). Similar concentrations of different samples were compared and $ indicates significance relative to each other ($ p-value<0.05, $$ p-value<0.01, $$$ p-value<0.001, $$$$ p-value<0.0001). Results were obtained from at least three independent experiments performed in triplicate. The concentrations are expressed as mols of astaxanthin per milliliter of culture medium.

The results obtained for the shrimp shell extract revealed to be very positive (Figure 3.21). All concentrations of extract tested were found to significantly decrease the level of ROS relative to the control, furthermore, the levels of ROS decreased with increase of the concentration off extract. These findings support the theory that the extract is composed by antioxidant molecules that are unable to permeate the cell membrane and reach the intracellular compartment, only being able to exert their antioxidant effect if entrapped in the SLCs or if the ROS are present extracellularly. Also, these antioxidant molecules could be in higher amounts or have higher antioxidant power than the pro-oxidant molecules, that might exist, thus the antioxidant effect overpowers the pro-oxidant effect.

When comparing the results obtained for the extract with those obtained for pure astaxanthin, even if the extract had a much lower concentration of astaxanthin than pure astaxanthin, it is clear that extract demonstrated significantly higher capacity to protect the cells against ROS than astaxanthin. This indicates that the extract is composed by other antioxidant molecules that together demonstrated a higher antioxidant effect than astaxanthin alone, and perhaps these molecules are more powerful than astaxanthin at directly scavenging ROS.

Regarding, the extract-loaded SLCs there was a significant increase in the level of ROS with the increase of the concentration (Figure 3.21). In the other approaches this sample was not found to increase the levels of ROS, but instead it was found to decrease them (Section 3.3.4.1 and 3.3.4.2). The increase verified in this approach might be attributed to the oxidation of the lipids that compose

the particles in the presence of the stress inducer, triggering the propagation of lipid oxidation. Further studies should be performed to confirm this result.

As for the extract-loaded NLCs all concentrations tested revealed to significantly increase the levels of ROS relative to the control (Figure 3.21). This increase can be attributed to the toxicity exhibited by the particles, and, additionally, to the oxidation of the lipids that compose the NLCs, caused by the stress inducer. Furthermore, as the concentration of extract-loaded NLCs increases, increases the amount of particles that can be oxidized, thus increases the amount of ROS produced, this explains why the level of ROS increase with the concentration of particles.

All in all, none of the concentrations tested of pure astaxanthin inhibited the production of intrinsic ROS, or were not able to prevent oxidative stress, and, in fact, the highest concentrations tested increased the levels of ROS when incubated with the cells prior to the stress induction. Although, the highest concentrations tested reduced the levels of ROS when co-incubated with the stressor. Future studies should be performed to confirm the results obtained, to better understand the mechanism of action of astaxanthin and to validate the hypothesis that astaxanthin increases the levels of ROS to activate the antioxidant pathways.

Regarding, astaxanthin-loaded SLCs this sample only displayed antioxidant activity in the inhibition of intrinsic ROS. None of the concentrations tested when pre-incubated with the cells prior to stress induction were able to prevent oxidative stress, nor decrease ROS production when co-incubated with the stress inducer.

As for the astaxanthin-loaded NLCs, none of the concentrations tested, in none of the approaches tested, revealed to inhibit the production of ROS. Furthermore, the highest concentrations tested revealed to increase the levels of ROS relative to the control in the intrinsic ROS and in the pre-incubation approaches, while in the co-incubation approach all concentrations revealed to increase the levels of ROS relative to the control. This is explained by possible toxicity of the particulate systems, as was observed for the extract-loaded NLCs, and possibly due to the increase of intracellular astaxanthin, which could induce the production of ROS. Moreover, the cytotoxicity studies indicate that the astaxanthin-loaded NLCs led to a cell viability enhancement, which is related to an increase of cell proliferation caused by the increase of intracellular ROS.

As for the shrimp shell extract, the highest concentrations tested were able to inhibit the production of endogenous ROS, thus indicating that extract is composed of molecules other than astaxanthin that possess antioxidant activity and that are able to permeate the cell membrane. Nonetheless, when pre-incubated with the cells prior to stress induction, the highest concentration tested increased the levels of ROS, thus indicating that some of the molecules that constitute the extract were acting as prooxidants. On the other hand, when co-incubated with the stress inducer it was able to significantly reduce the level of ROS.

Concerning the extract-loaded SLCs, the delivery system allowed the permeation of higher amounts of antioxidant molecules and perhaps molecules that if not entrapped would not be able to permeate the cell membrane. Therefore, the formulation improved the inhibition of the production of intrinsic ROS, comparatively to the extract (not-formulated). Furthermore, the highest concentration tested, when pre-incubated with the cells prior the stress induction, was able to decrease the levels of ROS relative to the control. However, when co-incubated with the stress inducer some of the concentrations tested increased the levels of ROS.

As for the extract-loaded NLCs, it revealed to stress cells by inducing the production of ROS, although not decreasing cell viability or affecting the mitochondrial integrity. Furthermore, these findings were confirmed by the cytotoxicity studies that revealed an enhancement of the cell viability, which is related to the increase of the cell proliferation caused by the increase of intracellular ROS. Moreover, the TEER values obtained during the permeability studies also confirm this toxicity, since the extract-loaded NLCs revealed to damage the cell monolayer. Nevertheless, in none of the concentrations tested the ROS produced affected the integrity of the mitochondria (at least during the period of the assay).

4 Conclusion

Astaxanthin is renowned for its powerful antioxidant and anti-inflammatory activities, furthermore, it could constitute a potential nutraceutical to be used in the prevention, treatment and maintenance of Inflammatory Bowel diseases (IBD). Incidentally, its potential use in the treatment of IBD has not been vastly researched. Regardless of its remarkable activities, the therapeutic use of astaxanthin is seriously limited by its instability and low bioavailability. Hence the author of this dissertation proposed the entrapment of astaxanthin into NLCs and SLCs, to improve its stability and oral bioavailability, having as a target the gastrointestinal tract.

A solid-liquid extraction from shrimp shells using chloroform was performed to obtain an extract rich in astaxanthin that could be used for the optimization of the production of particles. However, the yield of carotenoids and the yield of astaxanthin obtained in the extractions was low, and because the extract had a wax-like texture it was hard to work with. Additionally, the extract had very different physical characteristics than that of astaxanthin standard (that was the sample that was intended to be entrapped at the end of the optimizations), which was a powder. Hence, the extract did not replicate the characteristics of the substance to be entrapped, thus not being suitable for the optimization of the production of particles and was not used. However, after these optimizations were concluded, the extract was formulated and its antioxidant activity, and of its formulations, were evaluated through cell-based assays. Several factors can contribute to these low yields obtained, but the solvent used seems to be the major influencing factor. It is proposed that in the future other organic solvents ought to be tested, and a different extraction process that could provide higher yield of carotenoids, such as supercritical fluid extraction and extraction using vegetable oils, should be investigated.

Lipid-based formulations (NLCs and SLCs) of astaxanthin were developed through different approaches, conventional methods (NLCs) and supercritical fluid based-methods (SLCs), and their capacity to improve the bioavailability of the bioactive was assessed.

The NLCs were produced through melt-emulsification. Before producing astaxanthin- and extract-loaded NLCs, the formulation composition and the process parameters were optimized. All the formulations produced revealed low encapsulation efficiencies (<25%), this is explained by the loss of a big portion of the lipid phase during the production of the particles. This loss of the lipid phase was due to a limitation of the production process related to the equipment being used (ultraturrax) and only by using a different equipment would this be resolved. The most promising formulation composition contained half the initial amount of bioactive and did not contain organic solvent. The lack of organic solvent compensates the lower encapsulation efficiency obtained for this formulation, since no organic solvent residues contaminated the finished product, thus reducing potential toxicity and environmental issues associated with the use of these solvents. Furthermore, the production process was less complex, and more scalable. The ideal formulation composition (compritol 888 ato, olive oil, lecithin, half the initial amount of bioactive and water) and the optimum process parameters (21500 rpm and 20 min) led to the production of astaxanthin- and extract-loaded NLCs with the smallest particle size (365.43 ± 2.10 and 365.50 ± 3.7 nm, respectively) and lowest PDI values (0.15 ± 0.11 and 0.26 ± 0.11, respectively), but low encapsulation efficiencies (10.02 ± 0.22% and 6.853%).

The SLCs were produced through PGSS® co-precipitation process. It is important to mention that neither the production of structured lipid carriers nor the micronization of astaxanthin through PGSS® process have been vastly reported. Before producing astaxanthin- and extract-loaded SLCs, the lipid matrix and the process parameters were optimized. In every experiment, the encapsulation efficiency of the resulting particles was above 100%. This is explained by the fact that the experimental load of the bioactive was higher than the initial load, and it is hypothesized that this phenomenon occurred due to a preferential loss of compritol 888 ato during depressurization. Notwithstanding, higher experimental loads translate in the delivery of higher amounts of bioactive without the presence of large amounts of excipients. It was confirmed that by using a liquid lipid in the formulation, the bioactive loading and stability of the particles is increased. When testing the two different formulations containing liquid lipids (olive oil or peceol) it was demonstrated that the lipid used did not influence the experimental load. However, there is an indication of the degradation of the bioactive in the formulations containing peceol, and also this lipid was not suitable to produce NLCs, thus not being used in further experiments. The optimum lipid matrix, containing olive oil, and

process parameters, 250 bar, 70ºC, and 15 minutes as the contact time with $scCO_2$, led the production of astaxanthin-loaded SLCs with experimental load of 9.26 ± 0.80 mg/g and particle size ranging between 1.50 and 20 µm. While the shrimp shells extract-loaded SLCs had an experimental load of 2.9 µg/g.

After the production of astaxanthin- and extract-loaded NLCs and SLCs, the formulations, pure astaxanthin and the extract, were tested to assess possible cytotoxicity. None of the concentrations tested of astaxanthin, extract and respective formulations revealed to cause cytotoxicity.

The influence of pure astaxanthin, the extract and respective formulation, on the mitochondrial integrity was evaluated. None of the concentrations tested of astaxanthin, extract and respective formulations influenced mitochondrial integrity.

To evaluate if the NLCs and SLCs formulations improved the permeability of astaxanthin, and which delivery system improved its absorption the most, permeability studies were performed on a Caco-2 monoculture and in a triple co-culture Caco-2:HT29-MTX:Raji-B. Due to time constraints and because of the unavailability of equipments (mass spectrometer), the cellular uptake was not determined. Instead it was determined an estimation of the cellular uptake, that does not have in consideration the degradation and metabolization that the study compound can undergo in the media and once inside the cells. Thus, it does not provide conclusive results about the cellular uptake. Further studies, with an adequate lysis protocol and using a more sensitive quantification method than the one used in this work (HPLC), should be performed in order to quantity the cellular uptake of astaxanthin. The estimated cellular uptake was significantly higher in triple co-culture. Additionally, the entrapment of astaxanthin into NLCs and SLCs significantly improved the estimated cellular uptake of astaxanthin, therefore it could improve the bioactive effect in the intestinal epithelium. Furthermore, astaxanthin-loaded NLCs revealed to provide the highest estimated cellular uptake of astaxanthin.

The antioxidant activity of astaxanthin, extract and respective formulations were tested in Caco-2 monolayers. Only astaxanthin-loaded SLCs, the extract and extract-loaded SLCs revealed to inhibit the production of intrinsic ROS. Furthermore, due to time limitations it was only possible to perform two independent experiments, and since the results obtained did not lead to conclusive findings these experiments should be repeated. Only the extract-loaded SLCs revealed to exhibit protective effect against ROS in the pre-incubation approach. Interestingly, astaxanthin when pre-incubated with the cells prior to stress induction revealed to significantly increase the levels of ROS. It is theorized that astaxanthin is inducing ROS production to activate antioxidant pathways, such as the Nfr-2/ARE pathway. Moreover, the extract revealed to cause the highest decrease in ROS production when co-incubated with the stress inducer. On the contrary, the NLCs formulations of both samples increased the levels of ROS in the three different approaches, instead of decreasing them. Furthermore, extract-loaded NLCs revealed to have damaged the cell monolayer in the permeability studies. It is hypothesized that the NLCs are stressing the cells by increasing ROS production.

All in all, SLCs could be better delivery system than NLCs, since not only they might improve the cellular uptake of astaxanthin comparatively to the free compound, but also unlike NLCs, SLCs did not reveal to stress cells by increasing the production of ROS. Furthermore, SLCs allowed the production of particles with higher astaxanthin loading, and their production process is less complex (less steps in the production process) and more scalable, having a greater potential for future industrial applications.

Overall, the aim of this thesis was accomplished. Formulations of astaxanthin that could improve its oral bioavailability were developed, through its entrapment into NLCs and SLCs. For the first time, astaxanthin-loaded SLCs were produced through PGSS® process, thus revealing that the micronization of astaxanthin can be carried out at larger scales in the pharmaceutical industry. Moreover, the shrimp shell extract revealed to possess promising antioxidant activities.

In future work, the shrimp shell extract should be fully characterized through mass spectrometry. Regarding the NLCs production, it would be interesting to perform analysis to determine the most suitable proportion of carriers to entrap a sample high content of astaxanthin. Additionally, further studies should be performed to overcome ultraturrax limitations, or a different homogenization technique should be used. The production of SLCs should be repeated using a PGSS® with a different design than the one used, to confirm the theory provided to explain the encapsulation efficiencies above 100%. The SLCs particles should be further characterized in terms of size and polydispersity index through Laser Diffraction (Malvern Mastersizer 2000) also, NLCs and

SLCs should be further characterized through X-ray Diffraction to assess the crystalline order of the particles, and confirm the results obtained in the DSC analysis. Furthermore, the zeta-potential of both delivery systems should be determined. In vitro released studies and stability tests of the two delivery systems should be performed.

Regarding the cell-based assays, it would be interesting to test the cellular uptake of digested astaxanthin-loaded NLCs and SLCs, to acquire information about the uptake of astaxanthin in conditions that better resemble those found in vivo, and also to assess the effect of the gastrointestinal digestion on the particles. To confirm the results obtained, the antioxidant assays should be repeated for pure astaxanthin and astaxanthin-loaded SLCs, as well as the antioxidant activity of blank NLCs and SLCs should be assessed. Furthermore, it would be interesting to further study the antioxidant activity of astaxanthin: (1) to assess if the induction of ROS observed in the pure astaxanthin samples was to activate the antioxidant pathways, (2) to evaluate the role of astaxanthin in the activation of the Nfr-2/ARE pathway, and (3) its influence on the expression of phase II antioxidant enzymes, such as NAD(P)H: quinine oxidoreductase-1 (NQO1), glutathione S-transferase, glutamate-cysteine ligase, and HO-1. Finally, it would be interesting to study the protective role of astaxanthin against oxidative stress induced mitochondrial dysfunction.

5. References

1. Prabu, S. L., Narasimman, T., Suriyaprakash, K., Kumar, C. D. & Kumar, S. S. Nutraceuticals and their medicinal importance. **1**, 47–53 (2012).
2. Singh, U., Singh, S. & Kochhar, A. Therapeutic potential of antidiabetic nutraceuticals. **2**, 144–169 (2012).
3. Lee, S. *Strategic Design of Delivery Systems for Nutraceuticals*. *Nanotechnology Applications in Food* (Elsevier Inc., 2017). doi:10.1016/B978-0-12-811942-6.00004-2
4. Prakash, V. & Boekel, M. A. J. S. Van. Nutraceuticals : Possible Future Ingredients and Food Safety Aspects. 333–338 (2010). doi:10.1016/B978-0-12-374845-4.00019-9
5. Keservani, R. K., Kesharwani, R. K., Sharma, A. K., Gautam, S. P. & Verma, S. K. *Chapter 9 - Nutraceutical Formulations and Challenges*. *Developing New Functional Food and Nutraceutical Products* (Elsevier Inc., 2017). doi:10.1016/B978-0-12-802780-6/00009-2
6. Fakhri, S., Abbaszadeh, F., Dargahi, L. & Jorjani, M. Astaxanthin: A mechanistic review on its biological activities and health benefits. *Pharmacol. Res.* **136**, 1–20 (2018).
7. Mont, L. *et al.* Astaxanthin : structural and e funcionais. **23**, 1041–1050 (2010).
8. Hu, J. *et al.* Extraction and purification of astaxanthin from shrimp shells and the effects of different treatments on its content. *Brazilian J. Pharmacogn.* 4–9 (2018). doi:10.1016/j.bjp.2018.11.004
9. Zuluaga, M., Barzegari, A., Letourneur, D. & Gueguen, V. Oxidative Stress Regulation on Endothelial Cells by Hydrophilic Astaxanthin Complex : Chemical , Biological , and Molecular Antioxidant Activity Evaluation. **2017**, (2017).
10. Pashkow, F. J., Watumull, D. G. & Campbell, C. L. Astaxanthin : A Novel Potential Treatment for Oxidative Stress and Inflammation in Cardiovascular Disease. (2008). doi:10.1016/j.amjcard.2008.02.010
11. Iwata, S., Imai, T., Shimazawa, M., Ishibashi, T. & Hayashi, M. Protective e ff ects of the astaxanthin derivative , adonixanthin , on brain hemorrhagic injury. *Brain Res.* **1698**, 130–138 (2018).
12. Li, M. *et al.* Astaxanthin protects lipopolysaccharide-induced inflammatory response in Channa argus through inhibiting NF-κB and MAPKs signaling pathways. *Fish Shellfish Immunol.* (2018). doi:10.1016/j.fsi.2018.11.011
13. Li, J., Zhu, D., Niu, J., Shen, S. & Wang, G. An economic assessment of astaxanthin production by large scale cultivation of Haematococcus pluvialis. *Biotechnol. Adv.* **29**, 568–574 (2011).
14. Kishimoto, Y., Yoshida, H. & Kondo, K. Potential Anti-Atherosclerotic Properties of Astaxanthin. 1–13 (2016). doi:10.3390/md14020035
15. Hu, I.-C. *Production of potential coproducts from microalgae*. *Biofuels from Algae* (Elsevier B.V., 2019). doi:10.1016/b978-0-444-64192-2.00014-7
16. Ambati, R. R., Phang, S. M., Ravi, S. & Aswathanarayana, R. G. Astaxanthin: Sources, Extraction, Stability, Biological Activities and Its Commercial Applications—A Review. 128–152 (2014). doi:10.3390/md12010128
17. Dong, S., Huang, Y., Zhang, R., Wang, S. & Liu, Y. Four Different Methods Comparison for Extraction of Astaxanthin from Green Alga Haematococcus pluvialis. **2014**, (2014).
18. Hooshmand, H., Shabanpour, B. & Golmakani, M. T. Optimization of carotenoids extraction from blue crab (Portunus pelagicus) and shrimp (Penaeus semisulcatus) wastes using organic solvents and vegetable oils. 1–9 (2017). doi:10.1111/jfpp.13171
19. Hu, J. *et al.* Extraction and purification of astaxanthin from shrimp shells and the effects of different treatments on its content. *Rev. Bras. Farmacogn.* **29**, 24–29 (2019).
20. Prameela, K. *et al.* Department of Environmental sciences , GITAM Institute of Science , GITAM University , Department of Biotechnology. *Food Chem.* (2017). doi:10.1016/j.foodchem.2017.05.097
21. Quan, C. & Turner, C. Extraction of Astaxanthin from Shrimp Waste Using Pressurized Hot Ethanol. 247–251 (2009). doi:10.1365/s10337-009-1113-0
22. Li, J. *et al.* HIGH PRESSURE EXTRACTION OF ASTAXANTHIN FROM SHRIMP WASTE (PENAEUS VANNAMEI BOONE): EFFECT ON YIELD AND ANTIOXIDANT ACTIVITY.

(2016). doi:10.1111/jfpe.12353
23. Sánchez-camargo, A. P., Martinez-correa, H. A., Paviani, L. C. & Cabral, F. A. The Journal of Supercritical Fluids Supercritical CO 2 extraction of lipids and astaxanthin from Brazilian redspotted shrimp waste (Farfantepenaeus paulensis). **56**, 164–173 (2011).
24. Lee, S. H., Roh, S. K., Park, K. H. & Yoon, K. Effective Extraction of Astaxanthin Pigment from Shrimp Using Proteolytic Enzymes. 199–200 (1999).
25. Goycoolea, F. M. Astaxanthin : A Review of its Chemistry and Applications Astaxanthin : A Review of its. **8398**, (2007).
26. Membrane, C. amr. **16**, (2011).
27. López-cervantes, J. & Sánchez-machado, D. I. *Chapter 2.2 - Astaxanthin, Lutein, and Zeaxanthin*. *Nonvitamin and Nonmineral Nutritional Supplements* (Elsevier Inc., 2019). doi:10.1016/B978-0-12-812491-8.00003-5
28. AstaReal. AstaReal®- The Natural Astaxanthin of Choice. (2019). Available at: http://www.astareal.se/astareal-astaxanthin?informationmodal=true.
29. Liu, X. & Osawa, T. Cis astaxanthin and especially 9- cis astaxanthin exhibits a higher antioxidant activity in vitro compared to the all- trans isomer. **357**, 187–193 (2007).
30. Visioli, F. & Artaria, C. Function mechanisms of action , therapeutic merits , and. 39–63 (2017). doi:10.1039/c6fo01721e
31. Wang, C., Armstrong, D. W. & Chang, C. Rapid baseline separation of enantiomers and a mesoform of standards and commercial supplements. **1194**, 172–177 (2008).
32. Doktorovová, S. *et al.* Cationic solid lipid nanoparticles interfere with the activity of antioxidant enzymes in hepatocellular carcinoma cells. *Int. J. Pharm.* **471**, 18–27 (2014).
33. Floerkemeier, V. & Kerschbaum, T. Erstellung Von Multiple Choice Fragen. Objektivierte Leistungskontrollen in Der Medizinischen Und Zahnmedizinischen Ausbildung (Iii). *Dtsch. Arztebl.* **71**, 2479–2485 (1974).
34. Régnier, P. *et al.* Astaxanthin from Haematococcus pluvialis Prevents Oxidative Stress on Human Endothelial Cells without Toxicity. 2857–2874 (2015). doi:10.3390/md13052857
35. Gammone, M. A., Riccioni, G. & D'Orazio, N. Marine carotenoids against oxidative stress: Effects on human health. *Mar. Drugs* **13**, 6226–6246 (2015).
36. Mitochondrial, S. Inhibitory Effect of Astaxanthin on Oxidative. (2018). doi:10.3390/nu10081137
37. Review, A. C. Astaxanthin in Skin Health, Repair, and Disease: A Comprehensive Review. 1–12 (2018). doi:10.3390/nu10040522
38. Niu, T. *et al.* Astaxanthin Induces the Nrf2/HO-1 Antioxidant Pathway in Human Umbilical Vein Endothelial Cells by Generating Trace Amounts of ROS. *J. Agric. Food Chem.* **66**, 1551–1559 (2018).
39. Min, K. J., Lee, J. T., Joe, E. hye & Kwon, T. K. An IκBα phosphorylation inhibitor induces heme oxygenase-1(HO-1) expression through the activation of reactive oxygen species (ROS)-Nrf2-ARE signaling and ROS-PI3K/Akt signaling in an NF-κB-independent mechanism. *Cell. Signal.* **23**, 1505–1513 (2011).
40. Tripathi, D. N. & Jena, G. B. Astaxanthin intervention ameliorates cyclophosphamide-induced oxidative stress, DNA damage and early hepatocarcinogenesis in rat: Role of Nrf2, p53, p38 and phase-II enzymes. *Mutat. Res. - Genet. Toxicol. Environ. Mutagen.* **696**, 69–80 (2010).
41. Fakhri, S., Dargahi, L., Abbaszadeh, F. & Jorjani, M. Astaxanthin attenuates neuroinflammation contributed to the neuropathic pain and motor dysfunction following compression spinal cord injury. *Brain Res. Bull.* **143**, 217–224 (2018).
42. McNulty, H. P., Byun, J., Lockwood, S. F., Jacob, R. F. & Mason, R. P. Differential effects of carotenoids on lipid peroxidation due to membrane interactions: X-ray diffraction analysis. *Biochim. Biophys. Acta - Biomembr.* **1768**, 167–174 (2007).
43. Chen, J. & Kotani, K. Astaxanthin as a Potential Protector of Liver Function : A Review. **8**, 701–704 (2016).
44. Ni, Y. *et al.* Astaxanthin prevents and reverses diet-induced insulin resistance and steatohepatitis in mice: A comparison with Vitamin E. *Sci. Rep.* **5**, 1–15 (2015).
45. Ahmed, S. M. U., Luo, L., Namani, A., Wang, X. J. & Tang, X. Nrf2 signaling pathway: Pivotal roles in inflammation. *Biochim. Biophys. Acta - Mol. Basis Dis.* **1863**, 585–597 (2017).
46. Kaulmann, A. & Bohn, T. Carotenoids, inflammation, and oxidative stress-implications of

cellular signaling pathways and relation to chronic disease prevention. *Nutr. Res.* **34**, 907–929 (2014).
47. Speranza, L. *et al.* Astaxanthin treatment reduced oxidative induced pro-inflammatory cytokines secretion in U937: SHP-1 as a novel biological target. *Mar. Drugs* **10**, 890–899 (2012).
48. Kavitha, K., Kowshik, J., Kishore, T. K. K., Baba, A. B. & Nagini, S. Biochimica et Biophysica Acta Astaxanthin inhibits NF- κ B and Wnt / β -catenin signaling pathways via inactivation of Erk / MAPK and PI3K / Akt to induce intrinsic apoptosis in a hamster model of oral cancer. *BBA - Gen. Subj.* **1830**, 4433–4444 (2013).
49. Indo, H. P. *et al.* A mitochondrial superoxide theory for oxidative stress diseases and aging. *J. Clin. Biochem. Nutr.* **56**, 49–56 (2015).
50. Sowmya, P. R. R., Arathi, B. P., Vijay, K., Baskaran, V. & Lakshminarayana, R. Astaxanthin from shrimp efficiently modulates oxidative stress and allied cell death progression in MCF-7 cells treated synergistically with β-carotene and lutein from greens. *Food Chem. Toxicol.* **106**, 58–69 (2017).
51. Moura, F. A., de Andrade, K. Q., dos Santos, J. C. F., Araújo, O. R. P. & Goulart, M. O. F. Antioxidant therapy for treatment of inflammatory bowel disease: Does it work? *Redox Biol.* **6**, 617–639 (2015).
52. 1.609, Naito, Y., Uchiyama, K. & Takagi, T. Dual antiplatelet therapy does not affect the Society for Free Radical Research Japan 10.3164/j6cb .18-16 1880 50860912-0009 JJCBN Original Article Kyj bn18-1 c oto, Japan ournal of Clinical Biochemistry and Nutrition the incidence of low?dose aspirin?ind. *J. Clin. Biochem. Nutr.* **64**, 2016–2019 (2018).
53. Kim, S. H. & Kim, H. Inhibitory effect of astaxanthin on oxidative stress-induced mitochondrial dysfunction-a mini-review. *Nutrients* **10**, (2018).
54. Dias, D., Silva, E. & Carmo, H. Combination effects of amphetamines under hyperthermia - the role played by oxidative stress. (2013). doi:10.1002/jat.2889
55. Wolf, A. M. *et al.* Astaxanthin protects mitochondrial redox state and functional integrity against oxidative stress. *J. Nutr. Biochem.* **21**, 381–389 (2010).
56. Novak, E. A. & Mollen, K. P. Mitochondrial dysfunction in inflammatory bowel disease. *Front. Cell Dev. Biol.* **3**, 1–18 (2015).
57. Dashdorj, A. *et al.* Mitochondria-targeted antioxidant MitoQ ameliorates experimental mouse colitis by suppressing NLRP3 inflammasome-mediated inflammatory cytokines. *BMC Med.* **11**, 1 (2013).
58. Restivo, N. L., Srivastava, M. D., Schafer, I. A. & Hoppel, C. L. Mitochondrial dysfunction in a patient with crohn disease: Possible role in pathogenesis. *J. Pediatr. Gastroenterol. Nutr.* **38**, 534–538 (2004).
59. Zerôncio, M. A. the Pathogenesis of Inflammatory Bowel Disease. *Int. J. Inflamm. Bowel Dis.* **2**, 14–16 (2016).
60. Song, X. *et al.* Astaxanthin inhibits apoptosis in alveolar epithelial cells type II in vivo and in vitro through the ROS-dependent mitochondrial signalling pathway. *J. Cell. Mol. Med.* **18**, 2198–2212 (2014).
61. Verhoeckx, K. *et al. The Impact of Food Bioactives on Health*.
62. Odeberg, J. M., Lignell, Å., Pettersson, A. & Höglund, P. Oral bioavailability of the antioxidant astaxanthin in humans is enhanced by incorporation of lipid based formulations. *Eur. J. Pharm. Sci.* **19**, 299–304 (2003).
63. Tamjidi, F., Shahedi, M., Varshosaz, J. & Nasirpour, A. Design and characterization of astaxanthin-loaded nanostructured lipid carriers. *Innov. Food Sci. Emerg. Technol.* **26**, 366–374 (2014).
64. Khalid, N., Shu, G., Kobayashi, I., Nakajima, M. & Barrow, C. J. Formulation and characterization of monodisperse O/W emulsions encapsulating astaxanthin extracts using microchannel emulsification: Insights of formulation and stability evaluation. *Colloids Surfaces B Biointerfaces* **157**, 355–365 (2017).
65. Ribeiro, H. S. *et al.* Cellular uptake of carotenoid-loaded oil-in-water emulsions in colon carcinoma cells in vitro. *J. Agric. Food Chem.* **54**, 9366–9369 (2006).
66. Sangsuriyawong, A., Limpawattana, M. & Siriwan, D. Properties and bioavailability assessment of shrimp astaxanthin loaded liposomes. *Food Sci. Biotechnol.* (2018).

doi:10.1007/s10068-018-0495-x
67. Salatti-Dorado, J. A. *et al.* Multifunctional green supramolecular solvents for cost-effective production of highly stable astaxanthin-rich formulations from Haematococcus pluvialis. *Food Chem.* **279**, 294–302 (2019).
68. Peng, C. H., Chang, C. H., Peng, R. Y. & Chyau, C. C. Improved membrane transport of astaxanthine by liposomal encapsulation. *Eur. J. Pharm. Biopharm.* **75**, 154–161 (2010).
69. Viswanathan, P., Muralidaran, Y. & Ragavan, G. *Challenges in oral drug delivery: A nano-based strategy to overcome*. *Nanostructures for Oral Medicine* (Elsevier Inc., 2017). doi:10.1016/B978-0-323-47720-8.00008-0
70. Zhu, L. *et al. Oral absorption basics: Pathways and physicochemical and biological factors affecting absorption*. *Developing Solid Oral Dosage Forms: Pharmaceutical Theory and Practice: Second Edition* (2016). doi:10.1016/B978-0-12-802447-8.00011-X
71. Tamjidi, F., Shahedi, M., Varshosaz, J. & Nasirpour, A. Nanostructured lipid carriers (NLC): A potential delivery system for bioactive food molecules. *Innov. Food Sci. Emerg. Technol.* **19**, 29–43 (2013).
72. Poonia, N., Kharb, R., Lather, V. & Pandita, D. Fsoa-2016-0030. **2**, (2016).
73. Pyo, S., Müller, R. H. & Keck, C. M. *Lipid Carriers*. *Nanoencapsulation Technologies for the Food and Nutraceutical Industries* (Elsevier Inc., 2017). doi:10.1016/B978-0-12-809436-5/00004-5
74. Katouzian, I., Faridi Esfanjani, A., Jafari, S. M. & Akhavan, S. Formulation and application of a new generation of lipid nano-carriers for the food bioactive ingredients. *Trends Food Sci. Technol.* **68**, 14–25 (2017).
75. Kohane, D. S. Microparticles and nanoparticles for drug delivery. *Biotechnol. Bioeng.* **96**, 203–209 (2007).
76. Danaei, M. *et al.* Impact of particle size and polydispersity index on the clinical applications of lipidic nanocarrier systems. *Pharmaceutics* **10**, 1–17 (2018).
77. McClements, D. J. Crystals and crystallization in oil-in-water emulsions: Implications for emulsion-based delivery systems. *Adv. Colloid Interface Sci.* **174**, 1–30 (2012).
78. Madhavi, D., Kagan, D. & Seshadri, S. ORIGINAL RESEARCH A Study on the Bioavailability of a Proprietary , Sustained-release Formulation of Astaxanthin. (2018).
79. Liu, X., McClements, D. J., Cao, Y. & Xiao, H. Chemical and Physical Stability of Astaxanthin-Enriched Emulsion-Based Delivery Systems. *Food Biophys.* **11**, 302–310 (2016).
80. Khalid, N. *et al.* Formulation and characterization of O/W nanoemulsions encapsulating high concentration of astaxanthin. *Food Res. Int.* **102**, 364–371 (2017).
81. Shanmugapriya, K., Kim, H., Saravana, P. S., Chun, B. S. & Kang, H. W. Astaxanthin-alpha tocopherol nanoemulsion formulation by emulsification methods: Investigation on anticancer, wound healing, and antibacterial effects. *Colloids Surfaces B Biointerfaces* **172**, 170–179 (2018).
82. Shanmugapriya, K., Kim, H. & Kang, H. W. In vitro antitumor potential of astaxanthin nanoemulsion against cancer cells via mitochondrial mediated apoptosis. *Int. J. Pharm.* **560**, 334–346 (2019).
83. Pan, L., Wang, H. & Gu, K. Nanoliposomes as vehicles for astaxanthin: Characterization, in vitro release evaluation and structure. *Molecules* **23**, (2018).
84. Li, M., Zahi, M. R., Yuan, Q., Tian, F. & Liang, H. Preparation and stability of astaxanthin solid lipid nanoparticles based on stearic acid. *Eur. J. Lipid Sci. Technol.* **118**, 592–602 (2016).
85. Tamjidi, F., Shahedi, M., Varshosaz, J. & Nasirpour, A. EDTA and α-tocopherol improve the chemical stability of astaxanthin loaded into nanostructured lipid carriers. *Eur. J. Lipid Sci. Technol.* **116**, 968–977 (2014).
86. Tamjidi, F., Shahedi, M., Varshosaz, J. & Nasirpour, A. Stability of astaxanthin-loaded nanostructured lipid carriers as affected by pH, ionic strength, heat treatment, simulated gastric juice and freeze–thawing. *J. Food Sci. Technol.* **54**, 3132–3141 (2017).
87. Montes de Oca-Ávalos, J. M., Candal, R. J. & Herrera, M. L. Nanoemulsions: stability and physical properties. *Curr. Opin. Food Sci.* **16**, 1–6 (2017).
88. Ganesan, P. & Narayanasamy, D. Lipid nanoparticles: Different preparation techniques, characterization, hurdles, and strategies for the production of solid lipid nanoparticles and nanostructured lipid carriers for oral drug delivery. *Sustain. Chem. Pharm.* **6**, 37–56 (2017).

89. Fang, C.-L., A. Al-Suwayeh, S. & Fang, J.-Y. Nanostructured Lipid Carriers (NLCs) for Drug Delivery and Targeting. *Recent Pat. Nanotechnol.* **7**, 41–55 (2012).
90. Martínez-Delgado, A. A., Khandual, S. & Villanueva–Rodríguez, S. J. Chemical stability of astaxanthin integrated into a food matrix: Effects of food processing and methods for preservation. *Food Chem.* **225**, 23–30 (2017).
91. Li, Q. *et al.* A Review of the Structure, Preparation, and Application of NLCs, PNPs, and PLNs. *Nanomaterials* **7**, 122 (2017).
92. Iqbal, M. A. *et al.* Nanostructured lipid carriers system: Recent advances in drug delivery. *J. Drug Target.* **20**, 813–830 (2012).
93. Soulier, J. P. Les publications médicales: Vrais ou faux auteurs? *Rev. Med. Brux.* **30**, 115–117 (2009).
94. Pasquali, I. & Bettini, R. Are pharmaceutics really going supercritical? *Int. J. Pharm.* **364**, 176–187 (2008).
95. Padrela, L. *et al.* Supercritical carbon dioxide-based technologies for the production of drug nanoparticles/nanocrystals – A comprehensive review. *Adv. Drug Deliv. Rev.* **131**, 22–78 (2018).
96. Esfandiari, N. Production of micro and nano particles of pharmaceutical by supercritical carbon dioxide. *J. Supercrit. Fluids* **100**, 129–141 (2015).
97. Girotra, P., Singh, S. K. & Nagpal, K. Supercritical fluid technology: A promising approach in pharmaceutical research. *Pharm. Dev. Technol.* **18**, 22–38 (2013).
98. Pasquali, I., Bettini, R. & Giordano, F. Supercritical fluid technologies: An innovative approach for manipulating the solid-state of pharmaceuticals. *Adv. Drug Deliv. Rev.* **60**, 399–410 (2008).
99. Rodríguez-Rojo, S., Martín, Á. & Cocero, M. J. Encapsulation Methods with Supercritical Carbon Dioxide: Basis and Applications. *Encapsulation Nanotechnologies* 391–424 (2013). doi:10.1002/9781118729175.ch12
100. Yasuji, T., Takeuchi, H. & Kawashima, Y. Particle design of poorly water-soluble drug substances using supercritical fluid technologies. *Adv. Drug Deliv. Rev.* **60**, 388–398 (2008).
101. Janiszewska-Turak, E. Carotenoids microencapsulation by spray drying method and supercritical micronization. *Food Res. Int.* **99**, 891–901 (2017).
102. M. S. Gomes, M. T., T. Santos, D. & A. Meireles, M. A. Trends in Particle Formation of Bioactive Compounds Using Supercritical Fluids and Nanoemulsions. *Food Public Heal.* **2**, 142–152 (2012).
103. Tabernero, A., Martín del Valle, E. M. & Galán, M. A. Supercritical fluids for pharmaceutical particle engineering: Methods, basic fundamentals and modelling. *Chem. Eng. Process. Process Intensif.* **60**, 9–25 (2012).
104. Nunes, A. V. M. & Duarte, C. M. M. Dense CO2 as a Solute, Co-Solute or Co-Solvent in Particle Formation Processes: A review. *Materials (Basel).* **4**, 2017–2041 (2011).
105. Gonc, V. S. S., Matias, A. A., Rodríguez-rojo, S., Nogueira, I. D. & Duarte, C. M. M. Supercritical fluid precipitation of ketoprofen in novel structured lipid carriers for enhanced mucosal delivery – a comparison with solid lipid particles. **495**, 302–311 (2015).
106. Keven Silva, E. & Angela A. Meireles, M. Encapsulation of Food Compounds Using Supercritical Technologies: Applications of Supercritical Carbon Dioxide as an Antisolvent. *Food Public Heal.* **4**, 247–258 (2014).
107. Haq, M. & Chun, B. LWT - Food Science and Technology Microencapsulation of omega-3 polyunsaturated fatty acids and astaxanthin- rich salmon oil using particles from gas saturated solutions (PGSS) process. *LWT - Food Sci. Technol.* **92**, 523–530 (2018).
108. Sousa, A. R. S. De, Calderone, M., Rodier, E., Fages, J. & Duarte, C. M. M. Solubility of carbon dioxide in three lipid-based biocarriers. **39**, 13–19 (2006).
109. Kim, J. T. *et al.* Absorption study of genistein using solid lipid microparticles and nanoparticles: Control of oral bioavailability by particle sizes. *Biomol. Ther.* **25**, 452–459 (2017).
110. Desai, J. & Thakkar, H. *Effect of particle size on oral bioavailability of darunavir-loaded solid lipid nanoparticles*. *Journal of Microencapsulation* **33**, (Taylor & Francis, 2016).
111. Wong, C. Y., Al-Salami, H. & Dass, C. R. Microparticles, microcapsules and microspheres: A review of recent developments and prospects for oral delivery of insulin. *Int. J. Pharm.* **537**, 223–244 (2018).
112. O'Hagan, D. T. The intestinal uptake of particles and the implications for drug and antigen

delivery. *J. Anat.* **189**, 477–47782 (1996).
113. Siepmann, J. & Siepmann, F. Microparticles used as drug delivery systems. *Prog. Colloid Polym. Sci.* **133**, 15–21 (2006).
114. Park, C. G. *et al.* Nanostructured mucoadhesive microparticles to enhance oral drug bioavailability. *J. Ind. Eng. Chem.* **54**, 262–269 (2017).
115. Anchi, P., Khurana, A., Swain, D., Samanthula, G. & Godugu, C. Dramatic improvement in pharmacokinetic and pharmacodynamic effects of sustain release curcumin microparticles demonstrated in experimental type 1 diabetes model. *Eur. J. Pharm. Sci.* **130**, 200–214 (2019).
116. Antunes, F., Andrade, F., Araújo, F., Ferreira, D. & Sarmento, B. European Journal of Pharmaceutics and Biopharmaceutics Establishment of a triple co-culture in vitro cell models to study intestinal absorption of peptide drugs. *Eur. J. Pharm. Biopharm.* **83**, 427–435 (2013).
117. Lozoya-agullo, I. *et al.* Usefulness of Caco-2 / HT29-MTX and Caco- 2 / HT29-MTX / Raji B co-culture models to Predict Intestinal and Colonic Permeability compared to Caco-2 Monoculture. (2017). doi:10.1021/acs.molpharmaceut.6b01165
118. Shah, P., Jogani, V., Bagchi, T. & Misra, A. Role of Caco-2 Cell Monolayers in Prediction of Intestinal Drug Absorption. 186–198 (2006).
119. Scaldaferri, F., Pizzoferrato, M., Gerardi, V., Lopetuso, L. & Gasbarrini, A. The Gut Barrier. *J. Clin. Gastroenterol.* **46**, S12–S17 (2012).
120. Dosh, R. H., Jordan-Mahy, N., Sammon, C. & Le Maitre, C. L. Tissue Engineering Laboratory Models of the Small Intestine. *Tissue Eng. Part B Rev.* **24**, 98–111 (2017).
121. Norris, D. A., Puri, N. & Sinko, P. J. The effect of physical barriers and properties on the oral absorption of particulates. *Adv. Drug Deliv. Rev.* **34**, 135–154 (1998).
122. Araújo, F. & Sarmento, B. Towards the characterization of an in vitro triple co-culture intestine cell model for permeability studies. *Int. J. Pharm.* **458**, 128–134 (2013).
123. Hubatsch, I., Ragnarsson, E. G. E. & Artursson, P. Determination of drug permeability and prediction of drug absorption in Caco-2 monolayers. **2**, 2111–2119 (2007).
124. Lechanteur, A., Almeida, A. & Sarmento, B. Elucidation of the impact of cell culture conditions of Caco-2 cell monolayer on barrier integrity and intestinal permeability. *Eur. J. Pharm. Biopharm.* (2017). doi:10.1016/j.ejpb.2017.06.013
125. Lipka, E. *et al.* Caco-2 versus Caco-2/HT29-MTX Co-cultured Cell Lines: Permeabilities Via Diffusion, Inside- and Outside-Directed Carrier-Mediated Transport. *J. Pharm. Sci.* **89**, 63–75 (2003).
126. Pereira, I., Lechanteur, A. & Sarmento, B. Chapter 11 Drug Permeability. **1817**, 107–113 (2018).
127. Lesuffleur, T., Barbat, A., Dussaulx, E. & Zweibaum, A. Growth Adaptation to Methotrexate of HT-29 Human Colon Carcinoma Cells Is Associated with Their Ability to Differentiate into Columnar Absorptive and Mucus-secreting Cells. *Cancer Res.* **50**, 6334–6343 (1990).
128. Behrens, I., Stenberg, P., Artursson, P. & Kissel, T. <Transport of Lipophilic Drug Molecules in a new mucus-secreting cell culture model based on HT29-MTX Cells (Behrens, et. al., Pharm Research 2001 - Per Arturson group).pdf>. **18**, 1138–1145 (2001).
129. Artursson, P. SCINES. **3**, 171–183 (1995).
130. Walter, E., Janich, S., Roessler, B. J., Hilfinger, J. M. & Amidon, G. L. HT29-MTX/Caco-2 cocultures as an in vitro model for the intestinal epithelium: In vitro-in vivo correlation with permeability data from rats and humans. *J. Pharm. Sci.* **85**, 1070–1076 (1996).
131. Béduneau, A. *et al.* A tunable Caco-2/HT29-MTX co-culture model mimicking variable permeabilities of the human intestine obtained by an original seeding procedure. *Eur. J. Pharm. Biopharm.* **87**, 290–298 (2014).
132. Ohno, H., Kanaya, T. & Williams, I. R. M cell differentiation: Distinct lineage or phenotypic transition? Salmonella provides answers. *Cell Host Microbe* **12**, 607–609 (2012).
133. Pereira, C. *et al.* In vitro M-like cells genesis through a tissue-engineered triple-culture intestinal model. 782–788 (2015). doi:10.1002/jbm.b.33508
134. Debard, N., Sierro, F., Browning, J. & Kraehenbuhl, J. P. Effect of mature lymphocytes and lymphotoxin on the development of the follicle-associated epithelium and M cells in mouse peyer's patches. *Gastroenterology* **120**, 1173–1182 (2001).
135. C., S. *et al.* Development of an advanced intestinal in vitro triple culture permeability model to

study transport of nanoparticles. *Mol. Pharm.* **11**, 808–818 (2014).
136. Gullberg, E. *et al.* Expression of specific markers and particle transport in a new human intestinal M-cell model. *Biochem. Biophys. Res. Commun.* **279**, 808–813 (2000).
137. Clark, M. A., Jepson, M. A. & Hirst, B. H. Exploiting M cells for drug and vaccine delivery. *Adv. Drug Deliv. Rev.* **50**, 81–106 (2001).
138. Kernéis, S. *et al.* Molecular studies of the intestinal mucosal barrier physiopathology using cocultures of epithelial and immune cells: A technical update. *Microbes Infect.* **2**, 1119–1124 (2000).
139. Rieux, A. Des *et al.* Transport of nanoparticles across an in vitro model of the human intestinal follicle associated epithelium. *Eur. J. Pharm. Sci.* **25**, 455–465 (2005).
140. Li, L. *et al.* Microelectronic Engineering Sterilization on dextran-coated iron oxide nanoparticles : Effects of autoclaving , filtration , UV irradiation , and ethanol treatment. **111**, 310–313 (2013).
141. Ansel, H. C., Norred, W. P. & Roth, I. L. Antimicrobial activity of dimethyl sulfoxide against Escherichia coli, Pseudomonas aeruginosa, and Bacillus megaterium. *J. Pharm. Sci.* **58**, 836–839 (1969).
142. Xu, M., Mccanna, D. J. & Sivak, J. G. Journal of Pharmacological and Toxicological Methods Use of the viability reagent PrestoBlue in comparison with alamarBlue and MTT to assess the viability of human corneal epithelial cells. *J. Pharmacol. Toxicol. Methods* **71**, 1–7 (2015).
143. Vieira, E. F., Dias, D., Carmo, H. & Ferreira, I. M. P. L. V. O. Protective ability against oxidative stress of brewers ' spent grain protein hydrolysates. *Food Chem.* **228**, 602–609 (2017).
144. Using, R. O. S. & Dcfda, O. Chapter 4. **594**,
145. Waste, C. *et al.* Extraction and Characterization of Astaxanthin From the Crustacean. *Int. J. Pharm. Sci. Res.* **6**, 2532–2537 (2015).
146. S., S. Extraction, Characterization, Antioxidant and Anti-Inflammatory Properties of Carotenoids from the Shell Waste of Arabian Red Shrimp Aristeus alcocki, Ramadan 1938. *Open Conf. Proc. J.* **2**, 95–103 (2011).
147. Sachindra, N. M., Bhaskar, N. & Mahendrakar, N. S. Recovery of carotenoids from shrimp waste in organic solvents. *Waste Manag.* **26**, 1092–1098 (2006).
148. Taksima, T., Limpawattana, M. & Klaypradit, W. Astaxanthin encapsulated in beads using ultrasonic atomizer andapplication in yogurt as evaluated by consumer sensory profile. *LWT - Food Sci. Technol.* **62**, 431–437 (2015).
149. Boskou, D., Blekas, G. & Tsimidou, M. *Olive Oil Composition*. *Olive Oil: Chemistry and Technology: Second Edition* (AOCS Press, 2006). doi:10.1016/B978-1-893997-88-2.50008-0
150. Burapapadh, K., Takeuchi, H. & Sriamornsak, P. Development of pectin nanoparticles through mechanical homogenization for dissolution enhancement of itraconazole. *Asian J. Pharm. Sci.* **11**, 365–375 (2016).
151. Yuan, B. *et al.* Metastatic cancer cell and tissue-specific fluorescence imaging using a new DNA aptamer developed by Cell-SELEX. *Talanta* **170**, 56–62 (2017).
152. Oliveira, D. R. B., Michelon, M., de Figueiredo Furtado, G., Sinigaglia-Coimbra, R. & Cunha, R. L. β-Carotene-loaded nanostructured lipid carriers produced by solvent displacement method. *Food Res. Int.* **90**, 139–146 (2016).
153. Jia, L. *et al.* Nanostructured lipid carriers for parenteral delivery of silybin: Biodistribution and pharmacokinetic studies. *Colloids Surfaces B Biointerfaces* **80**, 213–218 (2010).
154. Frias, I., Neves, A. R., Pinheiro, M. & Reis, S. Design, development, and characterization of lipid nanocarriers-based epigallocatechin gallate delivery system for preventive and therapeutic supplementation. *Drug Des. Devel. Ther.* **10**, 3319–3528 (2016).
155. Babazadeh, A., Ghanbarzadeh, B. & Hamishehkar, H. Formulation of food grade nanostructured lipid carrier (NLC) for potential applications in medicinal-functional foods. *J. Drug Deliv. Sci. Technol.* **39**, 50–58 (2017).
156. Doktorovová, S., Araújo, J., Garcia, M. L., Rakovský, E. & Souto, E. B. Formulating fluticasone propionate in novel PEG-containing nanostructured lipid carriers (PEG-NLC). *Colloids Surfaces B Biointerfaces* **75**, 538–542 (2010).
157. Cocero, M. J., Martín, Á., Mattea, F. & Varona, S. Encapsulation and co-precipitation processes with supercritical fluids: Fundamentals and applications. *J. Supercrit. Fluids* **47**, 546–555 (2009).

158. Mezzomo, N. *et al.* Supercritical anti-solvent precipitation of carotenoid fraction from pink shrimp residue: Effect of operational conditions on encapsulation efficiency. *J. Supercrit. Fluids* **66**, 342–349 (2012).
159. Bikiaris, D. *et al.* Physicochemical studies on solid dispersions of poorly water-soluble drugs: Evaluation of capabilities and limitations of thermal analysis techniques. *Thermochim. Acta* **439**, 58–67 (2005).
160. Mainardes, R. M., Gremião, M. P. D. & Evangelista, R. C. Thermoanalytical study of praziquantel-loaded PLGA nanoparticles. *Rev. Bras. Ciencias Farm. J. Pharm. Sci.* **42**, 523–530 (2006).
161. Shen, X., Zhao, C., Lu, J. & Guo, M. Physicochemical Properties of Whey-Protein-Stabilized Astaxanthin Nanodispersion and Its Transport via a Caco-2 Monolayer. *J. Agric. Food Chem.* **66**, 1472–1478 (2018).
162. Manuscript, A. 基因的改变NIH Public Access. *Bone* **23**, 1–7 (2008).
163. de Paz, E., Martín, Á., Duarte, C. M. M. & Cocero, M. J. Formulation of β-carotene with poly-(ε-caprolactones) by PGSS process. *Powder Technol.* **217**, 77–83 (2012).
164. Nielsen, L. S., Schubert, L. & Hansen, J. Bioadhesive drug delivery systems. I. Characterisation of mucoadhesive properties of systems based on glyceryl mono-oleate and glyceryl monolinoleate. *Eur. J. Pharm. Sci.* **6**, 231–239 (1998).
165. Him, S. S. & Im, G. K. Technical paper Color Changes and Carotenoid Pigment Loss in Retentate from Star Ruby Grapefruit. **8**, 244–246 (2002).
166. Przybysz, M. A., Szterk, A., Symoniuk, E., Gäszczyk, M. & Dłuewska, E. α- and β-Carotene Stability during Storage of Microspheres Obtained from Spray-Dried Microencapsulation Technology. *Polish J. Food Nutr. Sci.* **68**, 45–55 (2018).
167. Knockaert, G. *et al.* Carrot β-carotene degradation and isomerization kinetics during thermal processing in the presence of oil. *J. Agric. Food Chem.* **60**, 10312–10319 (2012).
168. Jaspart, S., Piel, G., Delattre, L. & Evrard, B. is equivalent to SLNs. (2005).
169. de la Fuente, J. C., Oyarzún, B., Quezada, N. & del Valle, J. M. Solubility of carotenoid pigments (lycopene and astaxanthin) in supercritical carbon dioxide. *Fluid Phase Equilib.* **247**, 90–95 (2006).
170. Melgosa, R., Benito-Román, Ó., Sanz, M. T., de Paz, E. & Beltrán, S. Omega–3 encapsulation by PGSS-drying and conventional drying methods. Particle characterization and oxidative stability. *Food Chem.* **270**, 138–148 (2019).
171. Matias, A. *et al.* Food & Function. doi:10.1039/c4fo00071d.Please
172. Tsai, T. H., Chen, W. L. & Hu, F. R. Comparison of fluoroquinolones: Cytotoxicity on human corneal epithelial cells. *Eye* **24**, 909–917 (2010).
173. I.O. for Standardization,ISO 10993-5. (2009).
174. Day, R. & Suzuki, Y. Cell Proliferation, Reactive Oxygen and Cellular Glutathione. *Dose-Response* **3**, 425–442 (2005).
175. Diwanji, N. & Bergmann, A. An unexpected friend − ROS in apoptosis-induced compensatory proliferation: Implications for regeneration and cancer. *Semin. Cell Dev. Biol.* **80**, 74–82 (2018).
176. Yu, T., Dohl, J., Chen, Y., Gasier, H. G. & Deuster, P. A. Astaxanthin but not quercetin preserves mitochondrial integrity and function, ameliorates oxidative stress, and reduces heat-induced skeletal muscle injury. *J. Cell. Physiol.* **234**, 13292–13302 (2019).
177. des Rieux, A. *et al.* Helodermin-loaded nanoparticles: Characterization and transport across an in vitro model of the follicle-associated epithelium. *J. Control. Release* **118**, 294–302 (2007).
178. Akbari, A., Lavasanifar, A. & Wu, J. Interaction of cruciferin-based nanoparticles with Caco-2 cells and Caco-2/HT29-MTX co-cultures. *Acta Biomater.* **64**, 249–258 (2017).
179. Meor Mohd Affandi, M. M. R., Julianto, T. & Majeed, A. B. A. Enhanced oral bioavailability of astaxanthin with droplet size reduction. *Food Sci. Technol. Res.* **18**, 549–554 (2012).
180. Desai 1997.pdf. (1997).
181. Anarjan, N., Tan, C. P., Nehdi, I. A. & Ling, T. C. Colloidal astaxanthin: Preparation, characterisation and bioavailability evaluation. *Food Chem.* **135**, 1303–1309 (2012).
182. Emulsions, A., Shen, X., Fang, T., Zheng, J. & Guo, M. Physicochemical Properties and Cellular Uptake. 1–12 (2019). doi:10.3390/molecules24040727

183. Rodriguez-Ruiz, V. *et al.* Astaxanthin-loaded nanostructured lipid carriers for preservation of antioxidant activity. *Molecules* **23**, (2018).
184. Wolfe, K. L. & Rui, H. L. Cellular antioxidant activity (CAA) assay for assessing antioxidants, foods, and dietary supplements. *J. Agric. Food Chem.* **55**, 8896–8907 (2007).
185. Puglia, C. *et al.* Nanostructured Lipid Carriers (NLC) as Vehicles for Topical Administration of Sesamol: In Vitro Percutaneous Absorption Study and Evaluation of Antioxidant Activity. *Planta Med.* **83**, 398–404 (2017).
186. Pinto, F., de Barros, D. P. C. & Fonseca, L. P. Design of multifunctional nanostructured lipid carriers enriched with α-tocopherol using vegetable oils. *Ind. Crops Prod.* **118**, 149–159 (2018).
187. Chintong, S., Phatvej, W., Rerk-am, U. & Waiprib, Y. In Vitro Antioxidant , Antityrosinase , and Cytotoxic Activities of Astaxanthin from Shrimp Waste. 1–11 (2019).
188. Kang, H. & Kim, H. Astaxanthin and β-carotene in Helicobacter pylori-induced Gastric Inflammation: A Mini-review on Action Mechanisms. *J. Cancer Prev.* **22**, 57–61 (2017).
189. Doktorovova, S., Souto, E. B. & Silva, A. M. Nanotoxicology applied to solid lipid nanoparticles and nanostructured lipid carriers - A systematic review of in vitro data. *Eur. J. Pharm. Biopharm.* **87**, 1–18 (2014).
190. Fu, P. P., Xia, Q., Hwang, H. M., Ray, P. C. & Yu, H. Mechanisms of nanotoxicity: Generation of reactive oxygen species. *J. Food Drug Anal.* **22**, 64–75 (2014).
191. Bhattacharjee, S. *et al.* Role of surface charge and oxidative stress in cytotoxicity of organic monolayer-coated silicon nanoparticles towards macrophage NR8383 cells. *Part. Fibre Toxicol.* **7**, 25 (2010).
192. Wang, H. Q. *et al.* Astaxanthin upregulates heme oxygenase-1 expression through ERK1/2 pathway and its protective effect against beta-amyloid-induced cytotoxicity in SH-SY5Y cells. *Brain Res.* **1360**, 159–167 (2010).
193. Farruggia, C. *et al.* Astaxanthin exerts anti-inflammatory and antioxidant effects in macrophages in NRF2-dependent and independent manners. *J. Nutr. Biochem.* #pagerange# (2018). doi:10.1016/j.jnutbio.2018.09.005
194. Palozza, P. Can β-carotene regulate cell growth by a redox mechanism? An answer from cultured cells. *Biochim. Biophys. Acta - Mol. Basis Dis.* **1740**, 215–221 (2005).
195. Rao, B. N., Reddy, K. R., Mounika, B., Fathima, S. R. & Tejaswini, A. Vesicular Drug Delivery System: A Review. *Int. J. ChemTech Res.* **12**, 39–53 (2019).
196. Liao, X., Zhang, H. & He, T. Preparation of porous biodegradable polymer and its nanocomposites by supercritical CO 2 foaming for tissue engineering. *J. Nanomater.* **2012**, (2012).
197. Peterson, L. W. & Artis, D. Intestinal epithelial cells: Regulators of barrier function and immune homeostasis. *Nat. Rev. Immunol.* **14**, 141–153 (2014).

6. Appendix

Appendix 1- HPLC analysis to determine the content of astaxanthin in the extract

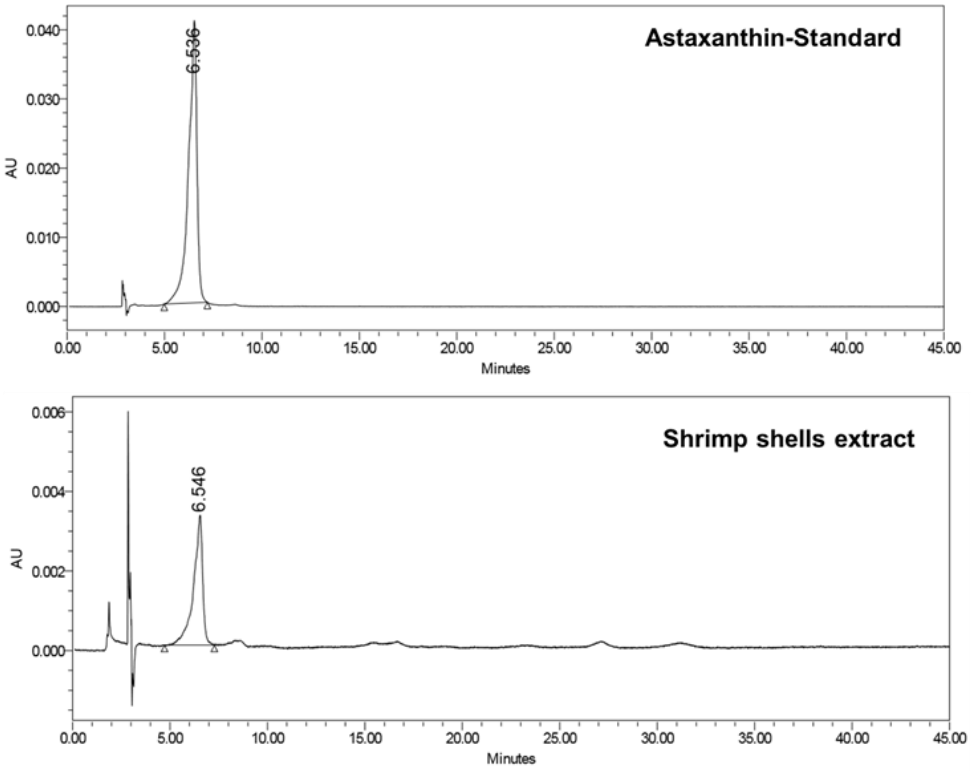

Figure 6.1- **HPLC chromatogram of astaxanthin standard, and shrimp shells extract**. HPLC method use described in Section 2.2.2.

Appendix 2- β-Carotene-loaded NLCs and Astaxanthin-loaded NLCs

Figure 6.2- β-carotene-loaded NLCs: Produced using a formulation without organic solvent through melt-emulsification using a homogenization time of 7 minutes and speed of 21500 rpm.

Figure 6.3- Astaxanthin-loaded NLCs: Produced using a formulation without organic solvent through melt-emulsification using a homogenization time of 20 minutes and speed of 21500 rpm.

Appendix 3- Statistical analysis performed for the experimental load of the β-carotene-loaded SLCs

Table 6.1- Summary of the results obtained for the statistical analysis performed for the experimental load obtained in the experiments performed for the B-carotene-loaded SLCs production optimization. Statistical analysis performed through One-way Anova and Tukey's multiple comparisons test The symbol * indicates significance between experiments (* p-value<0.05, ** p-value<0.01, *** p-value<0.001, **** p-value<0.0001).

Tukey's multiple comparisons test	Significant difference	Summary	Adjusted p-value
" **E.1 vs. E.2"**	Yes	****	< 0.0001
" **E.1 vs. E.3"**	Yes	****	< 0.0001
" **E.1 vs. E.4"**	Yes	***	0.0002
" **E.1 vs. E.5"**	Yes	***	0.0009
" **E.1 vs. E.6"**	Yes	****	< 0.0001
" **E.1 vs. E.7"**	Yes	****	< 0.0001
" **E.1 vs. E.8"**	Yes	****	< 0.0001
" **E.1 vs. E.9"**	Yes	****	< 0.0001
" **E.2 vs. E.3"**	No	ns	0.8702
" **E.2 vs. E.4"**	No	ns	0.2732
" **E.2 vs. E.5"**	No	ns	0.1038
" **E.2 vs. E.6"**	No	ns	0.2978
" **E.2 vs. E.7"**	No	ns	0.4527
" **E.2 vs. E.8"**	No	ns	0.7701
" **E.2 vs. E.9"**	No	ns	0.4543
" **E.3 vs. E.4"**	Yes	**	0.0082
" **E.3 vs. E.5"**	Yes	**	0.0020
" **E.3 vs. E.6"**	No	ns	0.9870
" **E.3 vs. E.7"**	No	ns	0.9986
" **E.3 vs. E.8"**	No	ns	> 0.9999
" **E.3 vs. E.9"**	No	ns	0.9986
" **E.4 vs. E.5"**	No	ns	> 0.9999
" **E.4 vs. E.6"**	Yes	***	0.0004
" **E.4 vs. E.7"**	Yes	***	0.0010
" **E.4 vs. E.8"**	Yes	**	0.0046
" **E.4 vs. E.9"**	Yes	***	0.0010
" **E.5 vs. E.6"**	Yes	****	< 0.0001
" **E.5 vs. E.7"**	Yes	***	0.0002
" **E.5 vs. E.8"**	Yes	**	0.0010
" **E.5 vs. E.9"**	Yes	***	0.0002
" **E.6 vs. E.7"**	No	ns	> 0.9999
" **E.6 vs. E.8"**	No	ns	0.9972
" **E.6 vs. E.9"**	No	ns	> 0.9999
" **E.7 vs. E.8"**	No	ns	0.9999
" **E.7 vs. E.9"**	No	ns	> 0.9999
" **E.8 vs. E.9"**	No	ns	0.9999

Appendix 4- Permeability studies: determination of the amount of permeated and absorbed astaxanthin

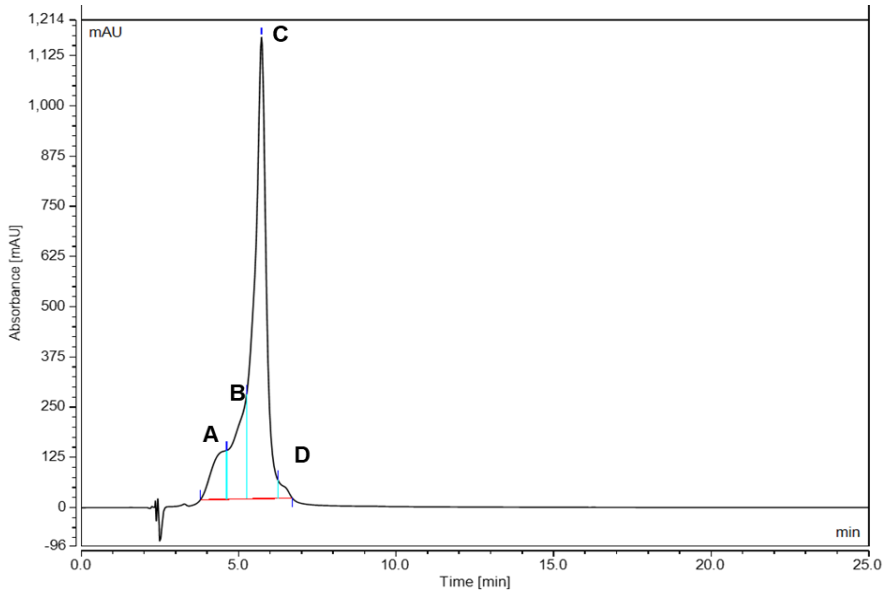

Figure 6.4- HPLC chromatogram of astaxanthin standard. HPLC method use described in Section 2.2.5.8.4

From Figure 6.4, it is possible to verify that it was not obtained only one peak corresponding to astaxanthin, but instead four peaks were obtained. From the UV spectra of each peak it is possible to verify that the four peaks correspond to astaxanthin (Figure 6.5). It is possible that the four different peaks correspond to astaxanthin isomers. Due to time limitations it was not possible to perform further optimizations on the HPLC process. Further studies should be performed in order to confirm if each peak corresponds to isomers of astaxanthin and which isomers.

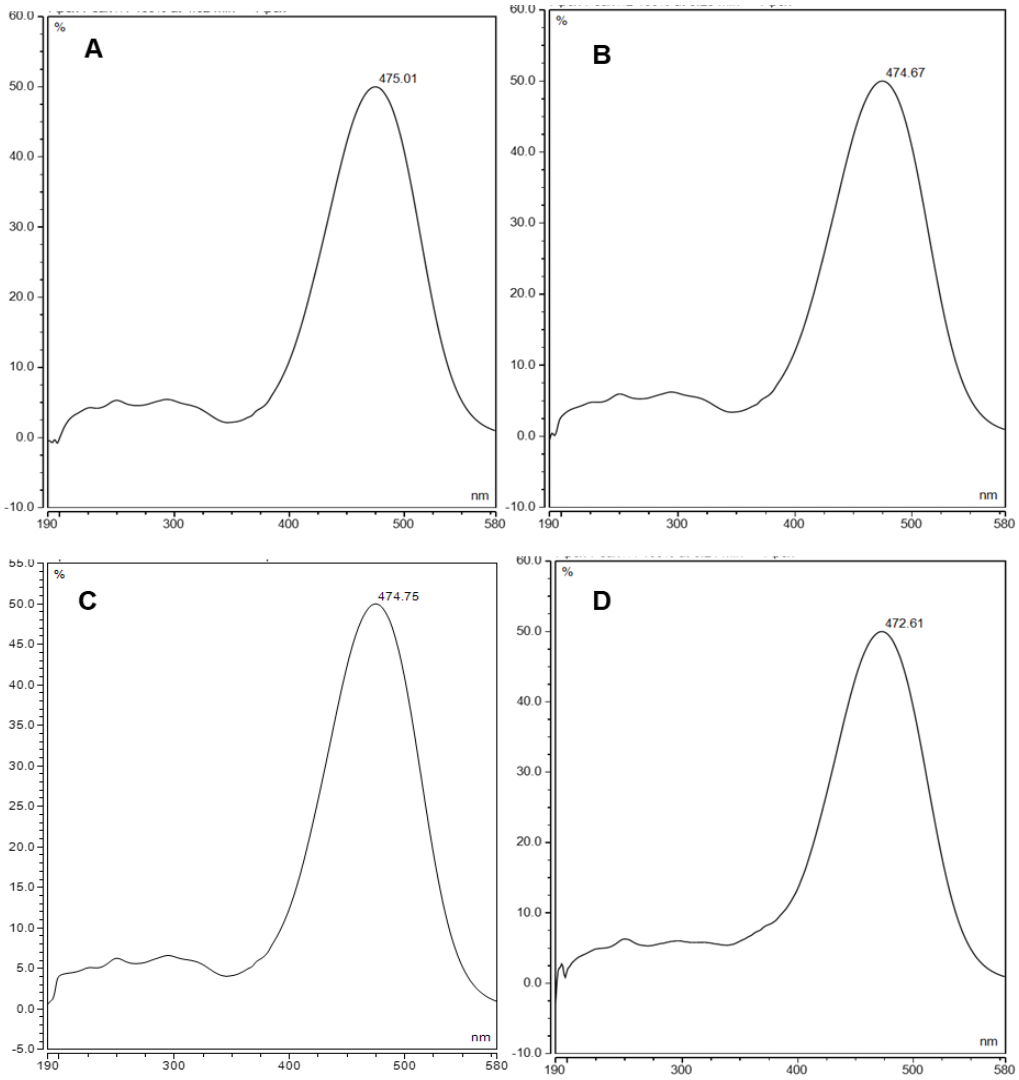

Figure 6.4- UV spectra of each peak obtained in the HPLC chromatogram of astaxanthin standard. HPLC method use described in Section 2.2.5.8.4

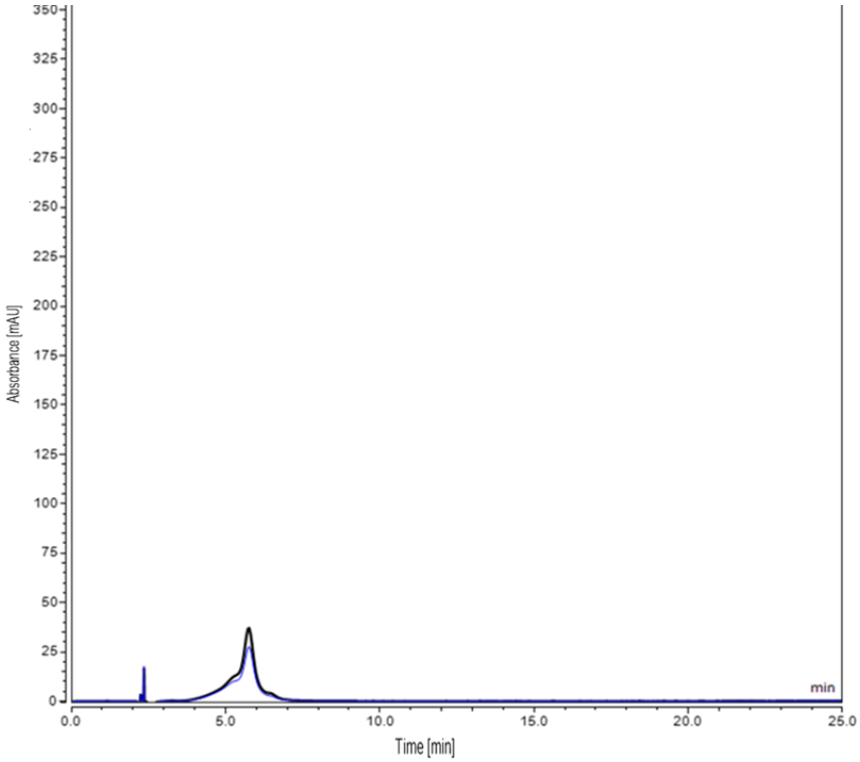

Figure 6.5- HPLC chromatogram: Permeability study to evaluate the permeability of astaxanthin-loaded SLCs in a triple co-culture Caco-2:HT29-MTX:-Raji-B. Black graph corresponds to astaxanthin standard and the blue graph corresponds to a sample of astaxanthin-loaded SLCs collected from the apical compartment. HPLC method use described in Section 2.2.5.8.4

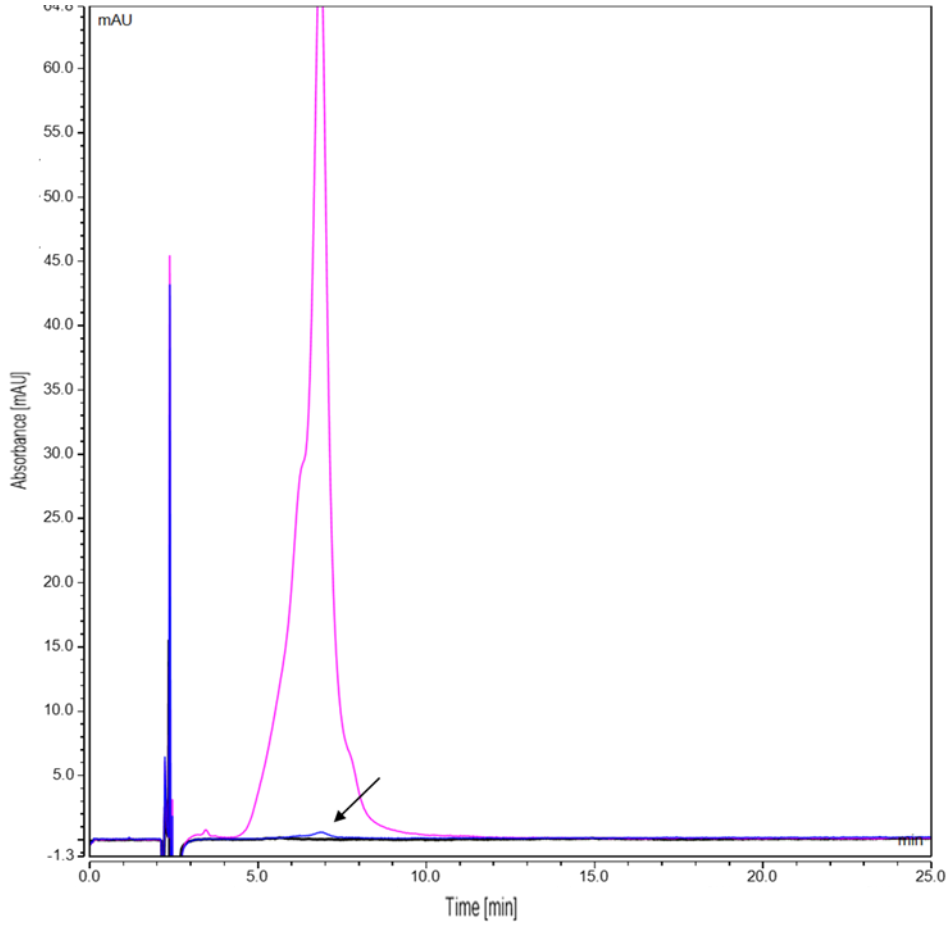

Figure 6.6- HPLC chromatogram: Permeability study to evaluate the permeability of astaxanthin-loaded SLCs in a triple co-culture Caco-2:HT29-MTX:Raji-B. Pink graph corresponds to astaxanthin standard and blue graph corresponds to a sample of astaxanthin-loaded NLCs collected from the basolateral compartment. HPLC method use described in Section 2.2.5.8.4